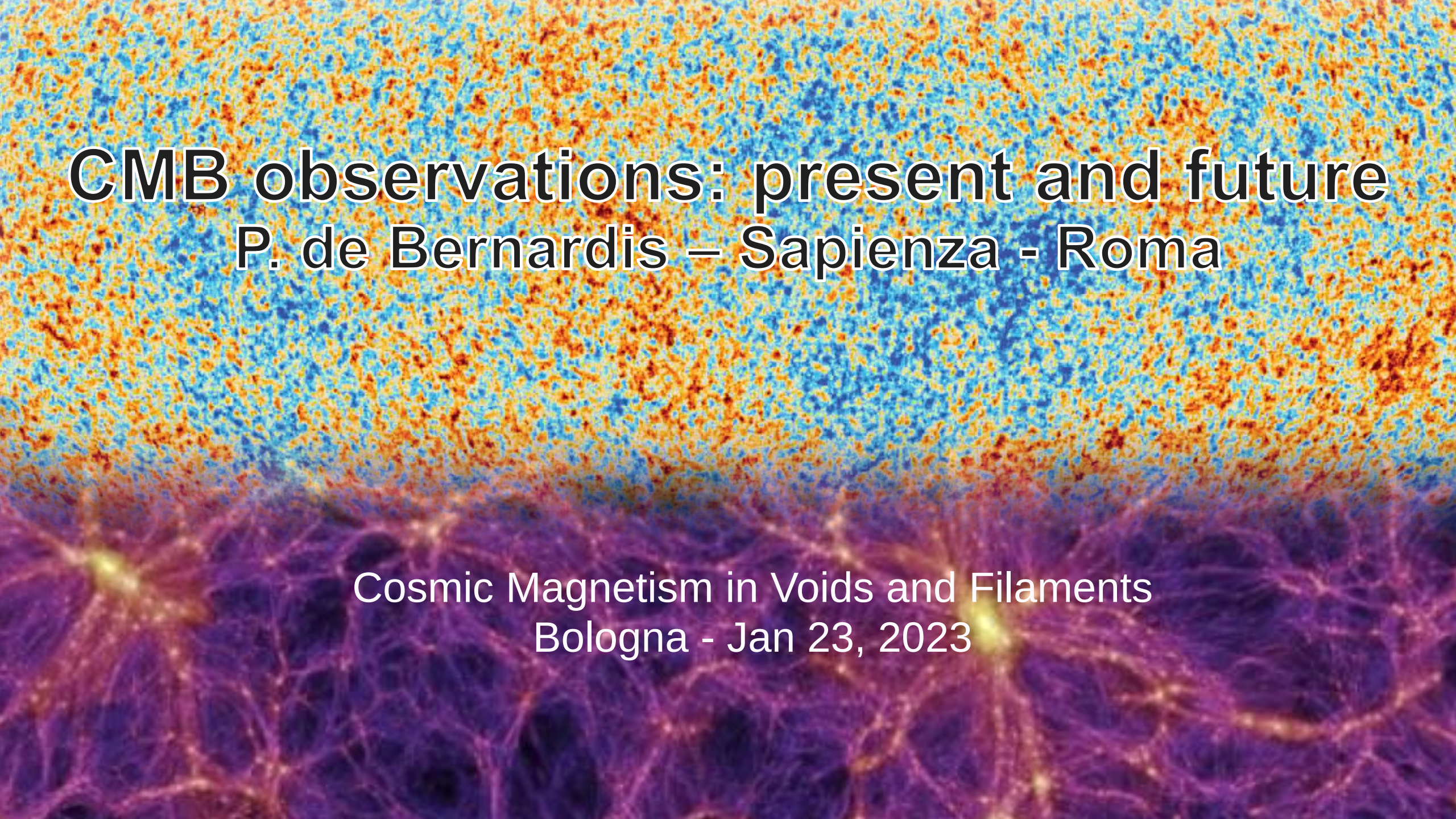

CMB observations: present and future

P. de Bernardis – Sapienza - Roma

Cosmic Magnetism in Voids and Filaments
Bologna - Jan 23, 2023

Origin of the Cosmic Microwave Background

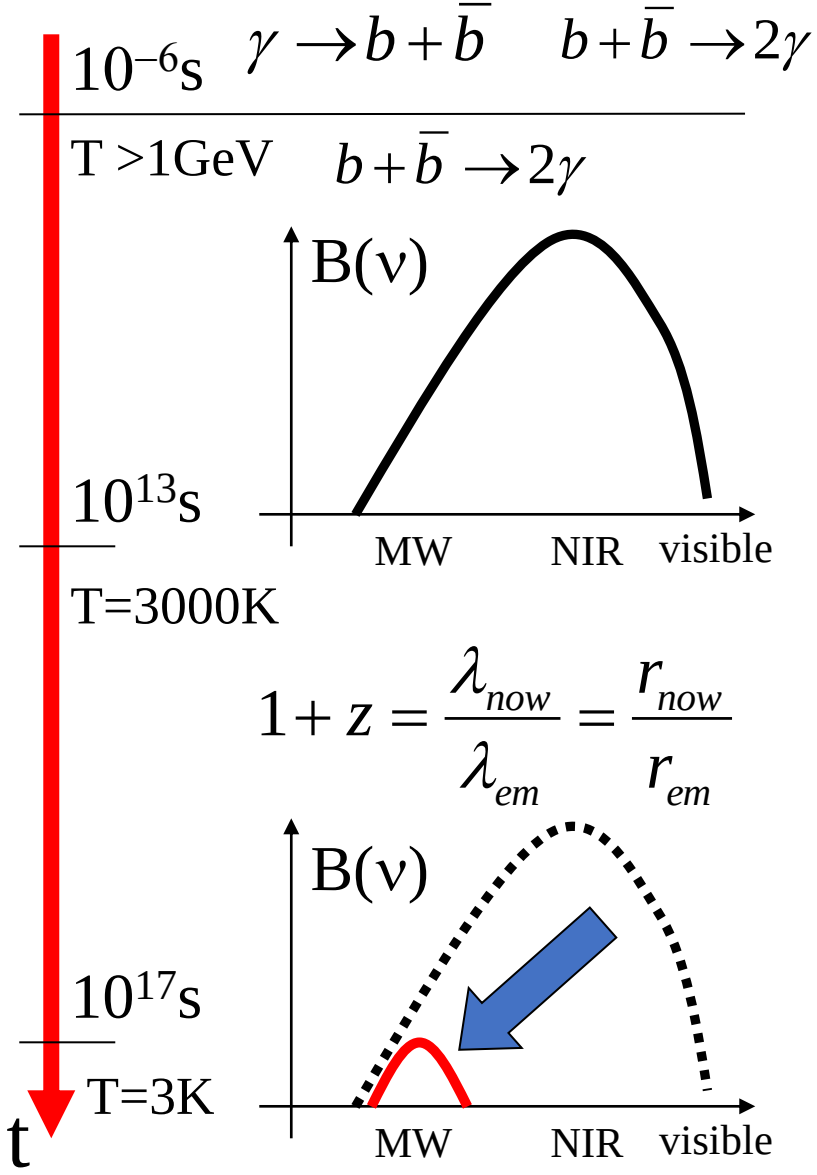

Today 411γ/cm^3

The CMB is an abundant background of photons, filling the whole Universe.

- **Generated** in the very early universe, less than 4 μs after the Big Bang, from a small $b-\bar{b}$ asymmetry ($10^9\gamma$ for each baryon)
- **Thermalized** in the primeval fireball (in the first 380000 years after the big bang) by repeated scattering against free electrons
- **Released, diluted and redshifted** to microwave frequencies (z_{CMB}=1100) in the subsequent 14 Gyrs of expansion of the Universe
- So CMB photons played a key role during baryogenesis, nucleosynthesis, recombination.
- **For us: they form our best tool for cosmological investigation, since they carry information about all the phases of the evolution of the universe.**

The CMB: a consolidated probe of the Universe

Empirically:

- The specific brightness of the CMB is *remarkably close to a blackbody* with T_o=2.725K
- The distribution is *remarkably isotropic* over the entire sky.

Spectrum: An accurate demonstration of the Hot Big Bang model for Cosmology

Around 1990:

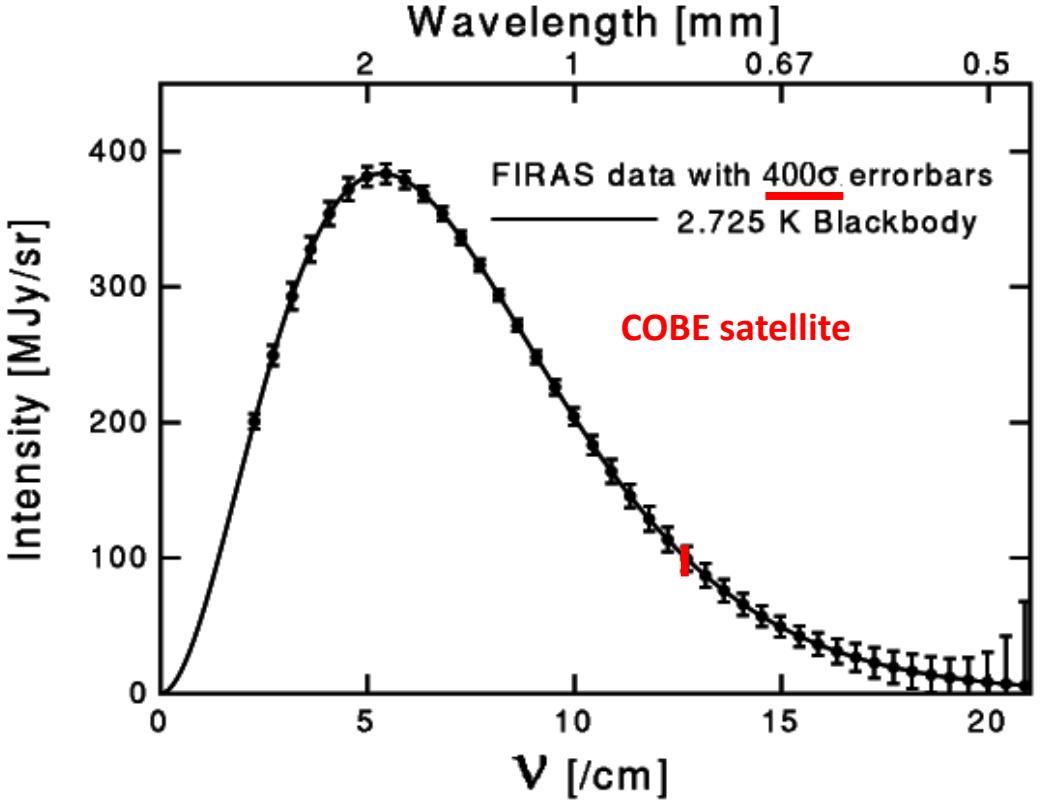

Isotropy: An accurate demonstration of the very high isotropy of the universe at large scales. However, faint anisotropies are expected.

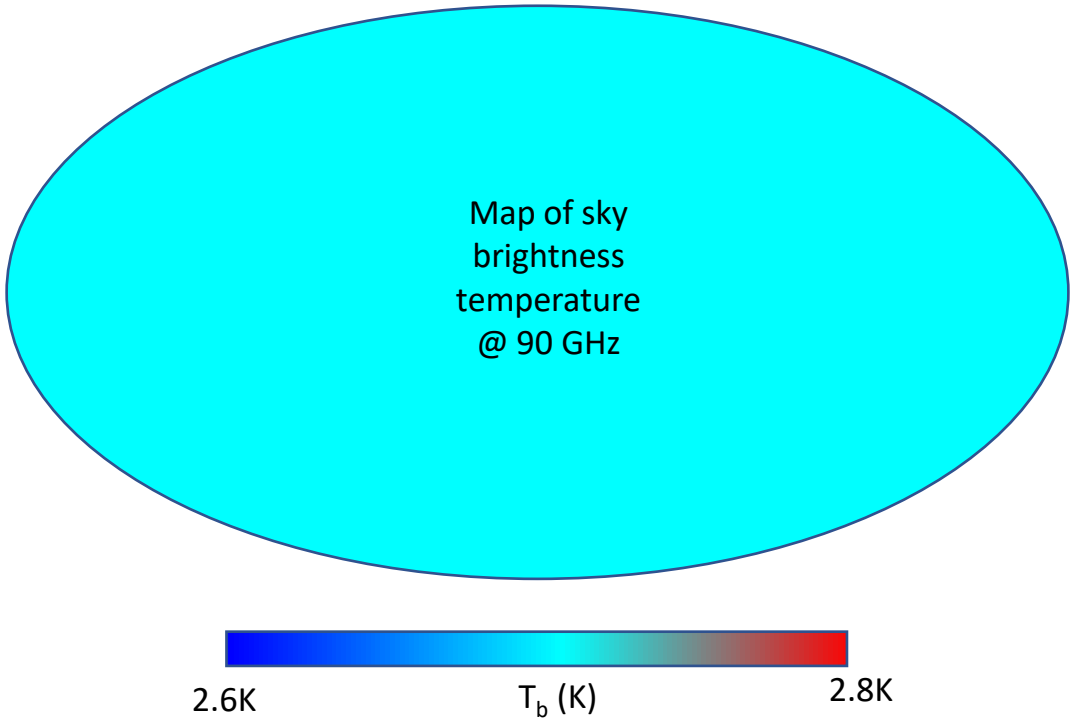

Faint anisotropies are expected

Density perturbations ($\Delta\rho/\rho$) were **oscillating** in the primeval plasma (as a result of the opposite effects of gravity and photon pressure).

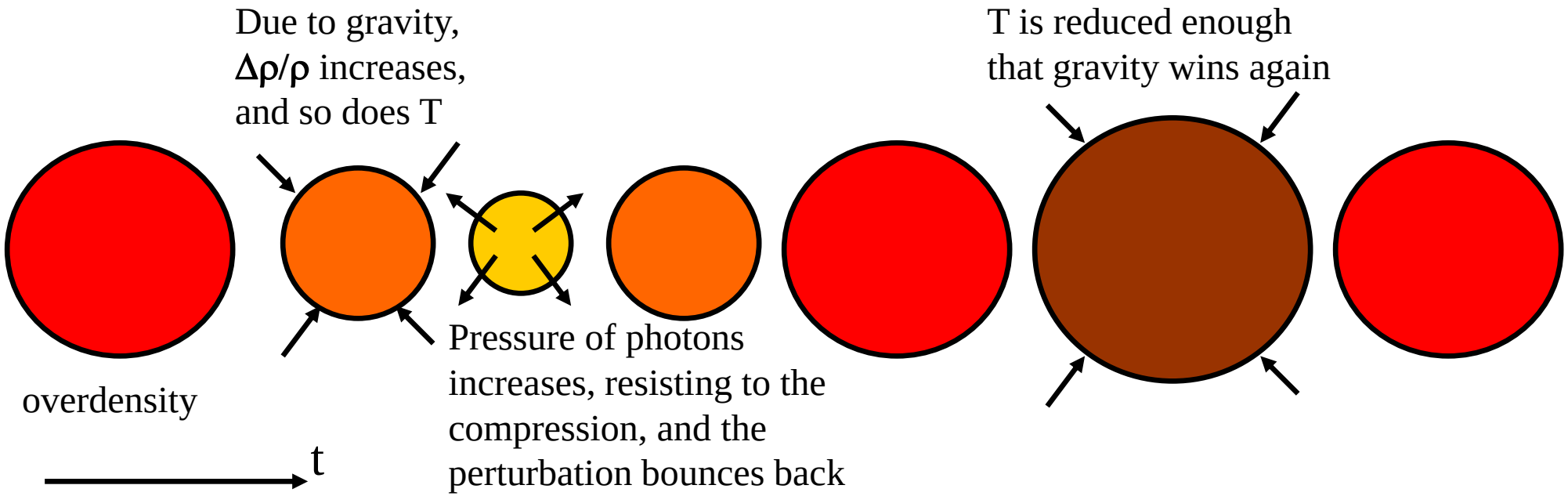

Before recombination $T > 3000$ K

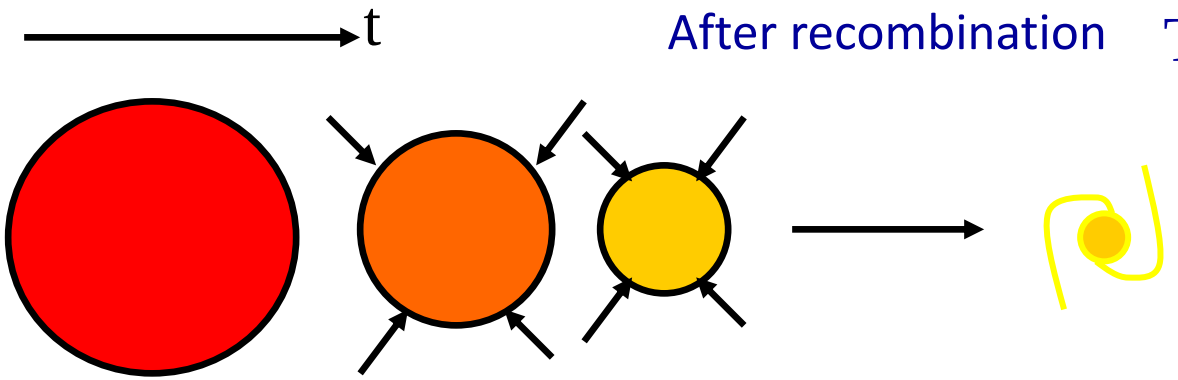

After recombination $T < 3000$ K

Here photons are not tightly coupled to matter, and their pressure is not effective. Perturbations can grow and form Galaxies.

After recombination, density perturbation can **grow** and create the hierarchy of structures we see in the nearby Universe.

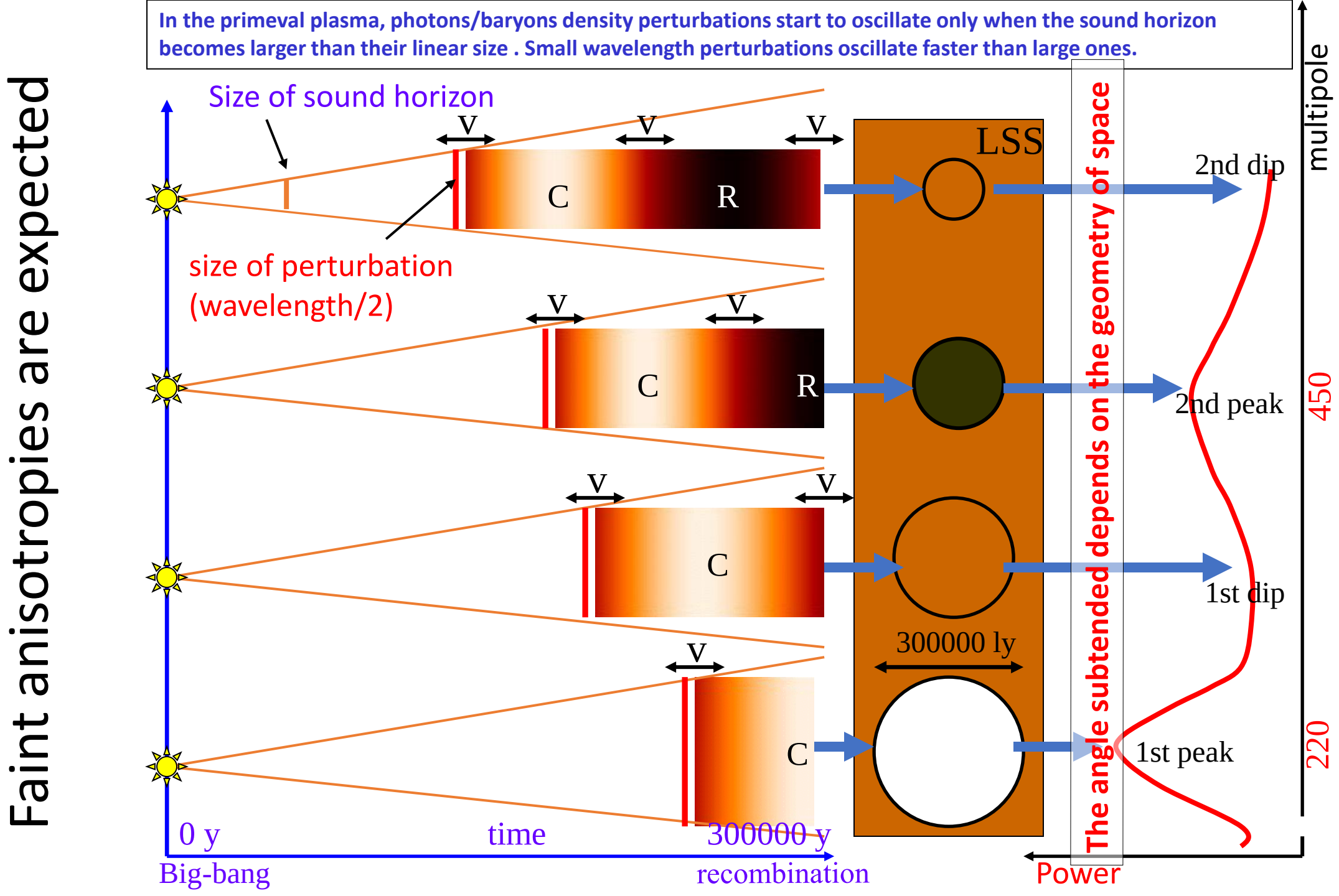
In the primeval plasma, photons/baryons density perturbations start to oscillate only when the sound horizon becomes larger than their linear size . Small wavelength perturbations oscillate faster than large ones.
Faint anisotropies are expected
Size of sound horizon
size of perturbation
(wavelength/2)
V
C
R
LSS
300000 ly
2nd dip
2nd peak
1st dip
1st peak
The angle subtended depends on the geometry of space
multipole
450
220
0 y
time
300000 y
Big-bang
recombination
Power

The CMB: a consolidated probe of the Universe

Around 2012:

Spectrum: An accurate demonstration of the Hot Big Bang model for Cosmology

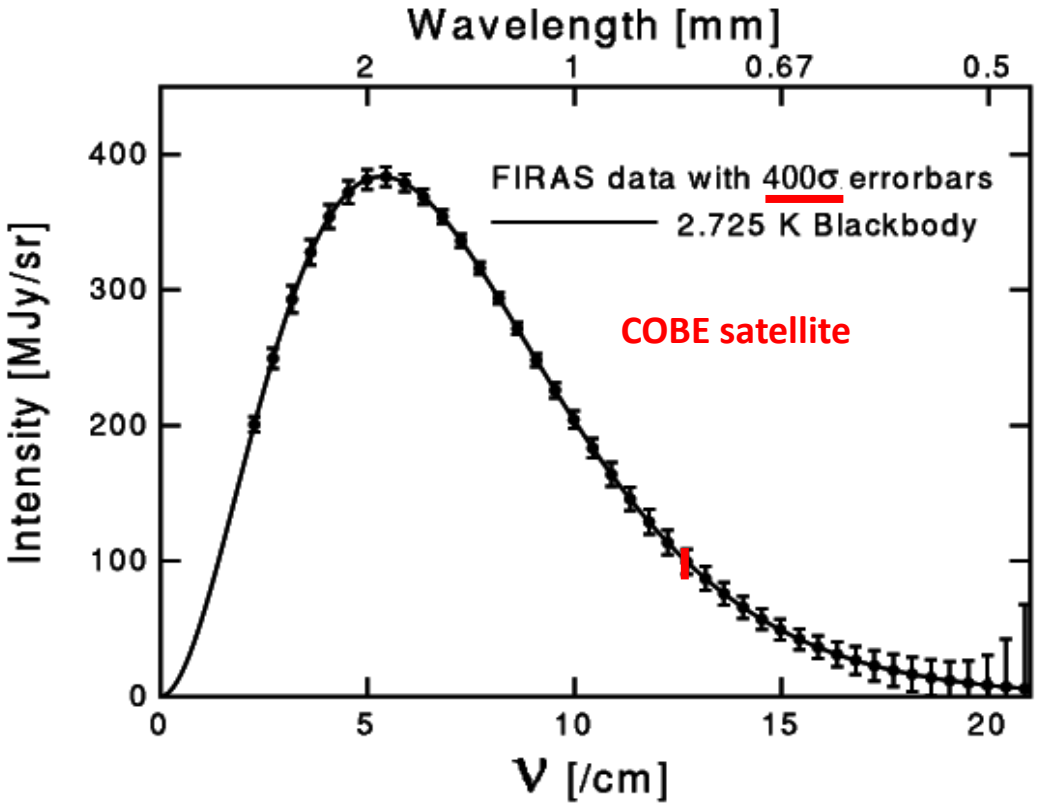

Faint Anisotropy: An accurate probe of the geometry, composition, and structure formation in the Universe

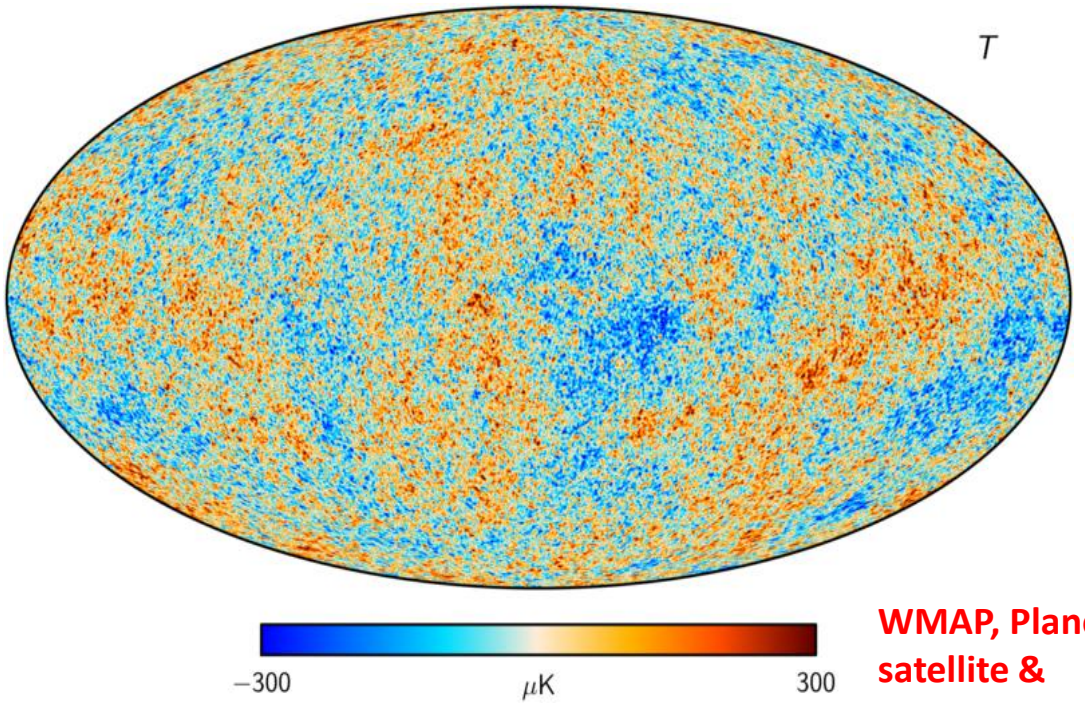

WMAP, Planck satellite &

The issue of **primary** CMB anisotropy is basically settled, and represents the backbone of the power of CMB data in constraining cosmological models. Important niches are still open for measurements of **secondary** anisotropies due to post recombination intreraction of CMB photons with the structures present in the universe (e.g. Sunyaev-Zeldovich effect).

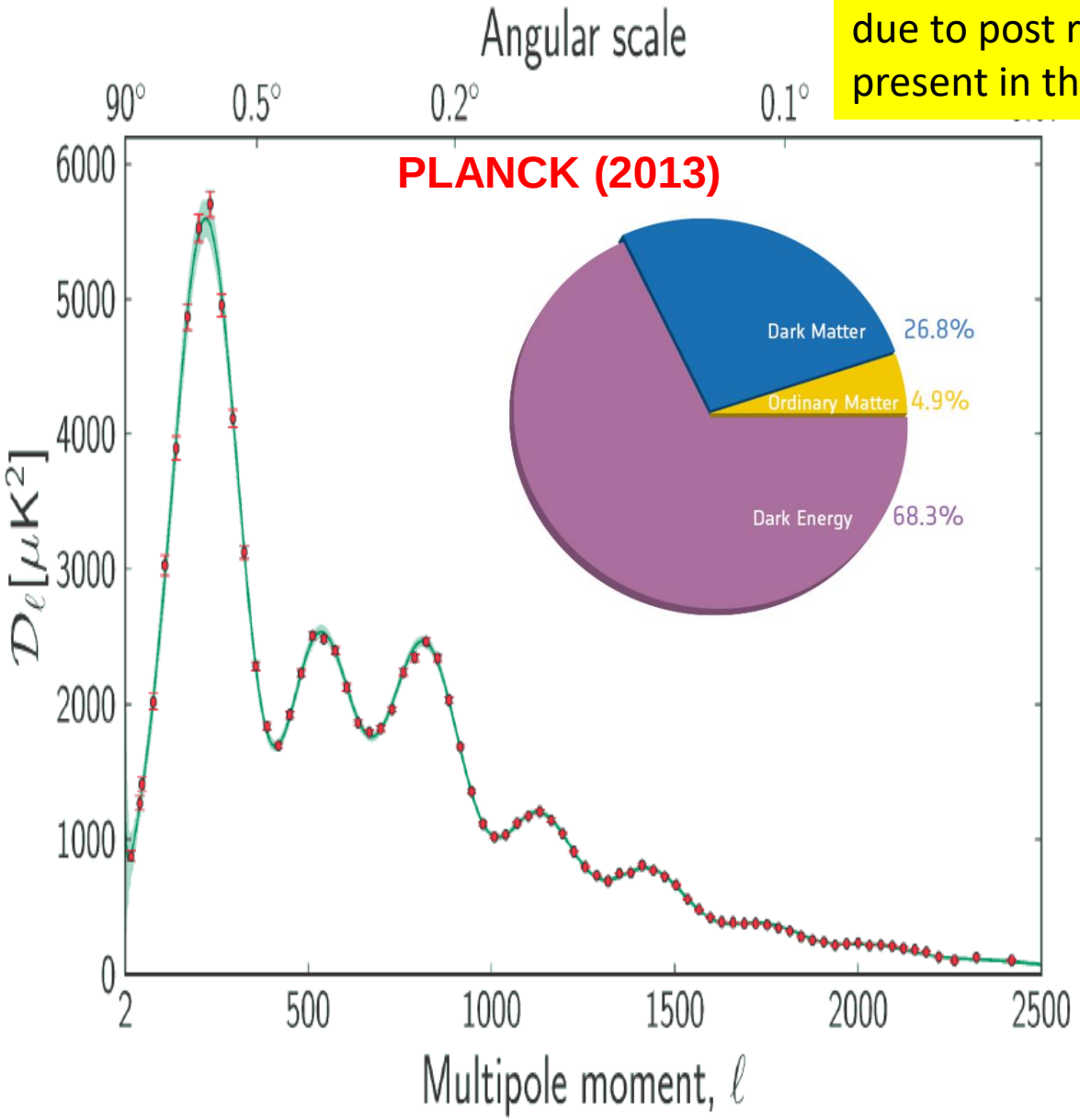

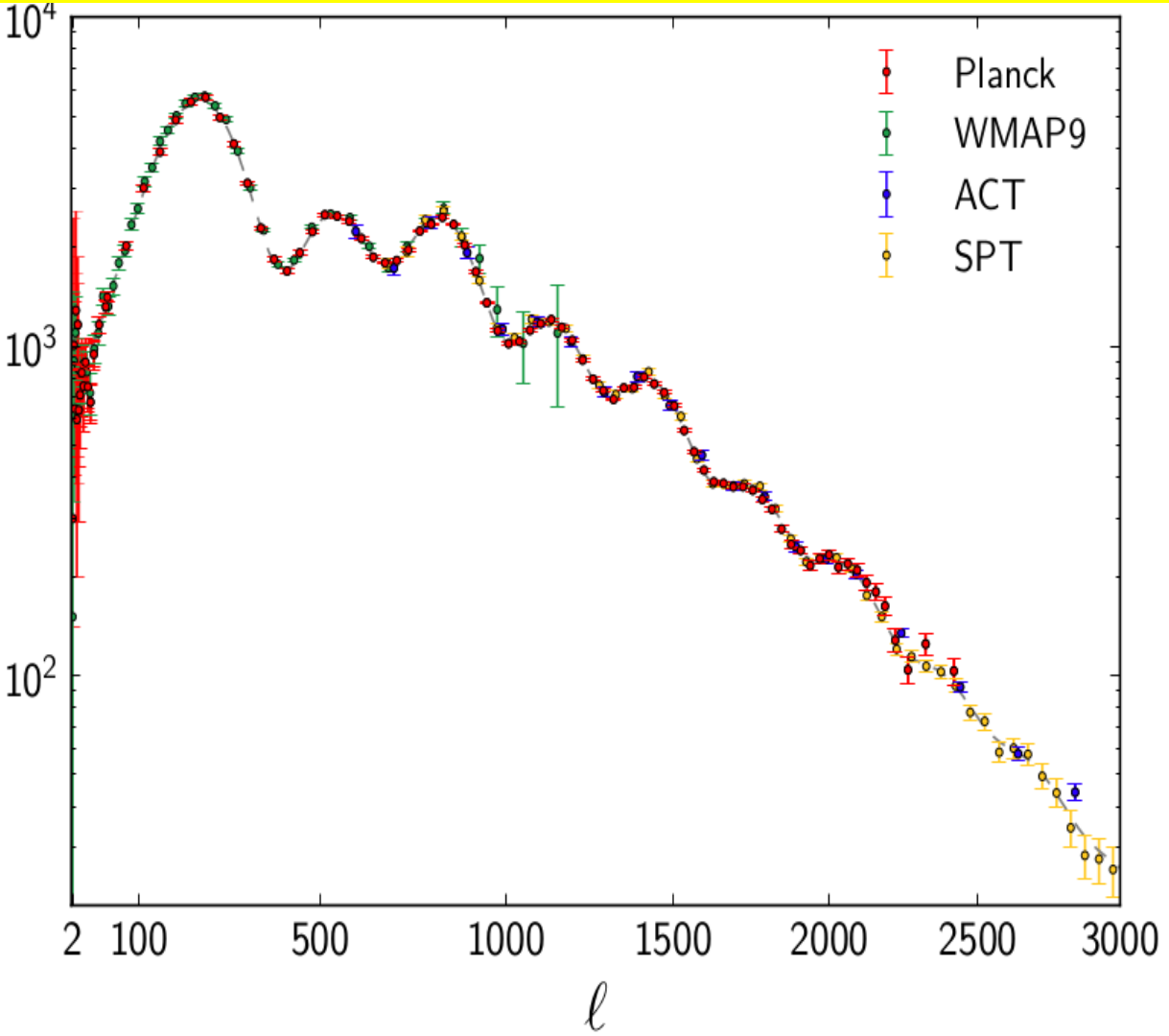

A small degree of linear polarization is expected

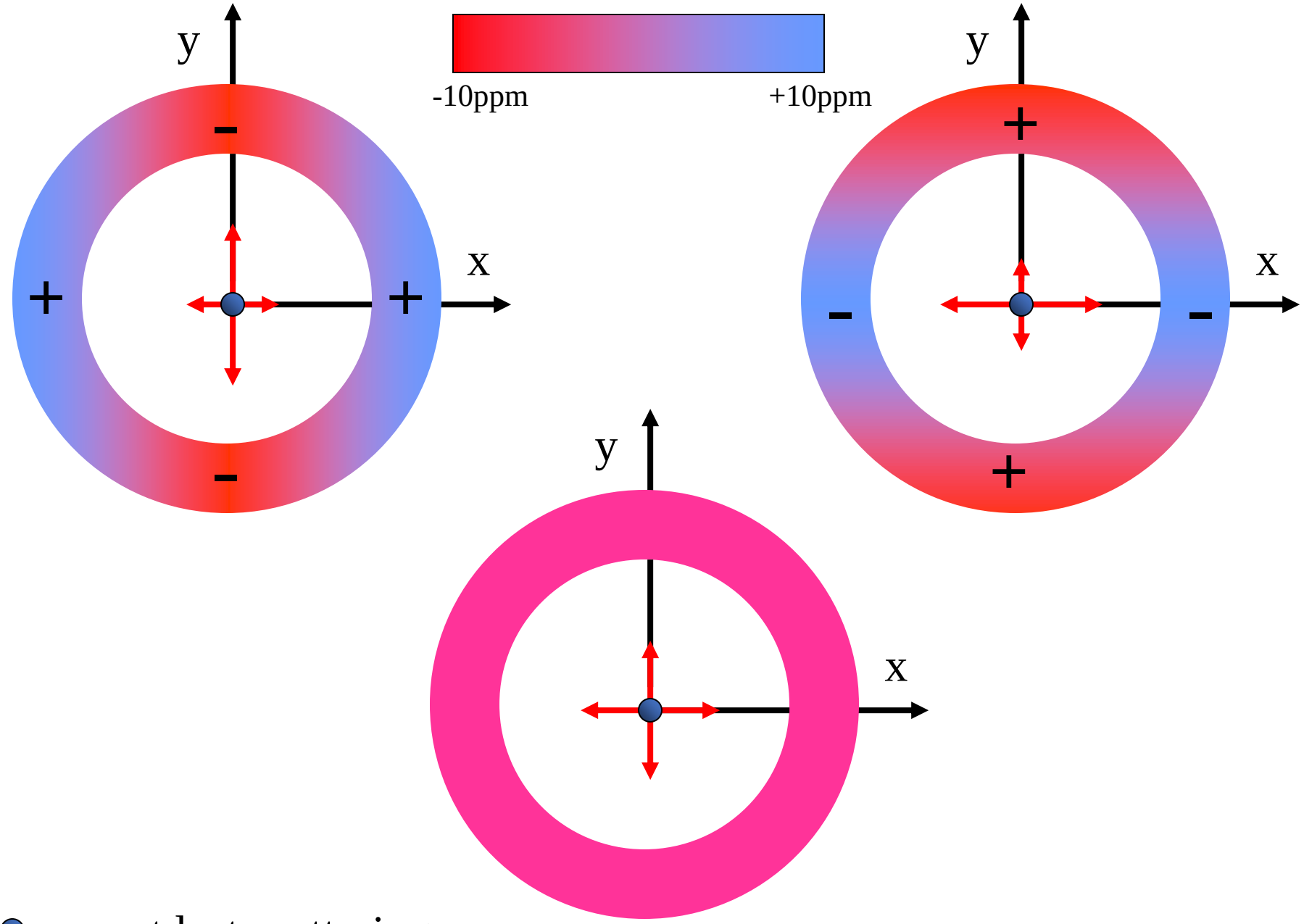

● = e^- at last scattering

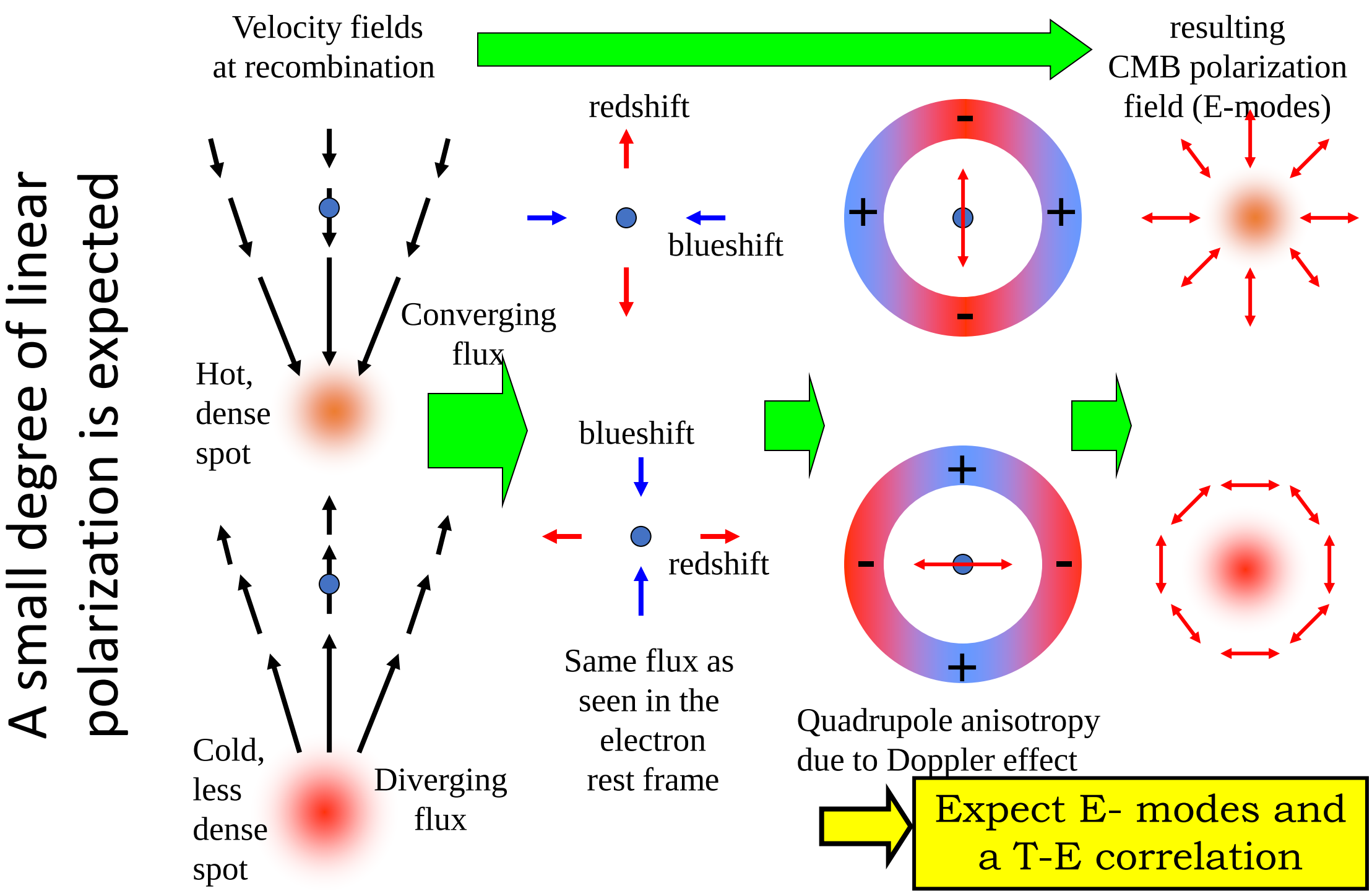
A small degree of linear polarization is expected
Velocity fields at recombination
resulting CMB polarization field (E-modes)
redshift
blueshift
Converging flux
Hot, dense spot
blueshift
redshift
Same flux as seen in the electron rest frame
Quadrupole anisotropy due to Doppler effect
Cold, less dense spot
Diverging flux
Expect E- modes and a T-E correlation

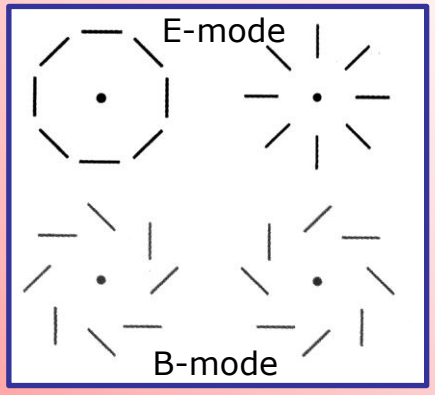

- If inflation really happened:
  - ✓ It stretched geometry of space to nearly Euclidean
  - ✓ It produced a nearly scale invariant spectrum of gaussian density fluctuations
  - ✓ It produced a stochastic background of gravitational waves: Primordial G.W. The background is so faint that even LISA will not be able to measure it.
- Tensor perturbations also produce quadrupole anisotropy. They generate irrotational (E-modes) **and rotational (B-modes) components** in the CMB polarization field.
- Since B-modes are not produced by scalar fluctuations, they represent a signature of inflation.

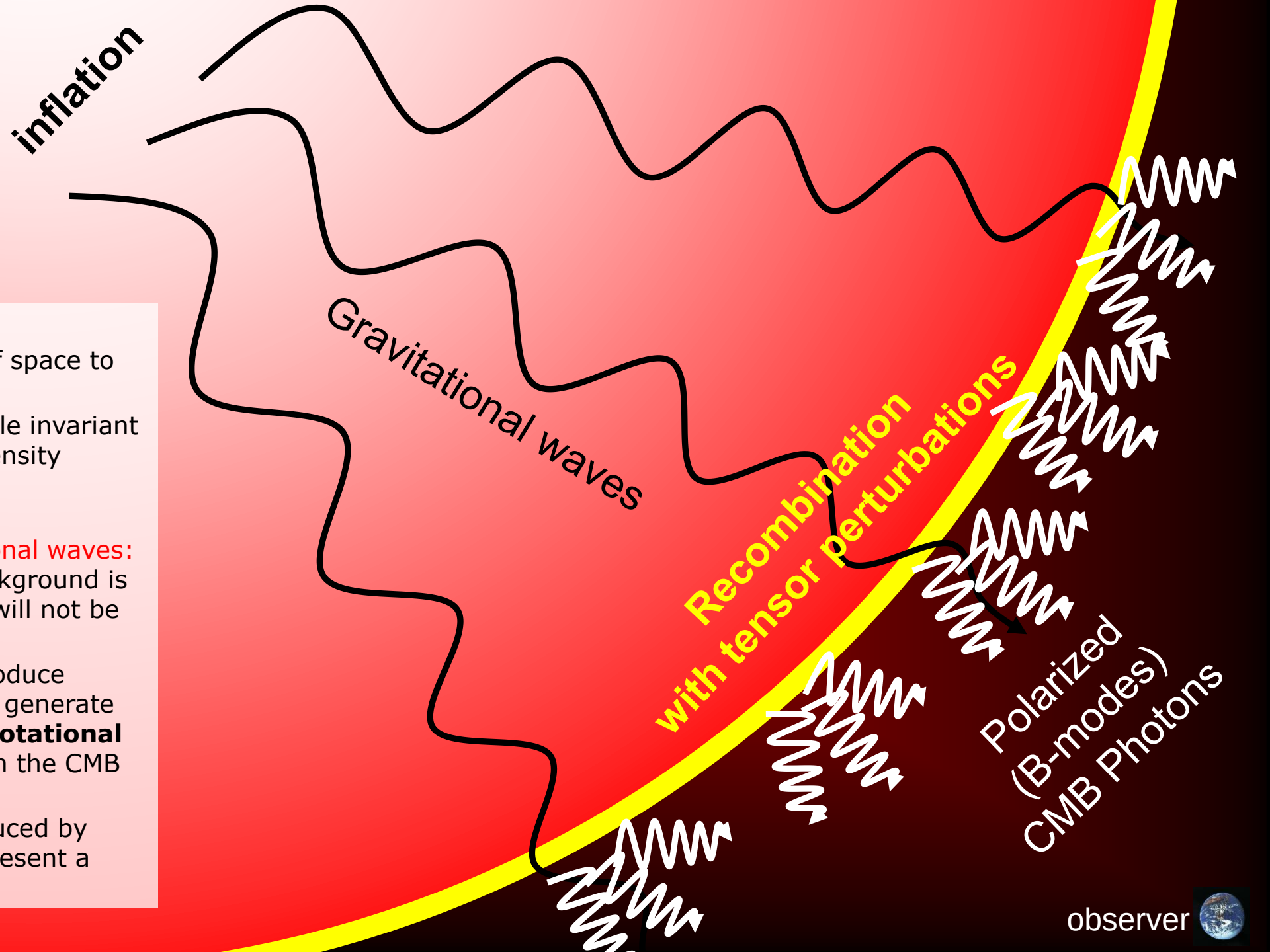

The CMB: a consolidated probe of the Universe

around 2017:

Spectrum: An accurate demonstration of the Hot Big Bang model for Cosmology

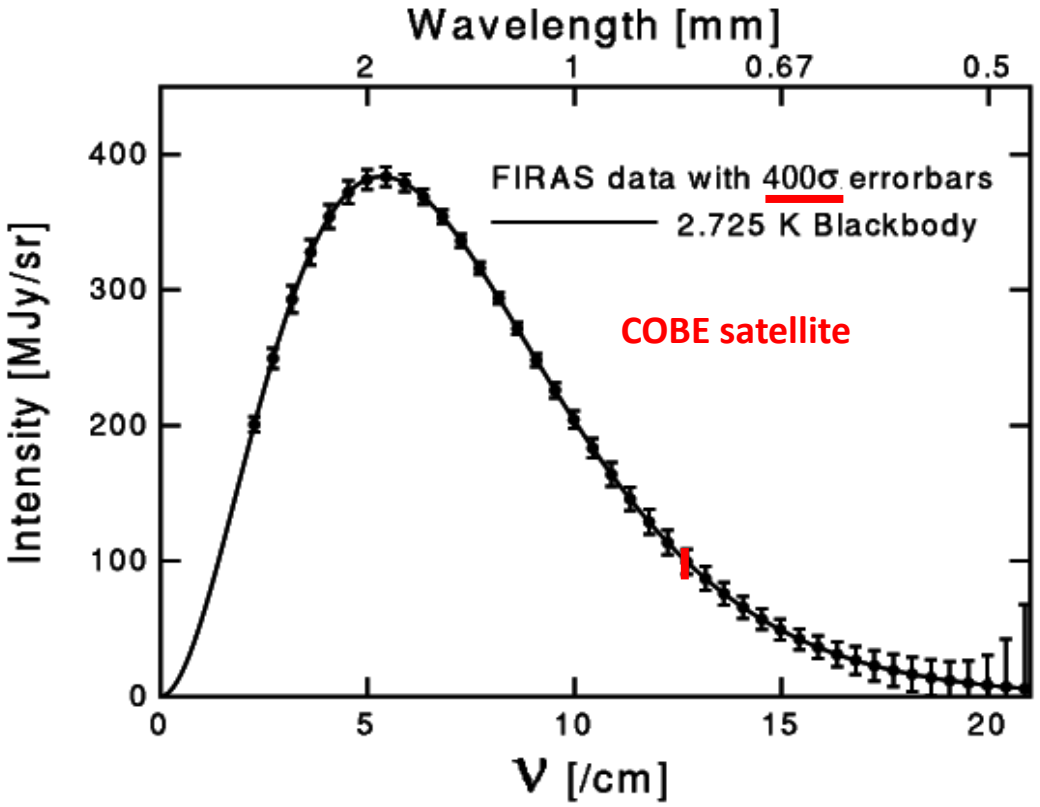

Polarization: A confirmation of the physics at recombination, and a possible probe of the very early universe (inflation) and physics at ultra high energy with the power spectrum of the rotational component (B-mode, BB in the figure).

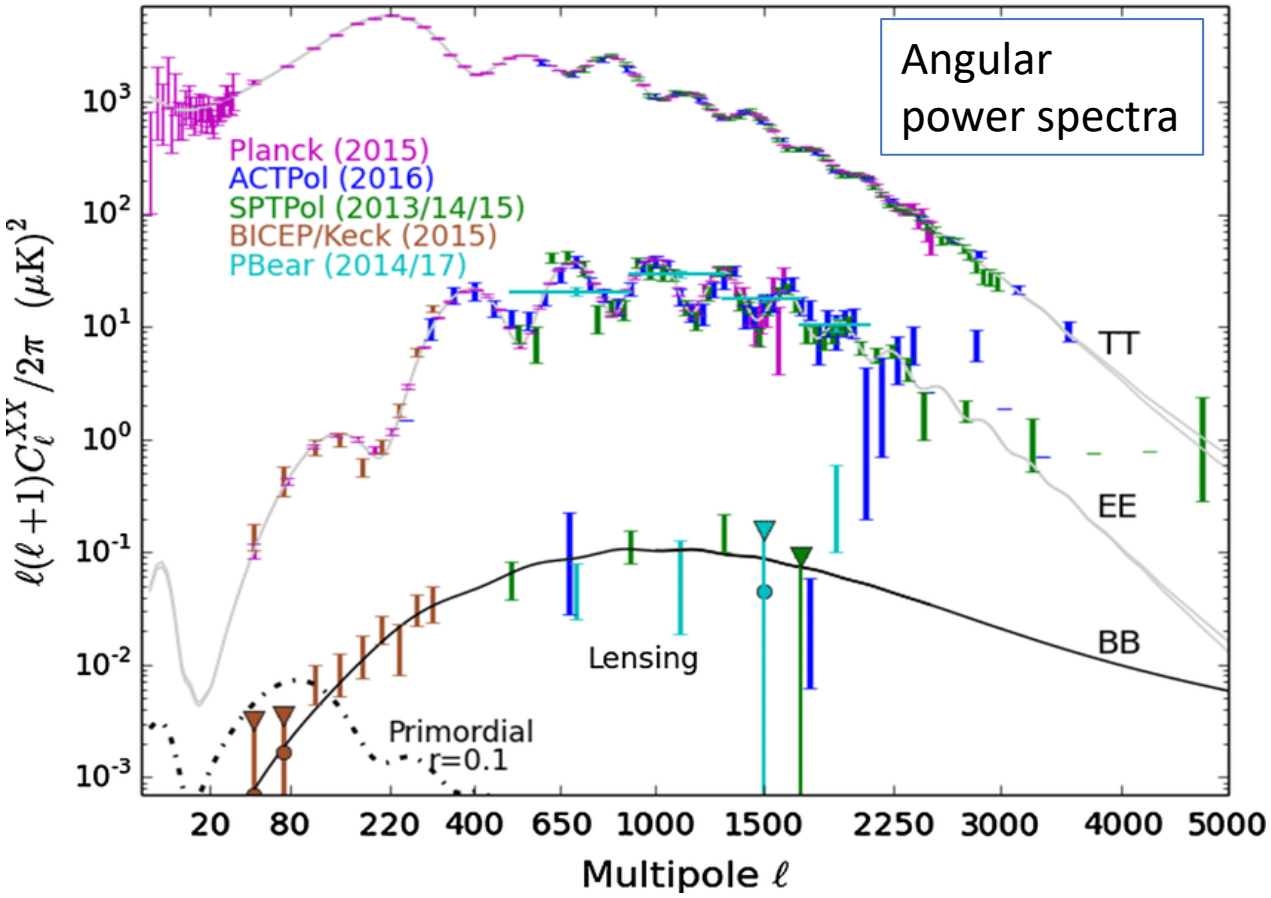

From the Planck survey

Polarization of the CMB

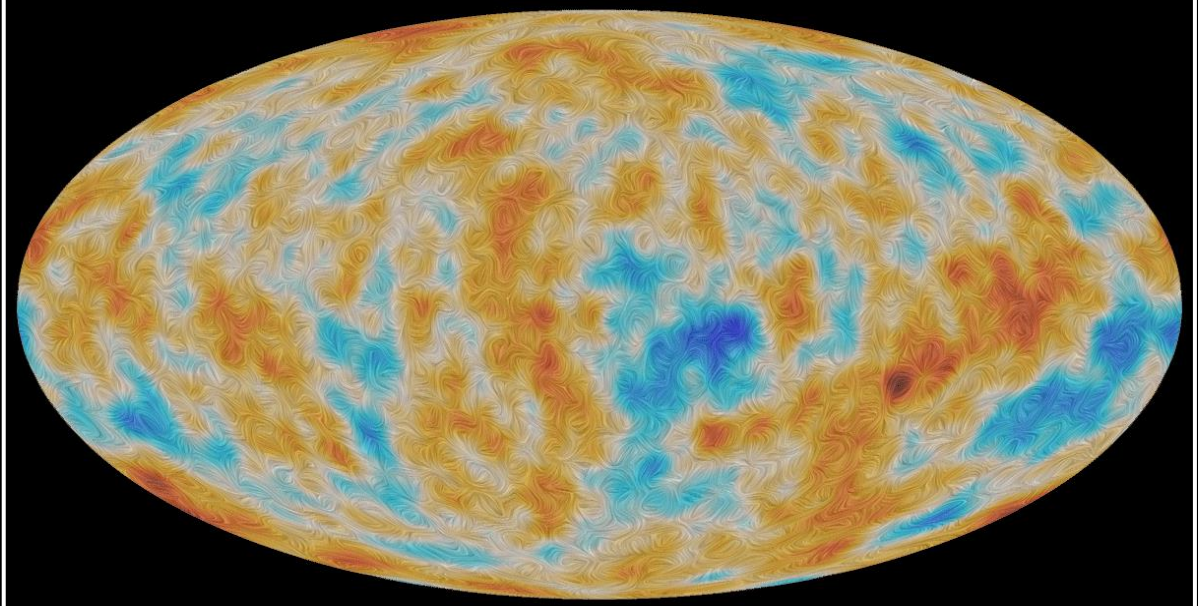

Polarization of ISD emission -> Galactic Magnetic Fields

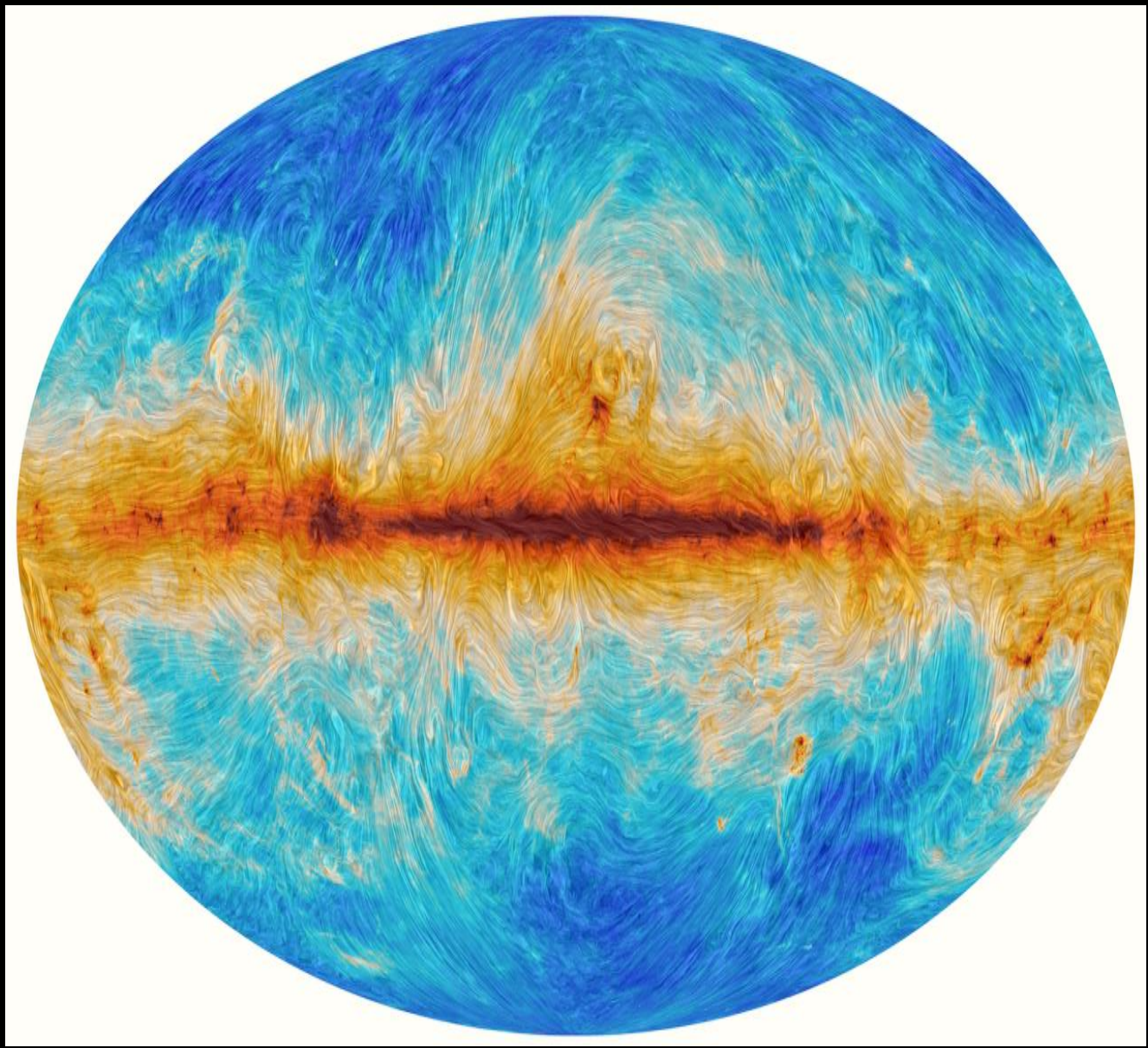

The CMB: a consolidated probe of the Universe

Tomorrow

Spectral distortions: (deviations from the 2.725K BB): a unique way to probe the very early universe and different pre-recombination phenomena

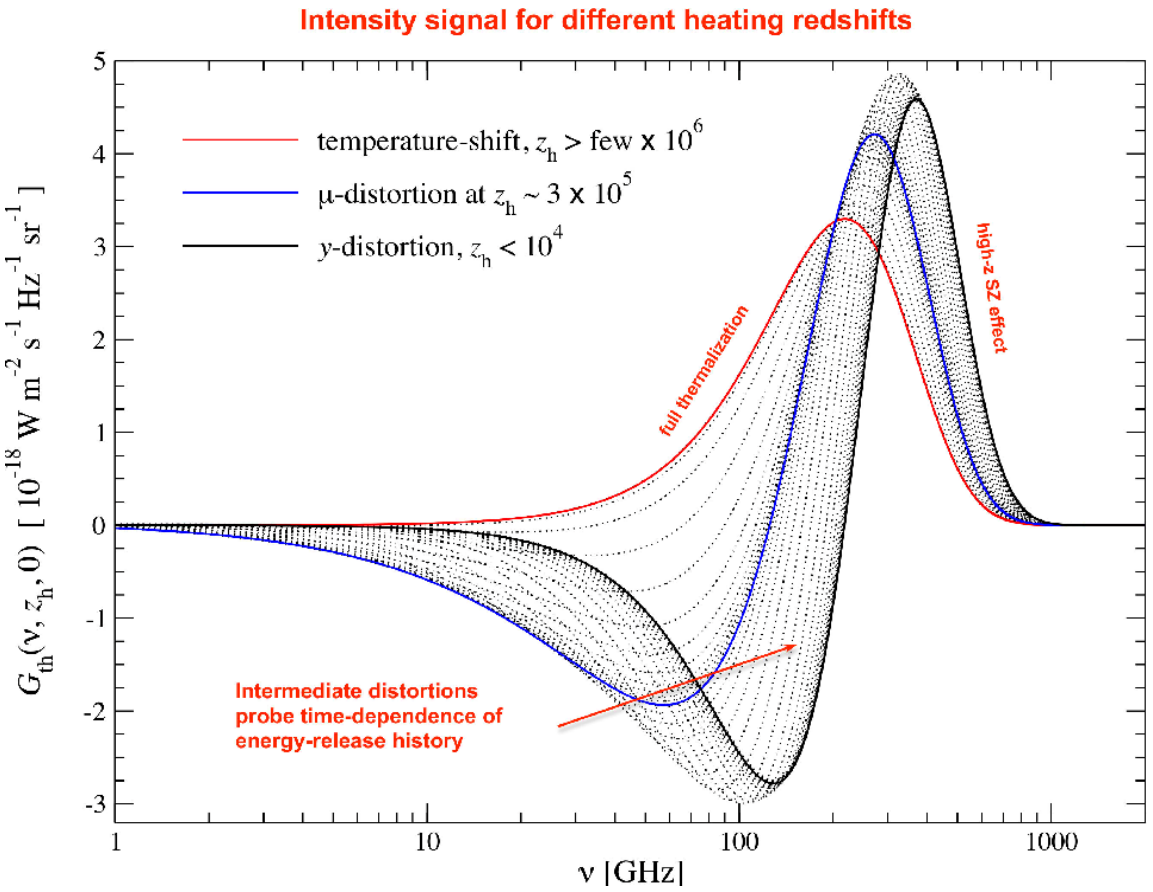

Polarization: Probing the very early universe (inflation) and physics at ultra high energy, with the **power spectrum of the B-mode, and a probe for cosmic magnetism.**

Polarized fraction **<< 1 ppm**

B-mode angular power spectra

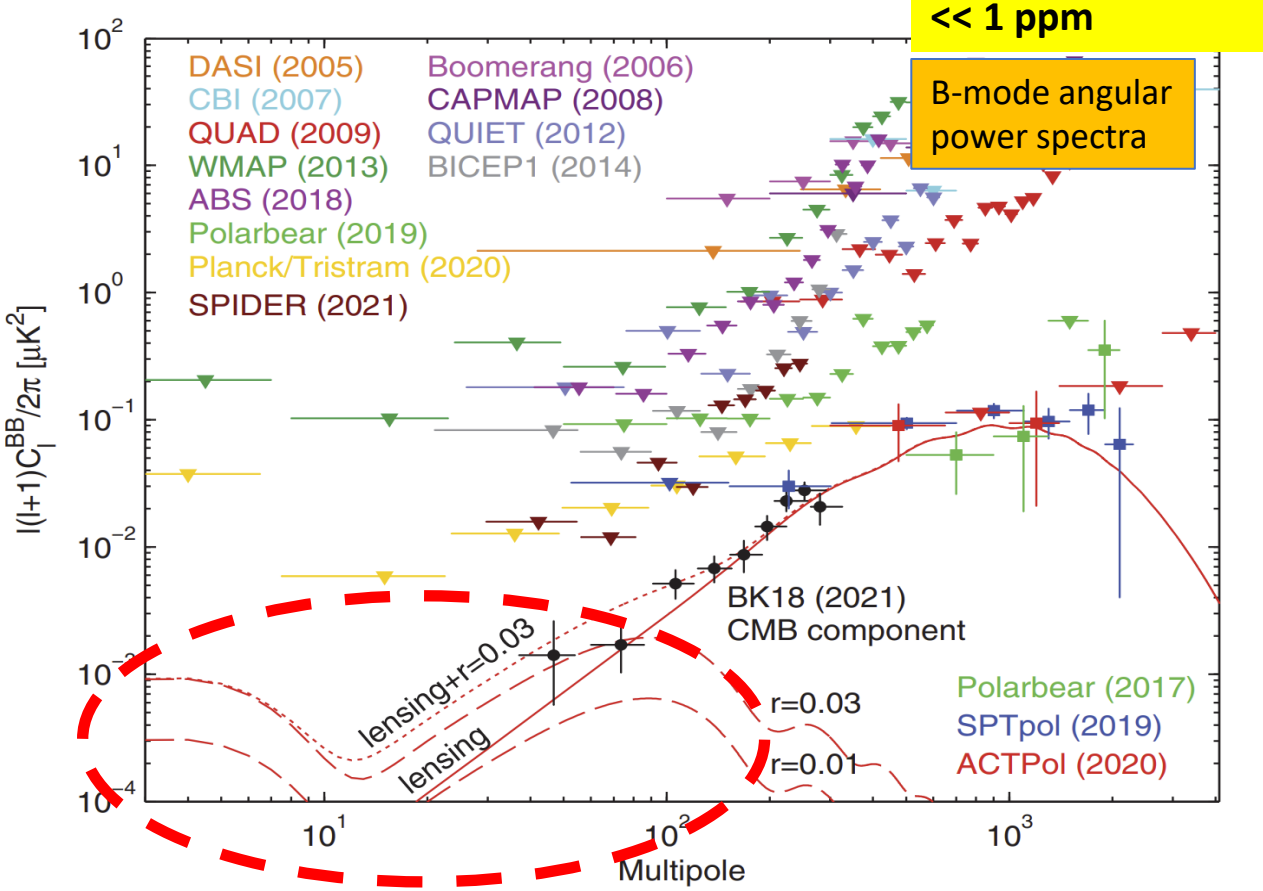

Modern CMB experiments

- How are CMB experiments carried out nowadays ? How are they evolving ?
- Current Stage-3 experiments aim at *CMB polarization* measurements with medium-sized collaborations, and arrays of order 10000 detectors.
  - Bicep Keck, QUIJOTE, GroundBIRD, LSPE-STRIP, … (ground, intermediate scales)
  - Polarbear, Simons Observatory, ACT, SPT, … (ground, smaller scales)
  - SPIDER, LSPE-SWIPE, Taurus, … (balloons)
- Smaller collaborations carry out measurements with non-standard configurations or with *different targets*. e.g. :
  - QUBIC – a bolometric interferometer for CMB polarization
  - OLIMPO – a balloon-borne telescope for Sunyaev-Zeldovich investigations at high frequency in clusters and filaments
  - MISTRAL – a W-band camera for high resolution Sunyaev-Zeldovich investigations in clusters and filaments
  - COSMO and BISOU – spectrometers for spectral distortions
- CMB *polarization* experiments in the 30s will be ***big science*** experiments, involving large collaborations and important resources (e.g. CMB-S4 on the ground, LiteBIRD in space). *Spectral distortions* experiments will hopefully converge in a medium-large space mission, as in ESA's Cosmic Voyage 2050
- To understand the experiments, it is good to start from the observable to be measured.

The *observable* :
brightness fluctuation for each multipole

$$\Delta T(\theta,\phi) = \sum_{\ell,m} a_{\ell m} Y_\ell^m(\theta,\phi)$$

$$c_\ell = \langle a_{\ell m}^2 \rangle$$

$$\langle \Delta T^2 \rangle = \frac{1}{4\pi}\sum_\ell \sigma_\ell^2 = \frac{1}{4\pi}\sum_\ell (2\ell+1) c_\ell$$

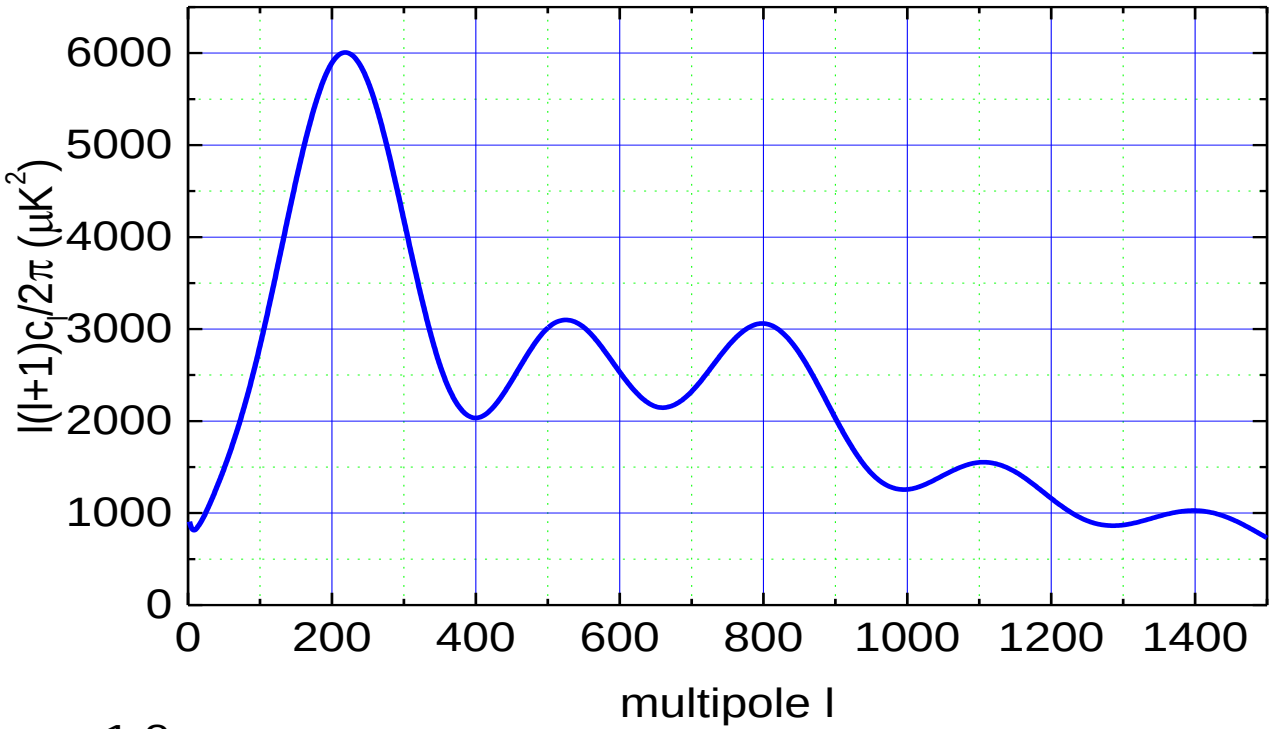

The *error* : cosmic variance and measurement noise

$$\Delta C_\ell = \sqrt{\frac{2}{(2\ell+1) f_{sky} \Delta\ell}} [C_\ell + N_\ell]$$

$$N_\ell = \frac{2(NET)^2 4\pi f_{sky}}{B_\ell^2 N_d t} \left[1 + \left[\frac{\ell}{\ell_k}\right]^{\alpha_k}\right]$$

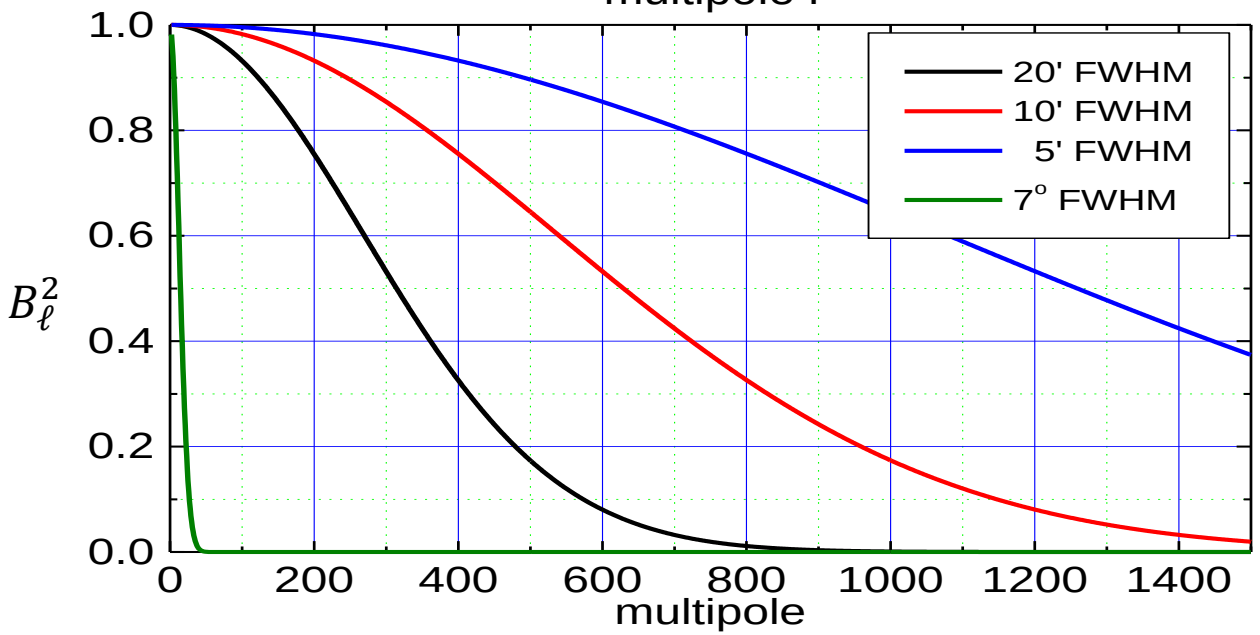

The *observable* :
rms brightness fluctuation for each multipole

$$\Delta T(\theta,\phi) = \sum_{\ell,m} a_{\ell m} Y_\ell^m(\theta,\phi)$$

$$c_\ell = \langle a_{\ell m}^2 \rangle$$

$$\langle \Delta T^2 \rangle = \frac{1}{4\pi}\sum_\ell \sigma_\ell^2 = \frac{1}{4\pi}\sum_\ell (2\ell+1)c_\ell$$

Plain unpolarized **anisotropy** power per multipole:

$$\sigma_{\ell,TT} = \frac{\sqrt{(2\ell+1)c_{\ell,TT}}}{T_{CMB}} \frac{xe^x}{e^x-1} B(\nu, T_{CMB}) \left[\frac{W}{cm^2 sr\ cm^{-1}}\right]$$

(no atmosphere, no foregrounds, no noise, no beam, no cosmic variance)

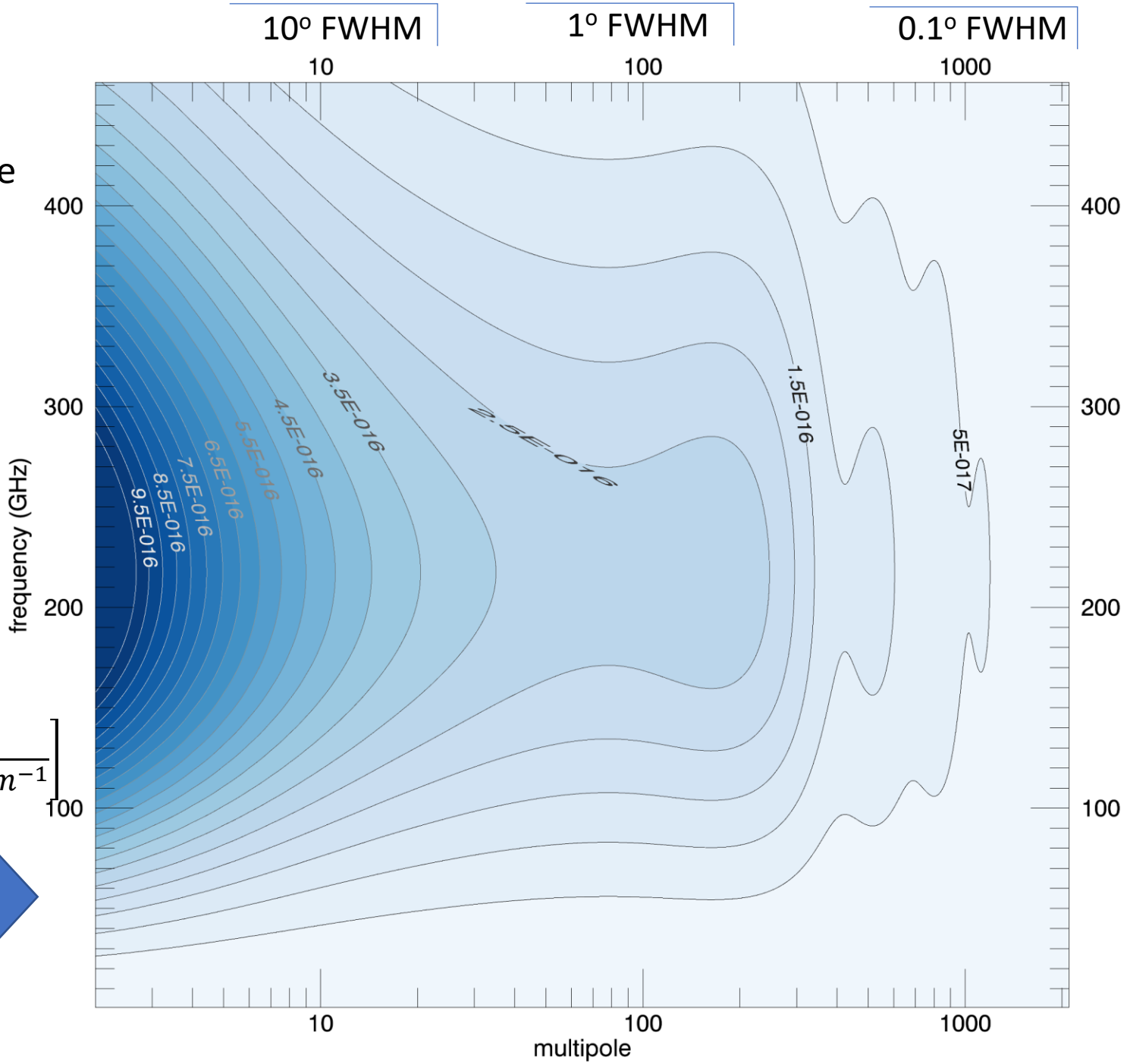

Plain **polarization** power

$$\sigma_{\ell,EE} = \frac{\sqrt{(2\ell+1)c_{\ell,EE}}}{T_{CMB}} \frac{xe^x}{e^x-1} B(\nu, T_{CMB}) \left[\frac{W}{cm^2 sr\ cm^{-1}}\right]$$

$$\sigma_{\ell,BB} = \frac{\sqrt{(2\ell+1)c_{\ell,BB}}}{T_{CMB}} \frac{xe^x}{e^x-1} B(\nu, T_{CMB}) \left[\frac{W}{cm^2 sr\ cm^{-1}}\right]$$

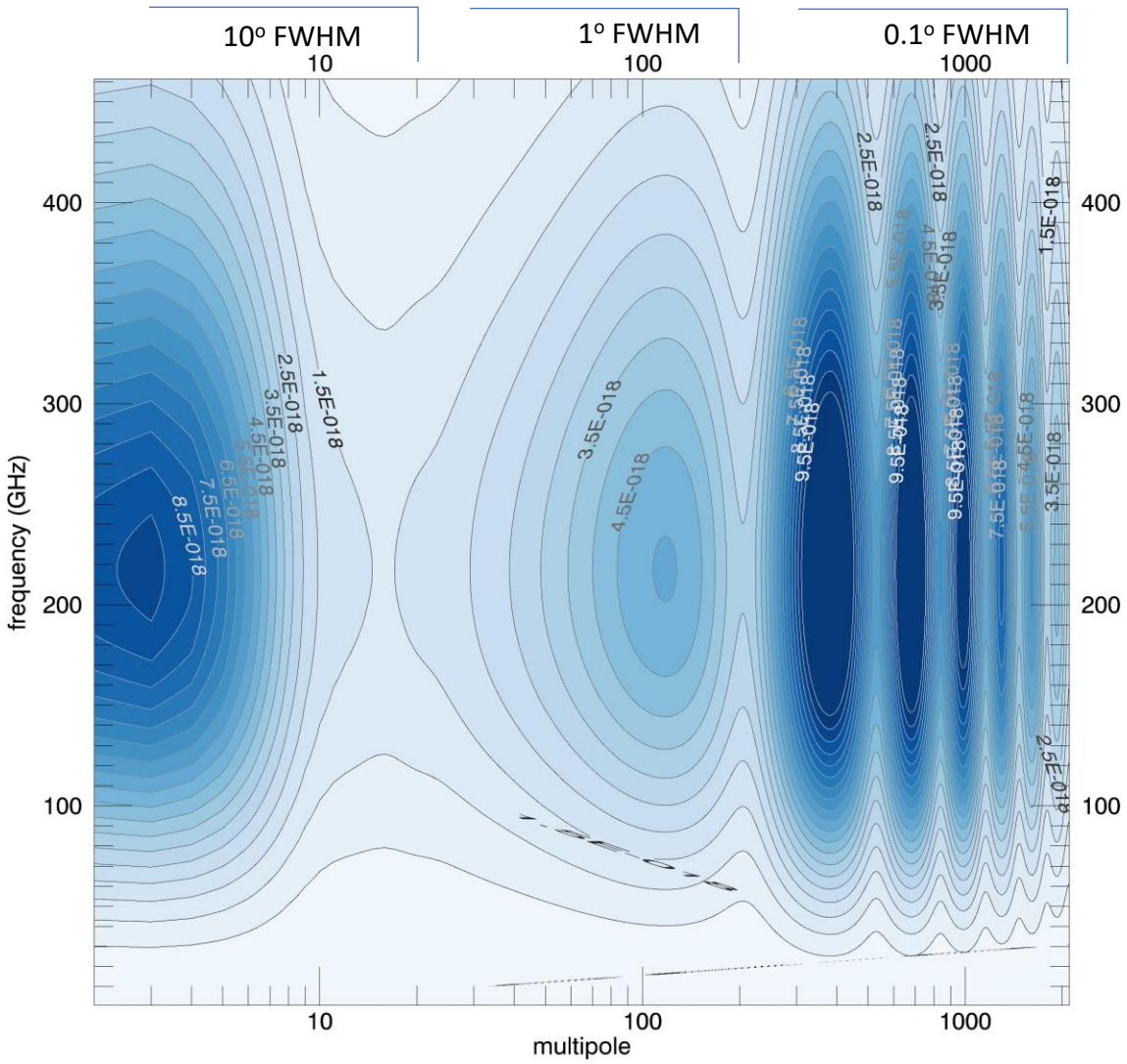

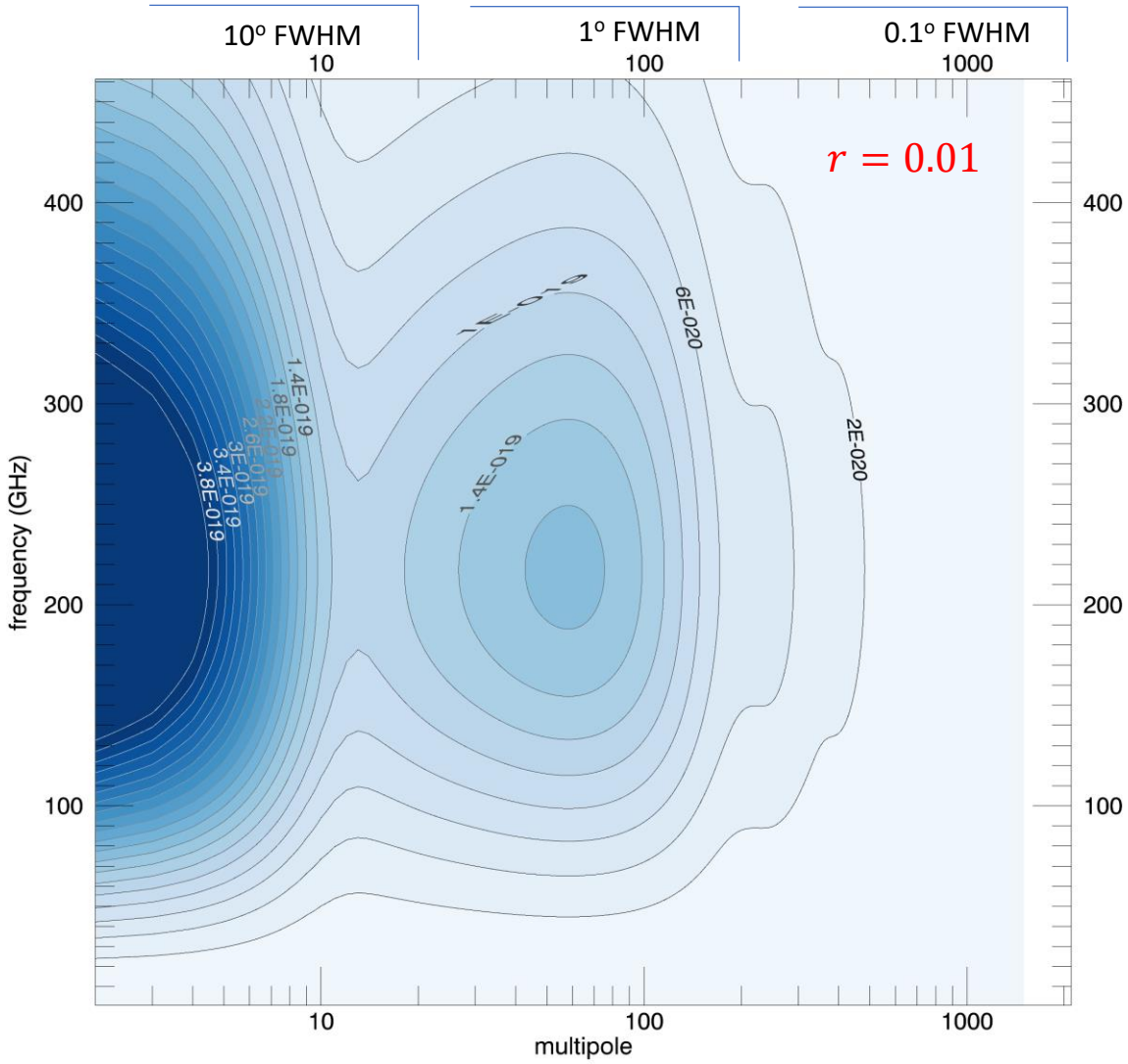

Effects of Earth's atmosphere

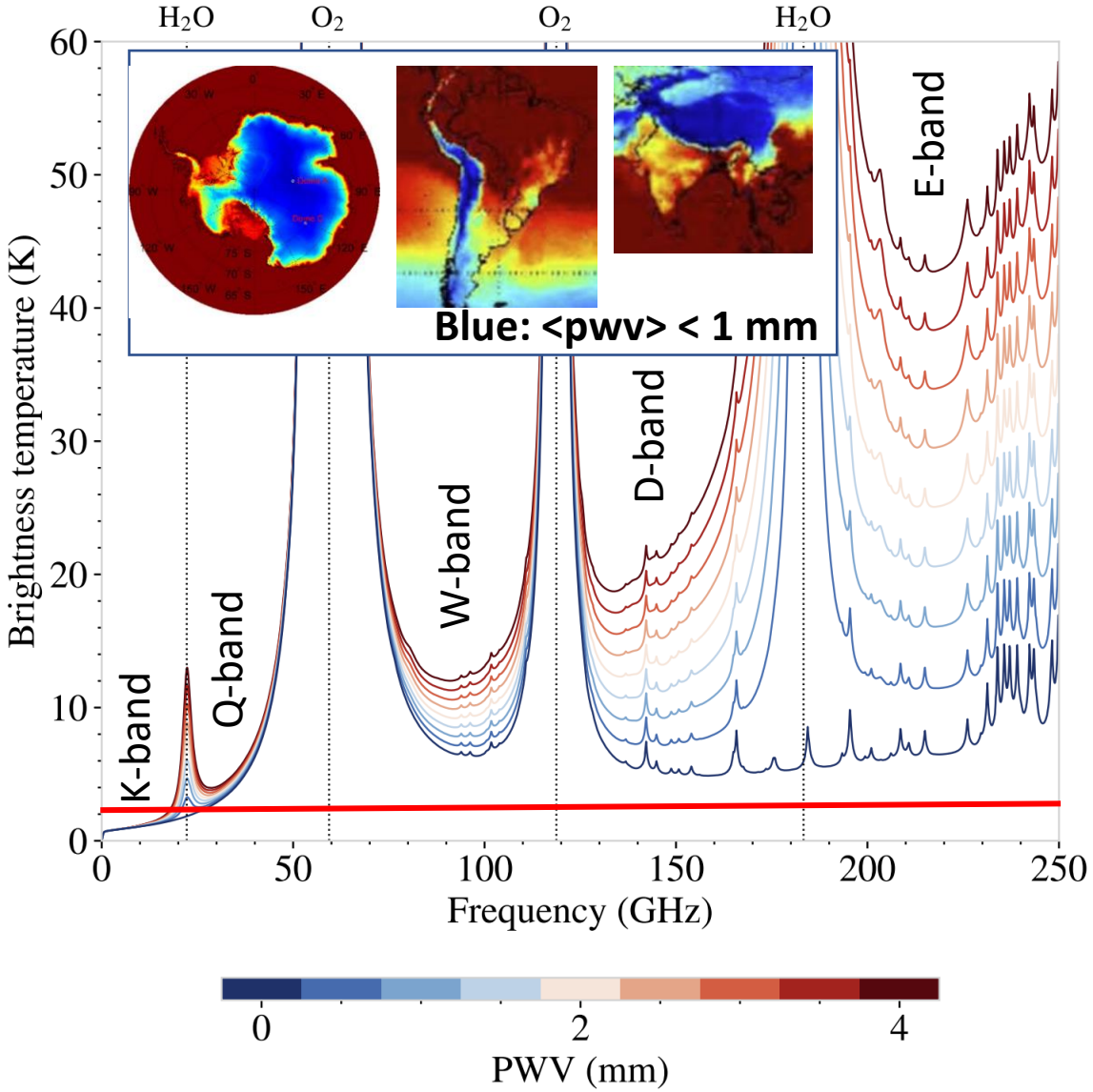

- Atmospheric emission in the best sites is a few K in the atmospheric windows corresponding to Q, W, D bands.
- We are interested to μK signals and the main issue will be the atmospheric fluctuations.
- These are due to quantum photon noise (subdominant) and to turbulence (1/f Kolmogorov).
- Once translated into multipoles, taking into account the scan strategy (typically azimuth scans), the angular part of atmospheric noise results in a $1/\ell$ like spectrum:

$$N_{\ell,atm} = A\left[1 + \left(\frac{\ell_o}{\ell}\right)^{\alpha}\right]$$

Adapted from Morris+ PRD **105**, 042004 (2022) and Y. Suen+ IEEE T. TeraHz Sci. Tech., **4**, 86,(2014)

rms brightness fluctuation for each multipole
Through atmospheric ***transmission*** (excellent site)

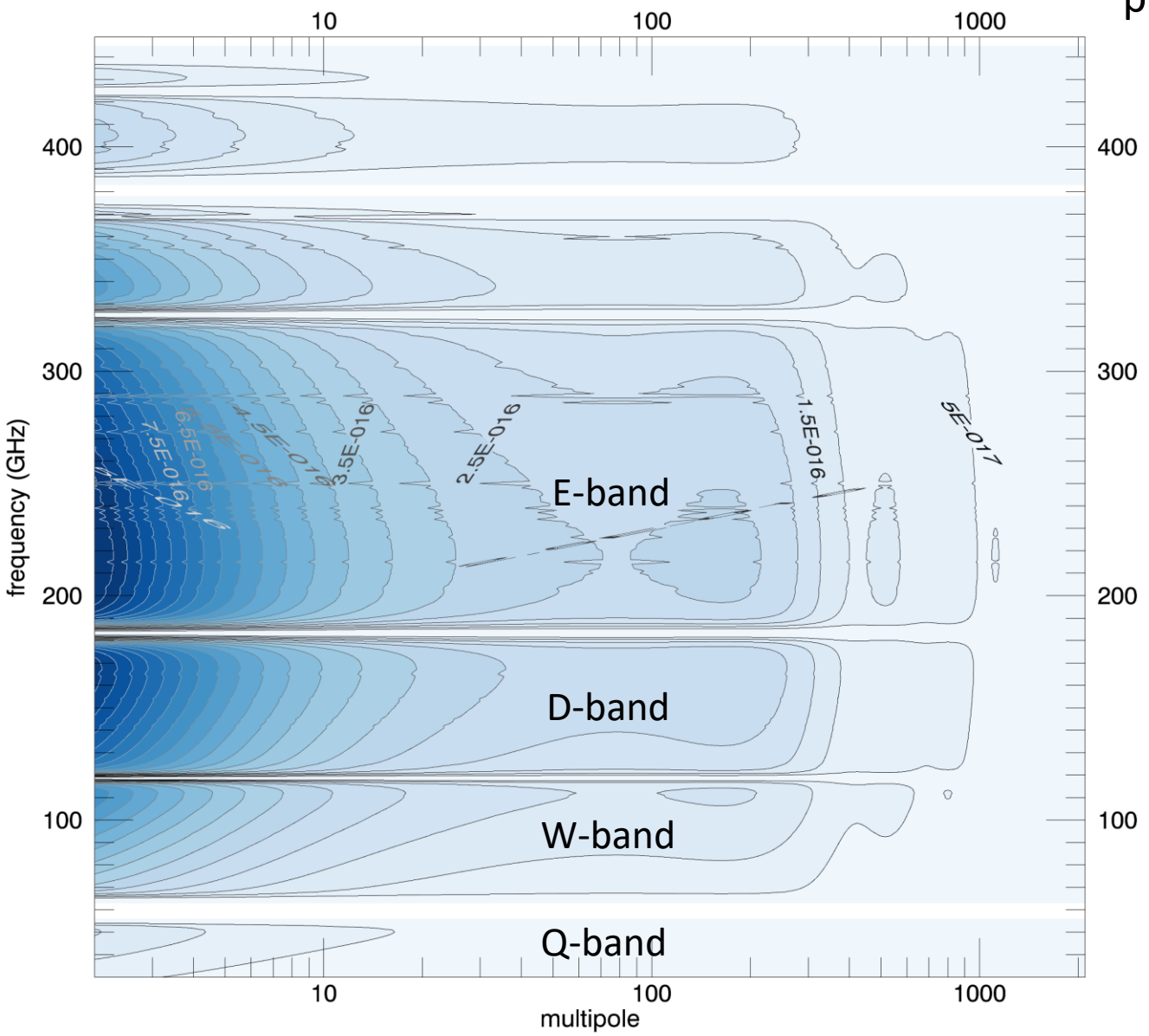

atmospheric brightness fluctuation for each multipole
In log scale (added **noise,** much more important than partial transmission).

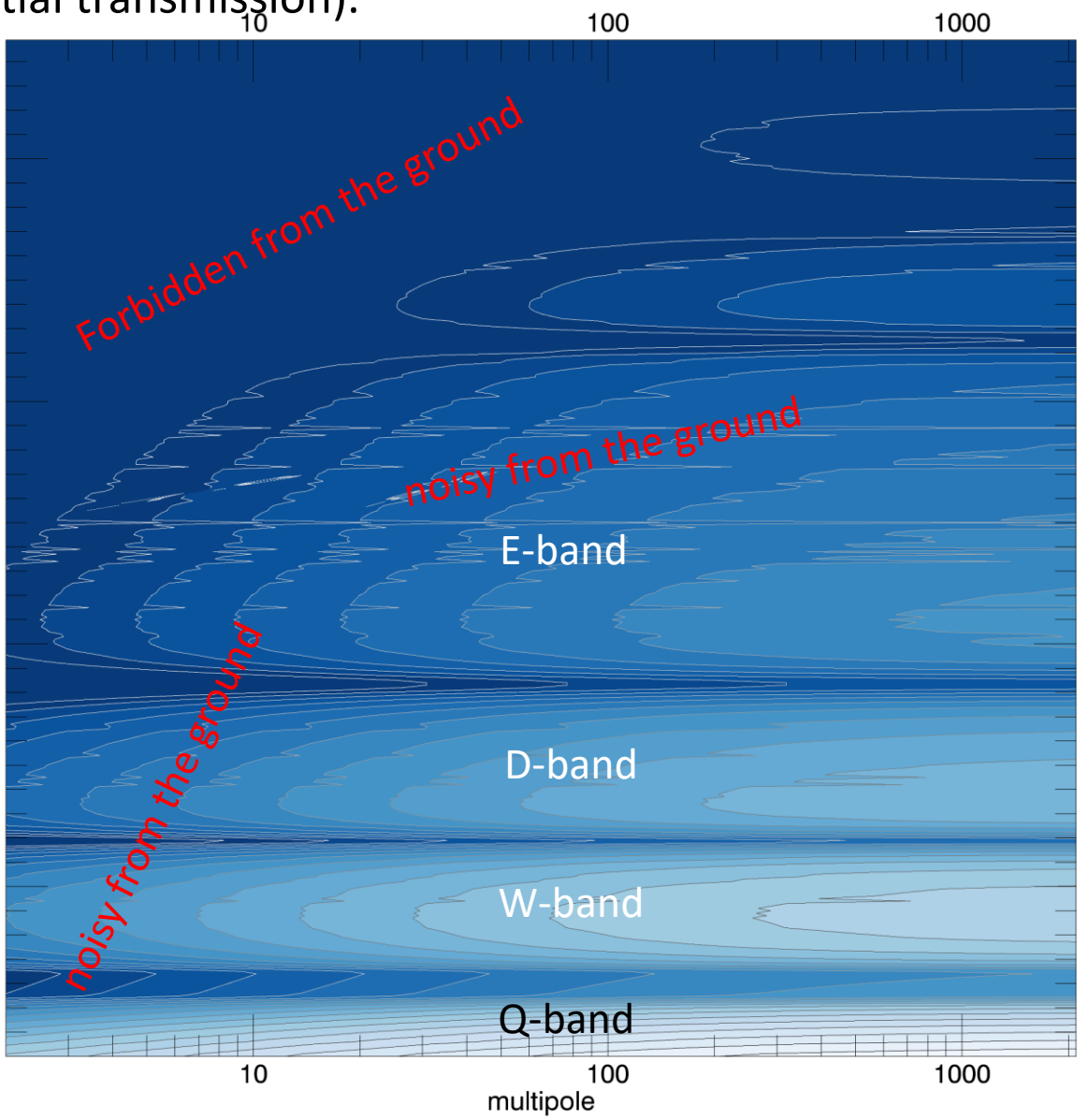

Effects of Galactic foregrounds

- Interstellar dust emission and Galactic synchrotron emission are polarized.
- Their anisotropic polarization signals dominate over CMB polarization signals.
- Their spectra (vs wavelength) are very different from the spectrum of CMB polarization.

Planck 2015 results X. Diffuse component separation: Foreground maps, A&A 594, A10 (2016)

unpolarized

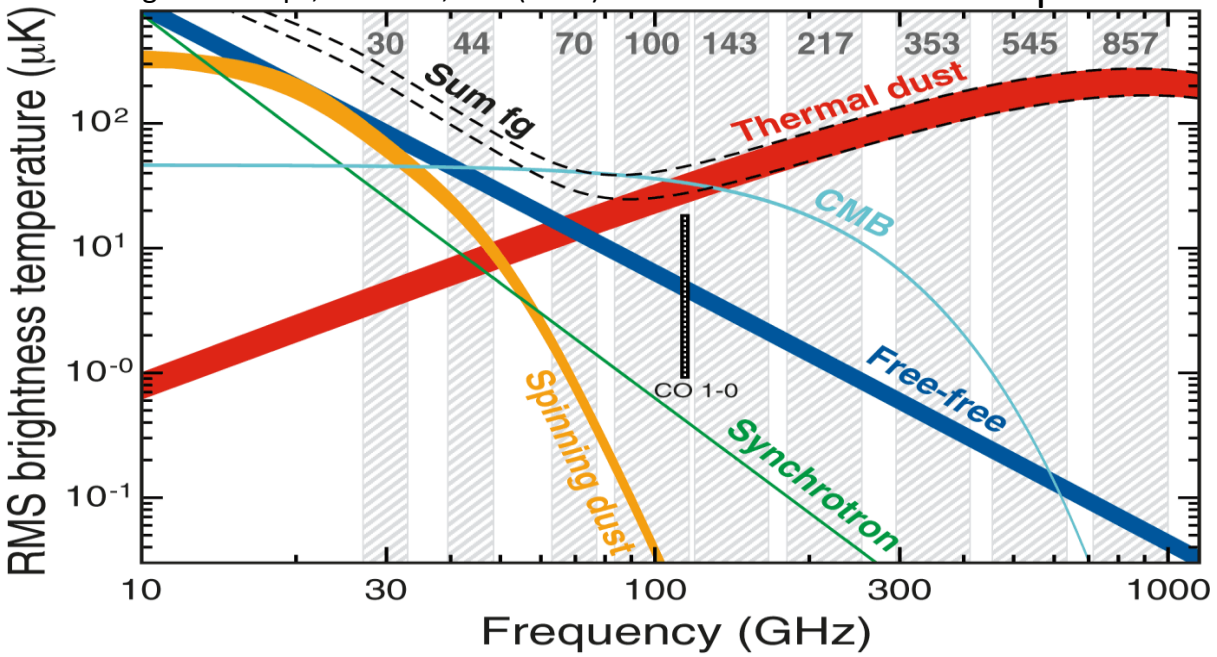

Planck 2018 results. IV. Diffuse component separation, A&A 641, A4 (2020)

Polarized EE

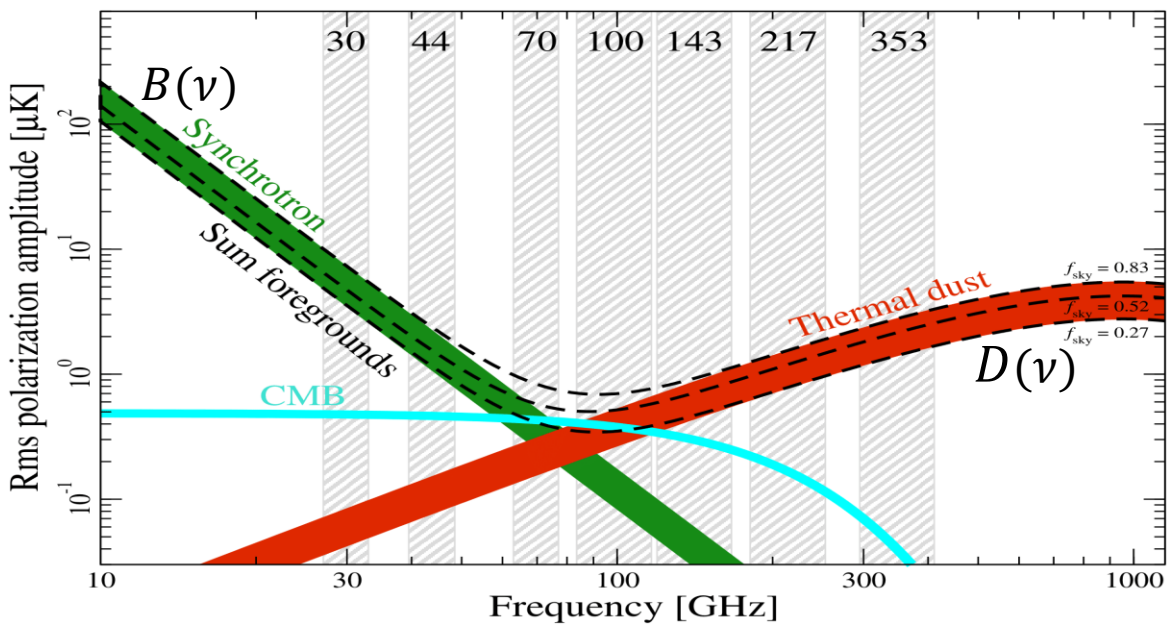

- Both foregrounds feature $1/\ell$–like angular spectra (see e.g. Choudhuri+ MNRAS 470, L11 (2017) and Planck intermediate results XXX, A&A 586, A133 (2016)) with

$$C_{\ell,synch} = B^2(\nu)\left(\frac{\ell_s}{\ell}\right)^{\beta} \qquad C_{\ell,dust} = D^2(\nu)\left(\frac{\ell_d}{\ell}\right)^{\delta}$$

- **Multiband** measurements are key for components separation (see https://lambda.gsfc.nasa.gov/toolbox/comp_separation.html)

BB polarized rms brightness fluctuation (r=0.01)

$$\sigma_{\ell,BB} = \frac{\sqrt{(2\ell+1)c_{\ell,BB}}}{T_{CMB}} \frac{xe^x}{e^x-1} B(\nu, T_{CMB}) \left[\frac{W}{cm^2 sr\ cm^{-1}}\right]$$

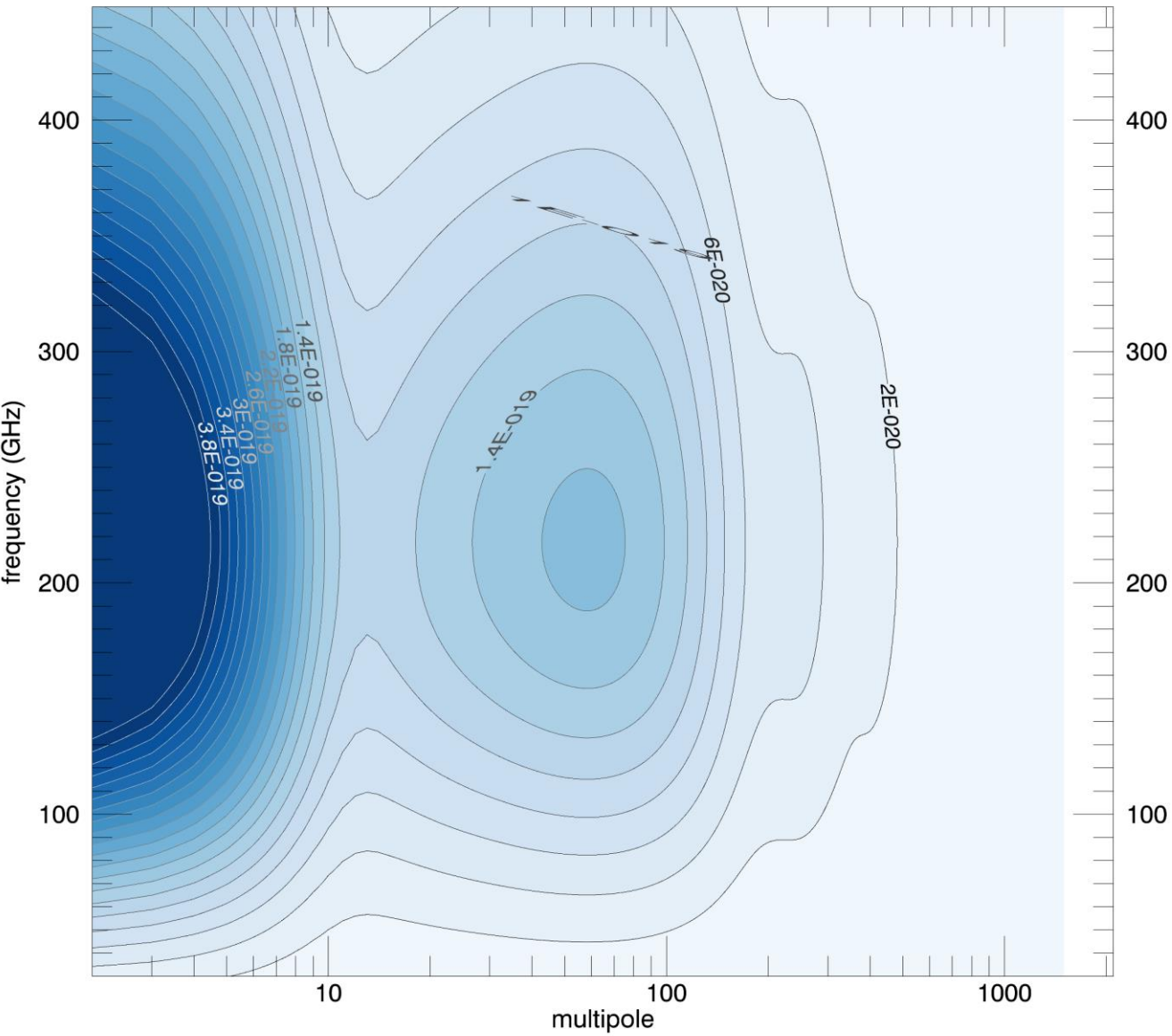

Rms brightness fluctuation from Galactic foregrounds

$$\sigma_{\ell,fg} = \sqrt{(2\ell+1)\left[c_{\ell,synch}B^2(\nu) + c_{\ell,dust}D^2(\nu)\right]} \left[\frac{W}{cm^2 sr\ cm^{-1}}\right]$$

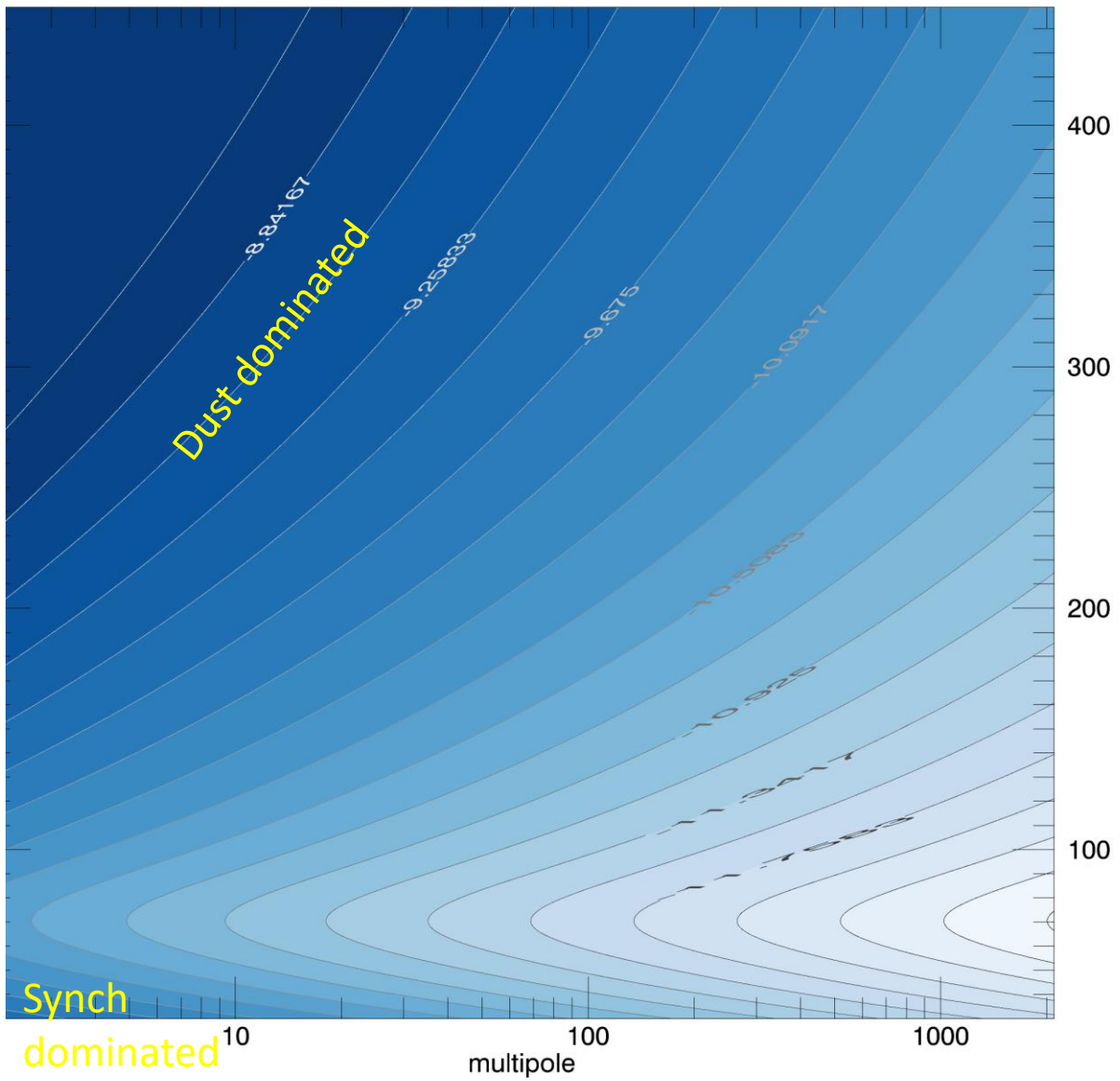

Microwave Detector Arrays Technology

- Error in the measurement of each sky pixel in a sky map :

$$\sigma_{pix} = \frac{NET}{\sqrt{t_{pix}}} = \frac{NET}{\sqrt{t_{surv} N_{det}/N_{pix}}} = \frac{NET}{\sqrt{t_{surv}}} \sqrt{\frac{4\pi f_{sky}}{N_{det}\Omega_{pix}}}$$

- Survey depth $\mathrm{w} = \sigma_{pix}\sqrt{\Omega_{pix}} = \frac{NET}{\sqrt{t_{surv}}} \sqrt{\frac{4\pi f_{sky}}{N_{det}}}$ usually in $\mu K \cdot arcmin$
- Required survey depth: order of 2 $\mu K \cdot$ arcmin for "final" CMB polarization surveys
- This implies N_{det}=2000 for a 3 years long full-sky survey in polarization, with the best available NET, of the order of 50 $\mu K\sqrt{s}$.
- Multifrequency coverage for components separation requirements boost this number to larger values (> 10000)
- **Large-format arrays** of microwave detectors are required, as well as large-throughput, low aberration optical systems (telescopes) to feed the detector array and obtain the necessary Ω_{pix} resolution.
- This excludes – *de facto* – coherent detectors, and favors TES bolometers and Kinetic Inductance Detectors, which can be easily replicated in large arrays, **but work best at *f* > 100GHz**.

Detectors for the CMB

- As of today, there are three ways to detect very-low energy CMB photons:
  - *Coherent detectors*, where the EM field produces an AC current in an antenna. The AC current is **amplified** coherently before rectification and detection. They are sensitive to amplitude and phase of the EM field. High-frequency extension of *radioastronomy* techniques, do not work well above 100 GHz. ***High cost per pixel. High power per pixel.***
  - *Thermal detectors*, integrating the thermal energy of a large number of absorbed photons (bolometers, **TESs**). They are sensitive to the amplitude of the EM field. Low-frequency extension of techniques used in *infrared astronomy*. Does not work well below 40 GHz. ***Low cost per pixel. Low power per pixel. Complex fabrication.***
  - *Quantum detectors*, exploiting low-binding-energy quantum systems which are affected by the energy of CMB quanta (**KIDs**). Recent development, exploiting *superconductivity effects*. They do not work below 70 GHz (unless they are used as thermometers in a bolometric detector: TKIDs). ***Very low cost per pixel. Low power per pixel. Easy fabrication.***

Bolometers

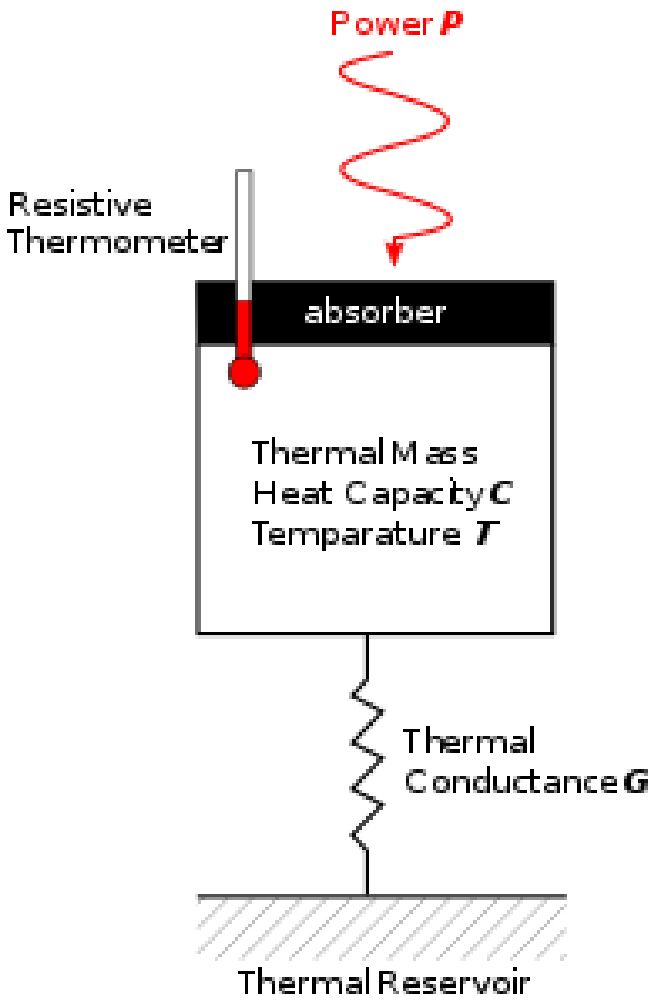

- A bolometer is a thermal sensor of EM radiation.
- A *radiation absorber* is thermally insulated from a *thermal reservoir*, and heats up when illuminated by radiation.
- A *thermistor* (a resistor with steep temperature dependance of the resistance) is used to measure the temperature change, and infer the absorbed power.
- A bolometer is able to absorb a wide range of wavelengths (depending on the technology of the absorber) and can be optimized for operation from radio frequencies to X-rays. They are optimal detectors in the mm/sub-mm/FIR range.
- Originally handcrafted suspending a tiny absorber square on thin nylon wires, have been modified in the last 3 decades to automate the fabrication using Si micromachining. BOOMERanG & Planck used cavity located spider webs with glued semiconductor thermistors. Now are fully micromachined, with a TES thermistor evaporated on the suspended Si island. TES provide important electrothermal feedback advantages (R vs τ)
- Typically background limited detectors (intrinsic noise < radiation noise) even in space (Planck, 30K mirror in L2).

Antenna-coupled bolometers

- Radiation is collected by a suitable (planar) antenna, and transferred via suitable waveguides (e.g. coplanar) to a matched resistor, where is dissipated.
- The resistor is placed on a thermally insulated island, and its temperature is sensed by a suitable thermistor (usually a superconducting Transition Edge Sensor - TES)
- All this is built **on a Si wafer**, using advanced microfabrication technology, **and can be replicated to obtain large-format detector arrays.** ***BOOST of the MAPPING SPEED.***
- Currently moving from laboratory developments to industrial production.

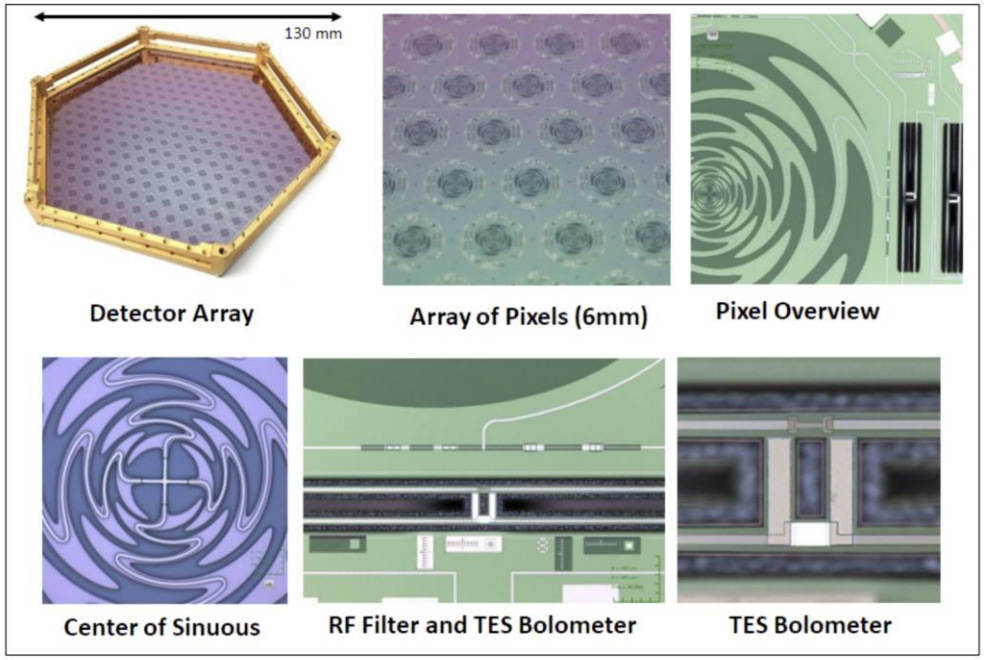

Detector Array Co-Fabricated with HYPRES

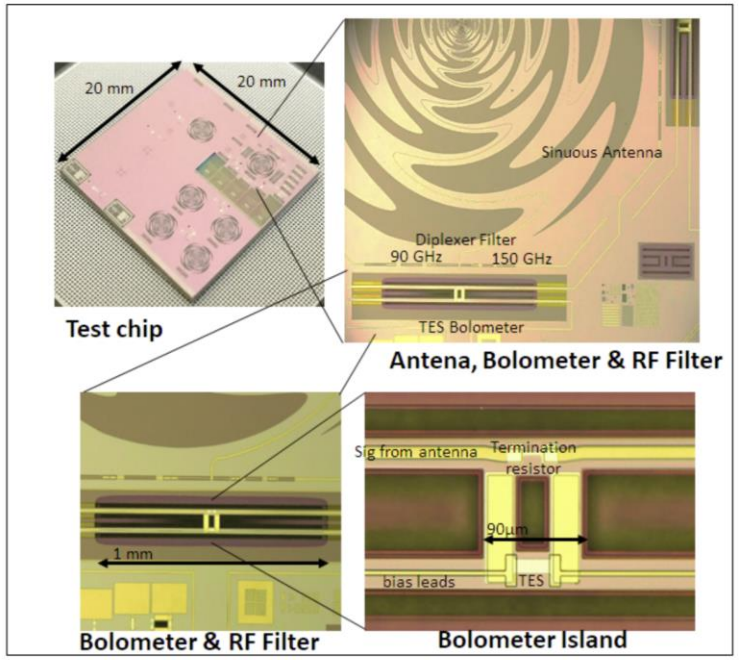

Prototype Chip Fabricated at StarCRYO

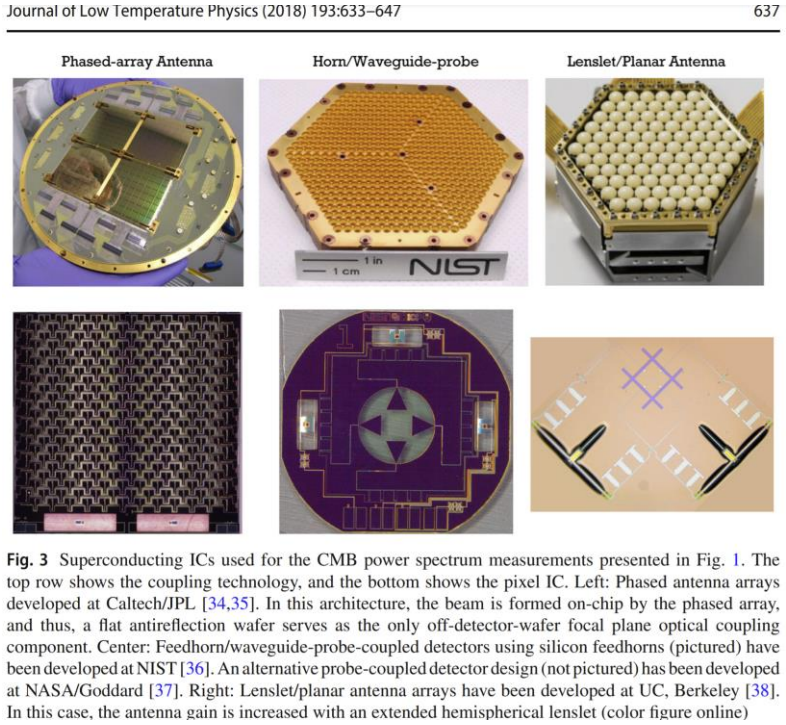

Fig. 3 Superconducting ICs used for the CMB power spectrum measurements presented in Fig. 1. The top row shows the coupling technology, and the bottom shows the pixel IC. Left: Phased antenna arrays developed at Caltech/JPL [34,35]. In this architecture, the beam is formed on-chip by the phased array, and thus, a flat antireflection wafer serves as the only off-detector-wafer focal plane optical coupling component. Center: Feedhorn/waveguide-probe-coupled detectors using silicon feedhorns (pictured) have been developed at NIST [36]. An alternative probe-coupled detector design (not pictured) has been developed at NASA/Goddard [37]. Right: Lenslet/planar antenna arrays have been developed at UC, Berkeley [38]. In this case, the antenna gain is increased with an extended hemispherical lenslet (color figure online)

Figure from https://export.arxiv.org/pdf/1801.06991

Antenna coupled *multichroic* pixels to increase the *density* of bolometers in the focal plane

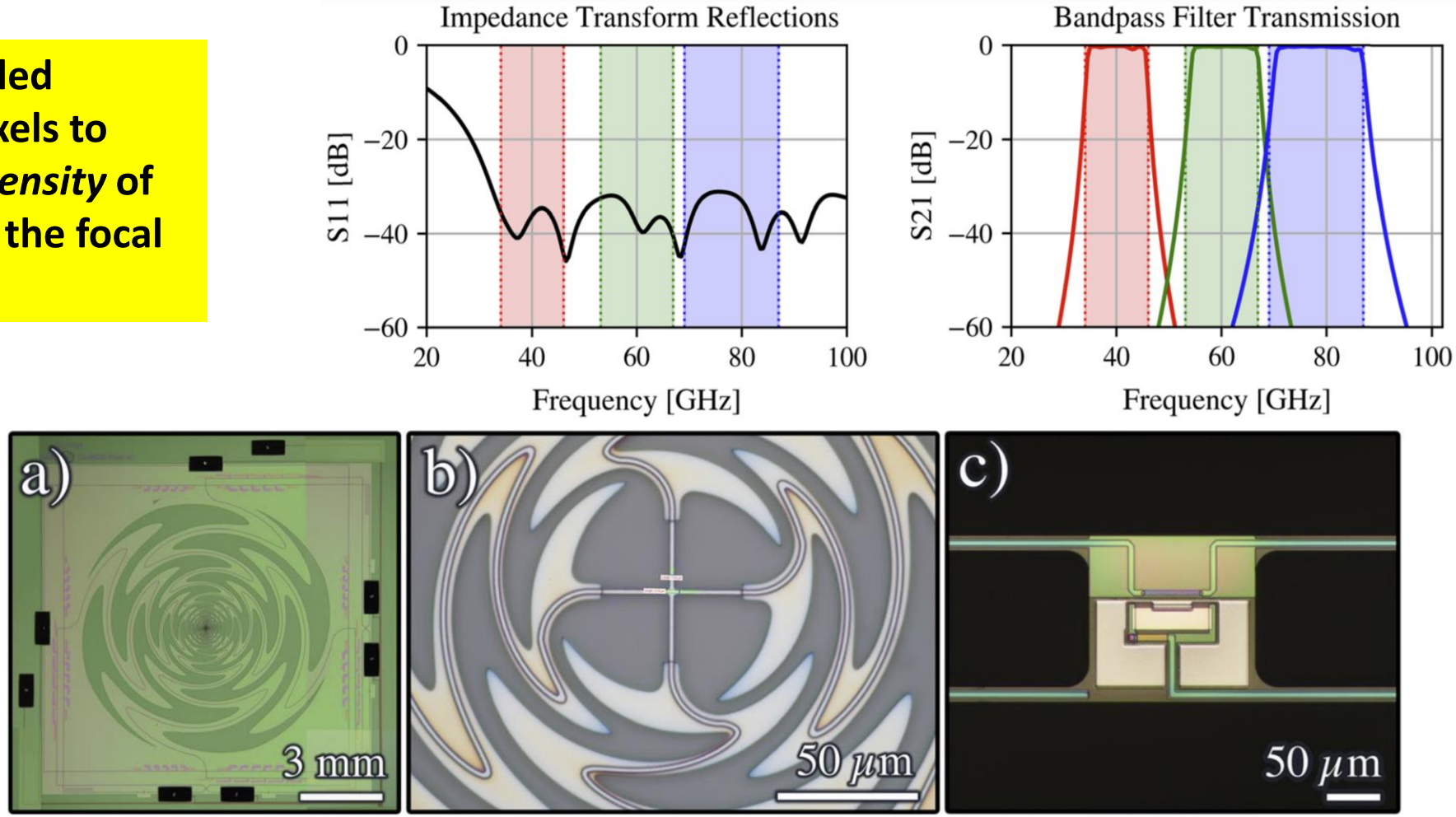

Fig. 3 **a** LF-1 prototype pixel with sinuous antenna in the center, the microstrip transmission line is routed between antenna arms, bandpass filters with mitered stubs surround the antenna, and the bolometers appear as rectangles. **b** Antenna feedline coupling with line widths at the center of 600 ± 50 nm. **c** The bolometer island with TES in the center, thermal ballast on the lower half of the island, readout wires routed to the lower right split the ballast, and antenna feedlines in the upper left and right lead to the load resistor above the TES (Color figure online)

G.C. Jaehnig *et al.* *J.Low Temp.Phys.* 199, 646-653 (2020)

The alternative for large arrays :

Kinetic Inductance Detectors (KIDs)

- Each sensor/pixel is a planar, superconducting *LC* resonator, where the number of quasiparticles is modulated by the incoming CMB photons, in turn modulating the resonance frequency.
- Intrinsically multiplexable; order of 10^2-10^3 pixels read with a single coaxial cable
- *Extremely simple cold electronics:* one single LNA can be used for 10^2-10^3 pixels. No SQUIDs. The rest of the readout is warm.
- *Ease of fabrication:* one single layer of material is needed.
- *Very flexible:* different materials and geometries can be chosen to tune detectors to specific needs.
- *Very robust:* no suspended islands, materials are all suitable for satellite and space missions.

TES

Deployed TES ARRAY (~ 2000 Detectors)
- 1000's wire bonds
- 1000's SQUID amplifiers
- hundreds of additional SC components
- dozens of cables

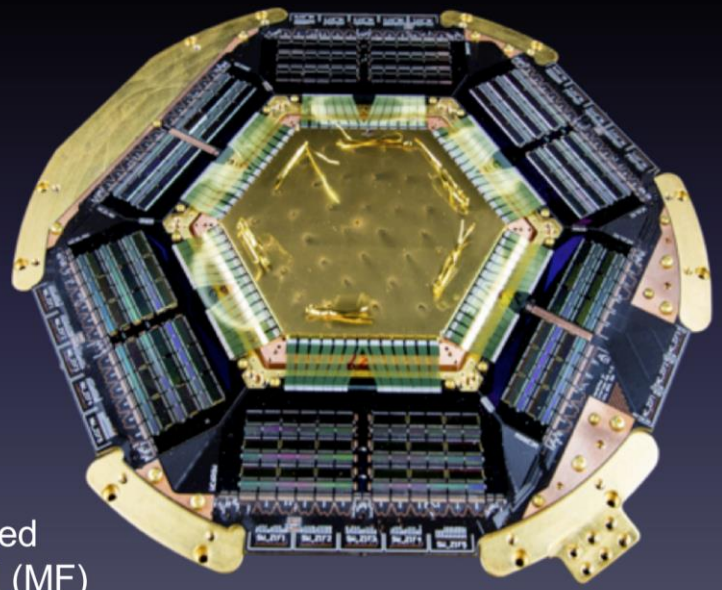

Advanced ACTPol (MF)

(Shown at same scale)

MKID

Integrated readout
e.g. Toltec MKID (4000 detectors)
- 14 wire bonds
- 14 Coax cables
- 7 LNAs (at 4K stage)

Toltec 1.1 mm

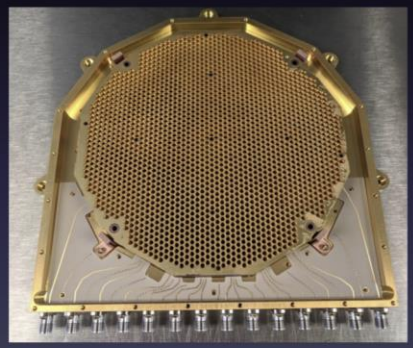

KIDs arrays recently qualified in near space

Kinetic Inductance Detectors for the OLIMPO experiment: in-flight operation and performance

S. Masi[1,2], P. de Bernardis[1,2], A. Paiella[1,2], F. Piacentini[1,2], L. Lamagna[1,2], A. Coppolecchia[1,2], P.A.R. Ade[3], E.S. Battistelli[1,2], M.G. Castellano[4], I. Colantoni[4,5] + Show full author list

Published 1 July 2019 • © 2019 IOP Publishing Ltd and Sissa Medialab

Journal of Cosmology and Astroparticle Physics, Volume 2019, July 2019

Citation S. Masi *et al* JCAP07(2019)003

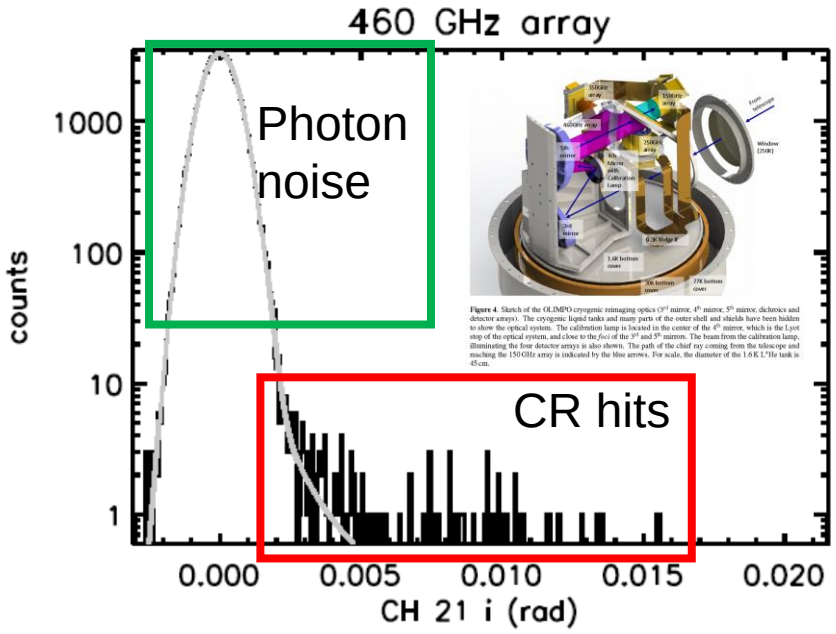

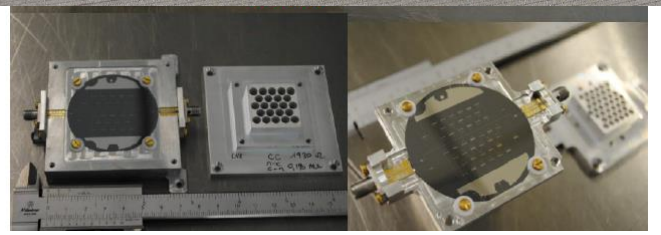

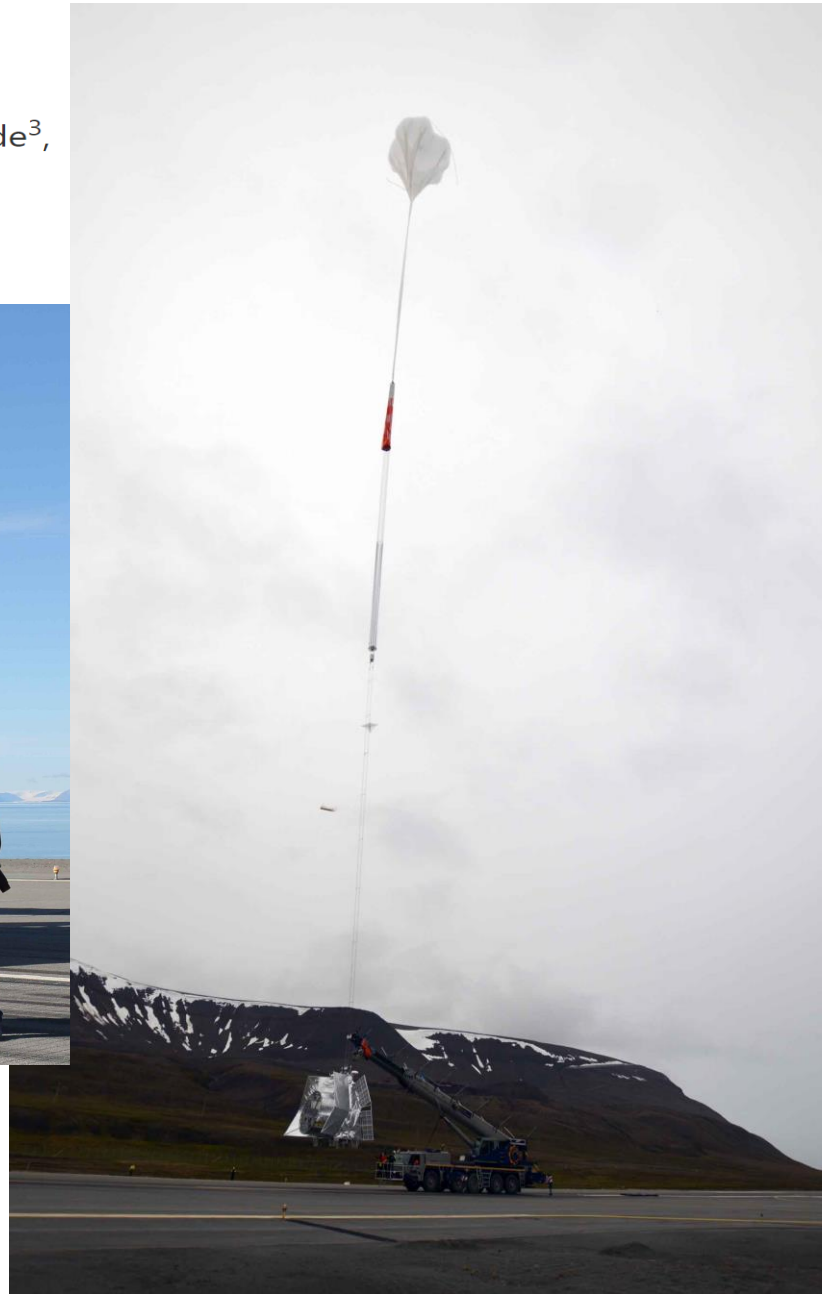

- Given the properties of the observable(s), of the foregrounds, and of the noise (detector and atmosphere), it is not surprising that current ground-based Stage-3 experiments aimed at B-mode CMB polarization exploit mostly the region ℓ=50-1000 and f>90 GHz.

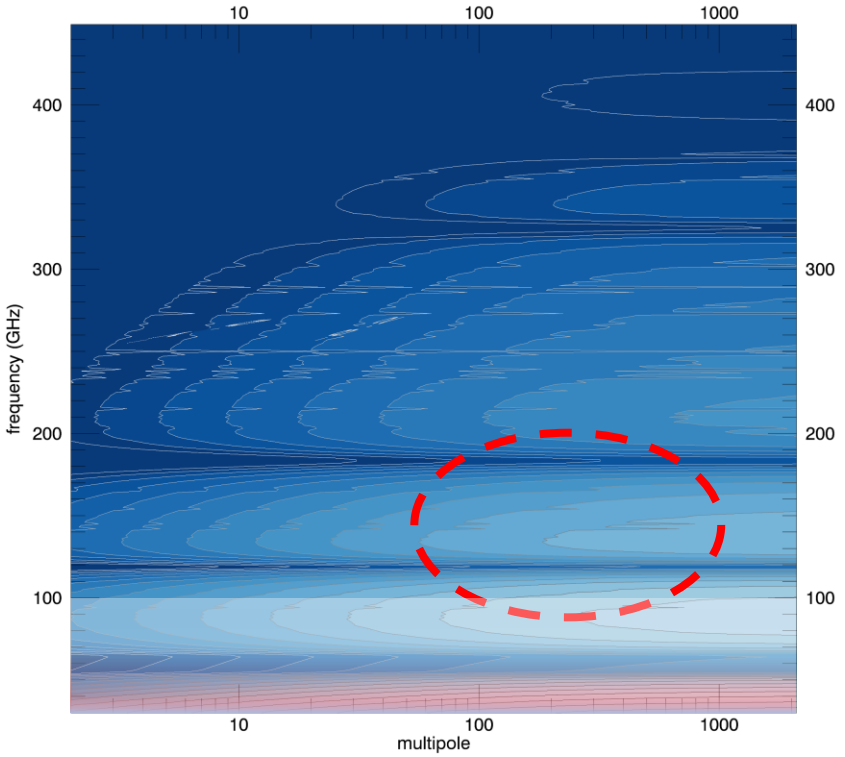

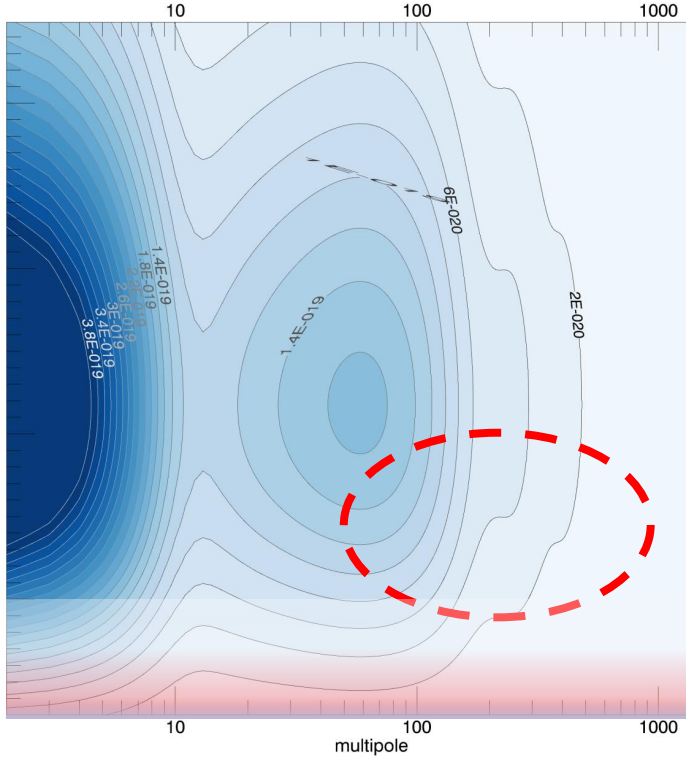

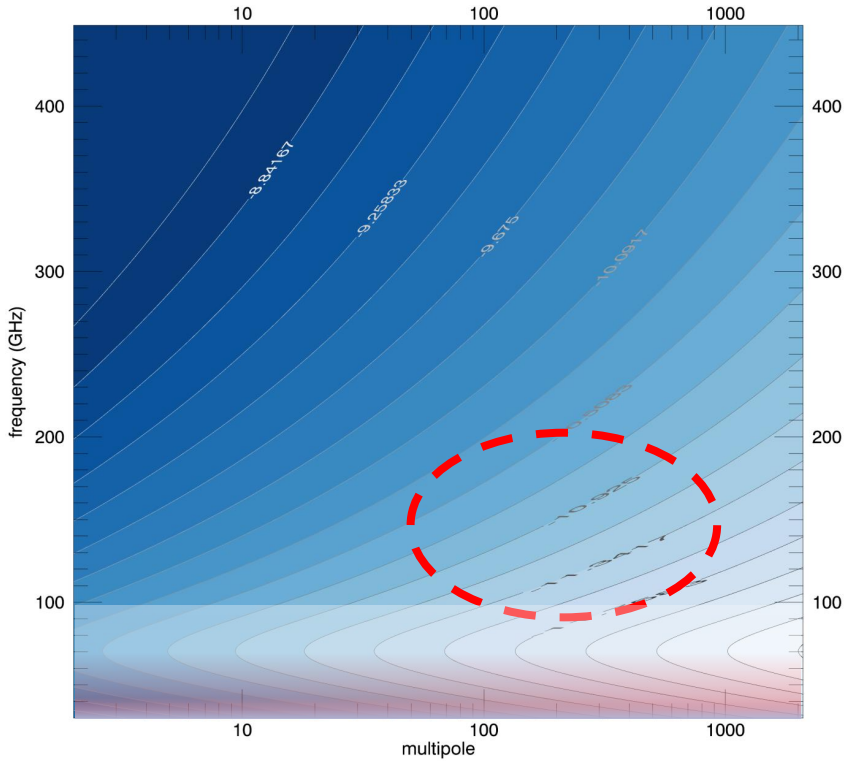

- Given the properties of the observable(s), of the foregrounds, and of the noise (detector and atmosphere), it is not surprising that current ground-based Stage-3 experiments aimed at B-mode CMB polarization exploit mostly the region ℓ=50-1000 and f>100 GHz.

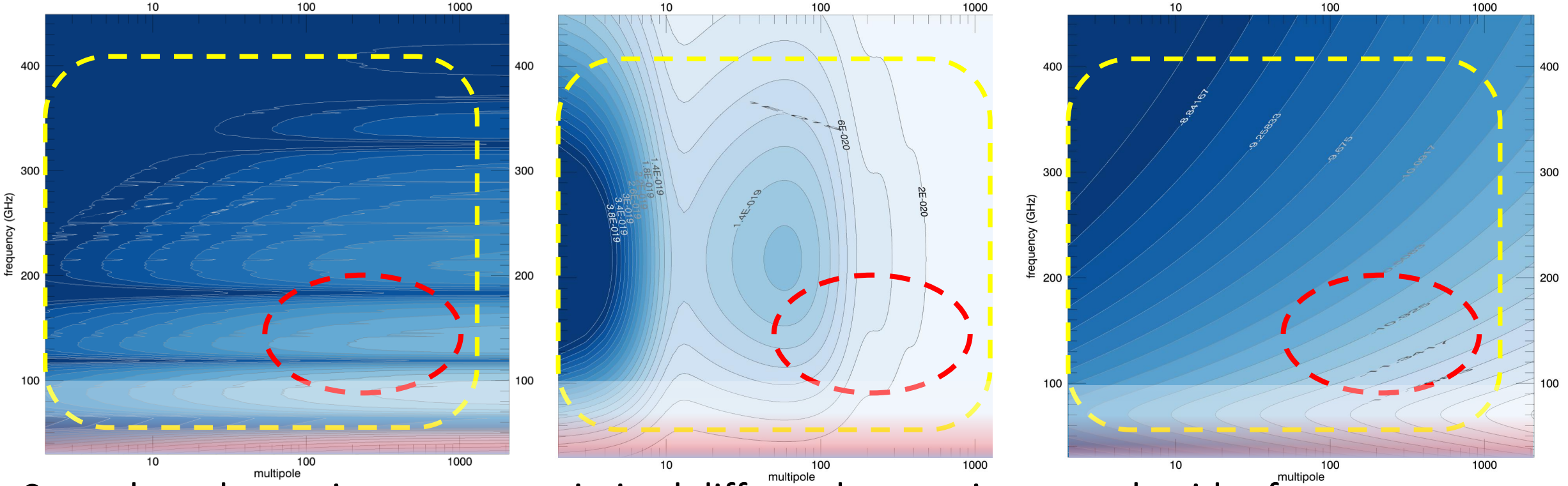

- Space based experiments are optimized differently, covering a much wider frequency range, forbidden from the ground, to allow effective monitoring of foregrounds, and extend to lower multipoles (larger angular scales) to cover the reionization peak of the B-mode spectrum. Note that higher frequency detectors require a smaller area in the focal plane ($A\Omega = \lambda^2$), so it is easier to accommodate large detector-count arrays.
- In the following I'll go through a few examples of current and future **configurations.**

BICEP Keck

- Ground based instruments (Atmospheric emission is not linearly polarized)
- South pole (the best site on Earth ?) in the Antarctic winter for high transmission and stability
- Heavily filter the data to remove large-scale fluctuations
- Massive increase in the number of detectors to boost the survey speed
- Polarization modulated by fast azimuth scan + rotation of the instrument around the boresight. $s = \frac{1}{2}\left[(1+\epsilon)\,\mathcal{I} + (1-\epsilon)\left(\mathcal{Q}\,cos(2\psi) + \mathcal{U}\,sin(2\psi)\right)\right]$

BICEP-3 (100 GHz)

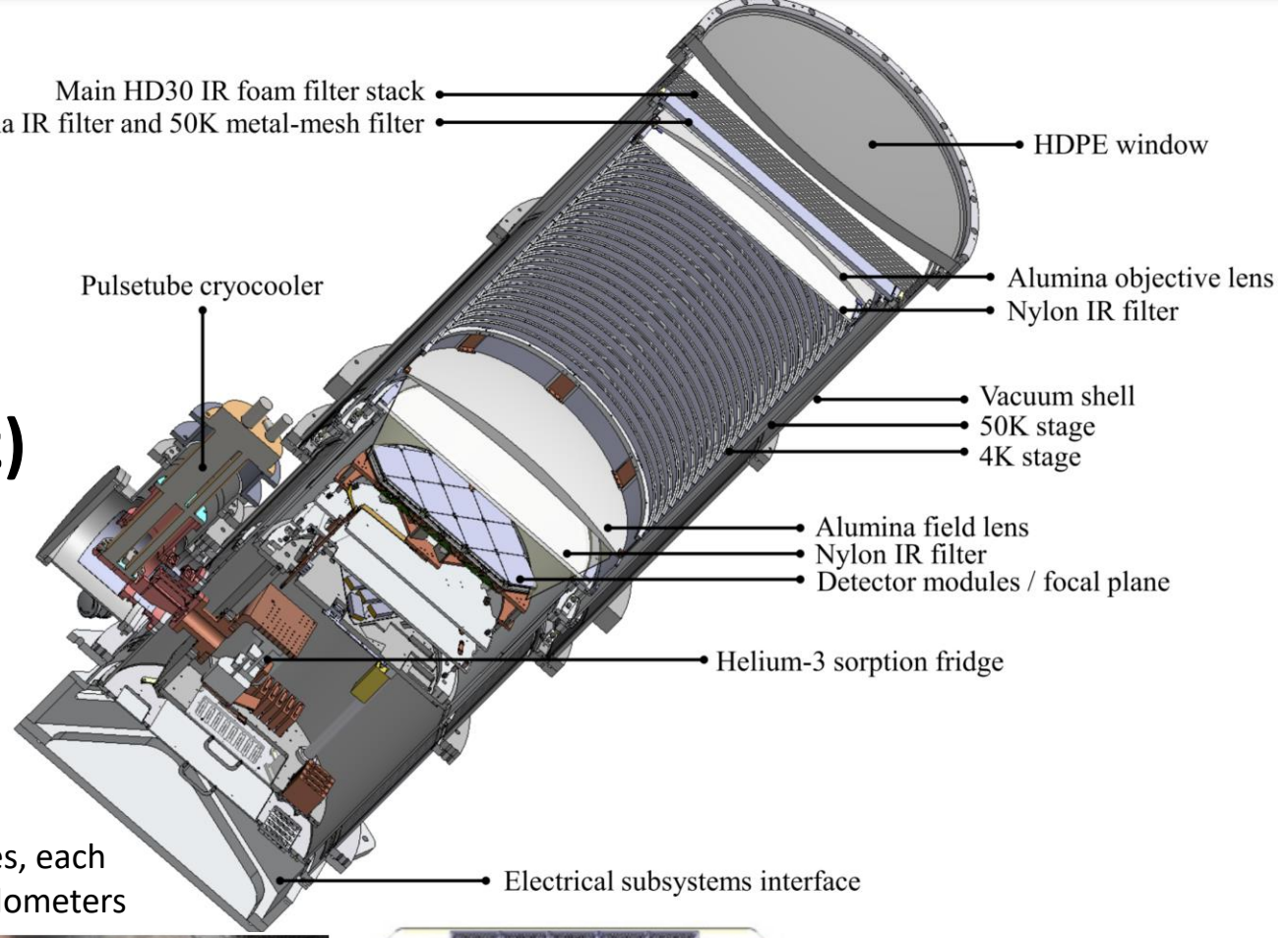

20 detector tiles, each with 60 TES bolometers

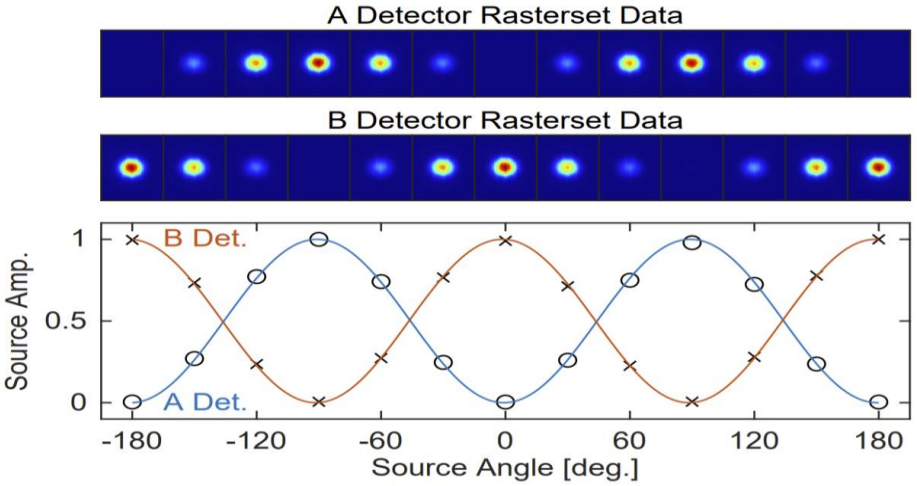

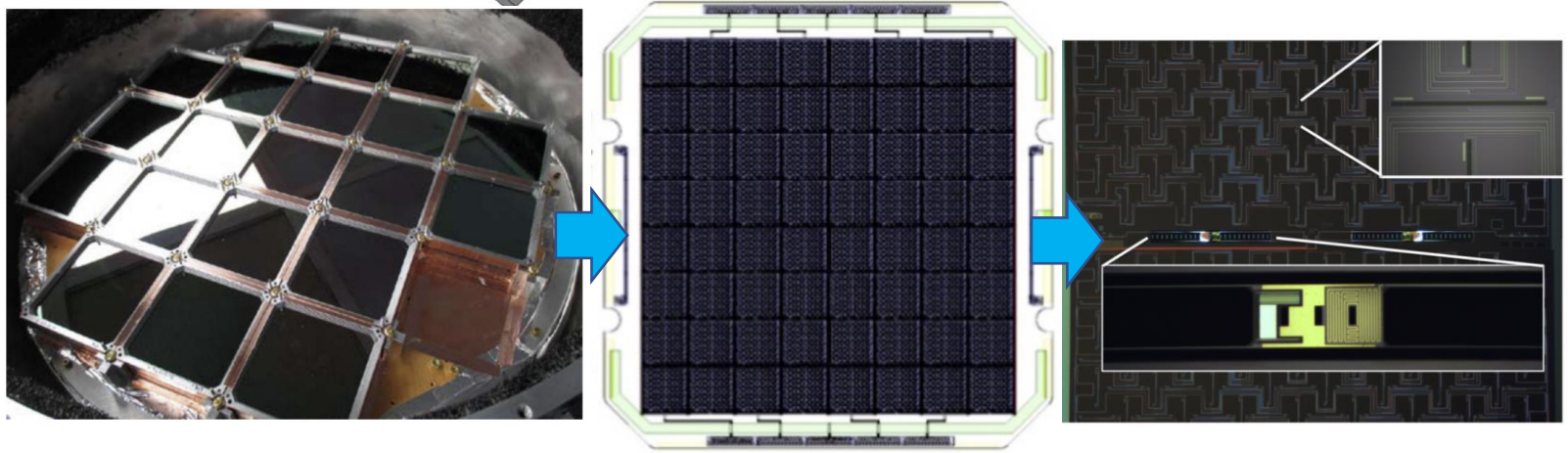

arXiv:2110.00482

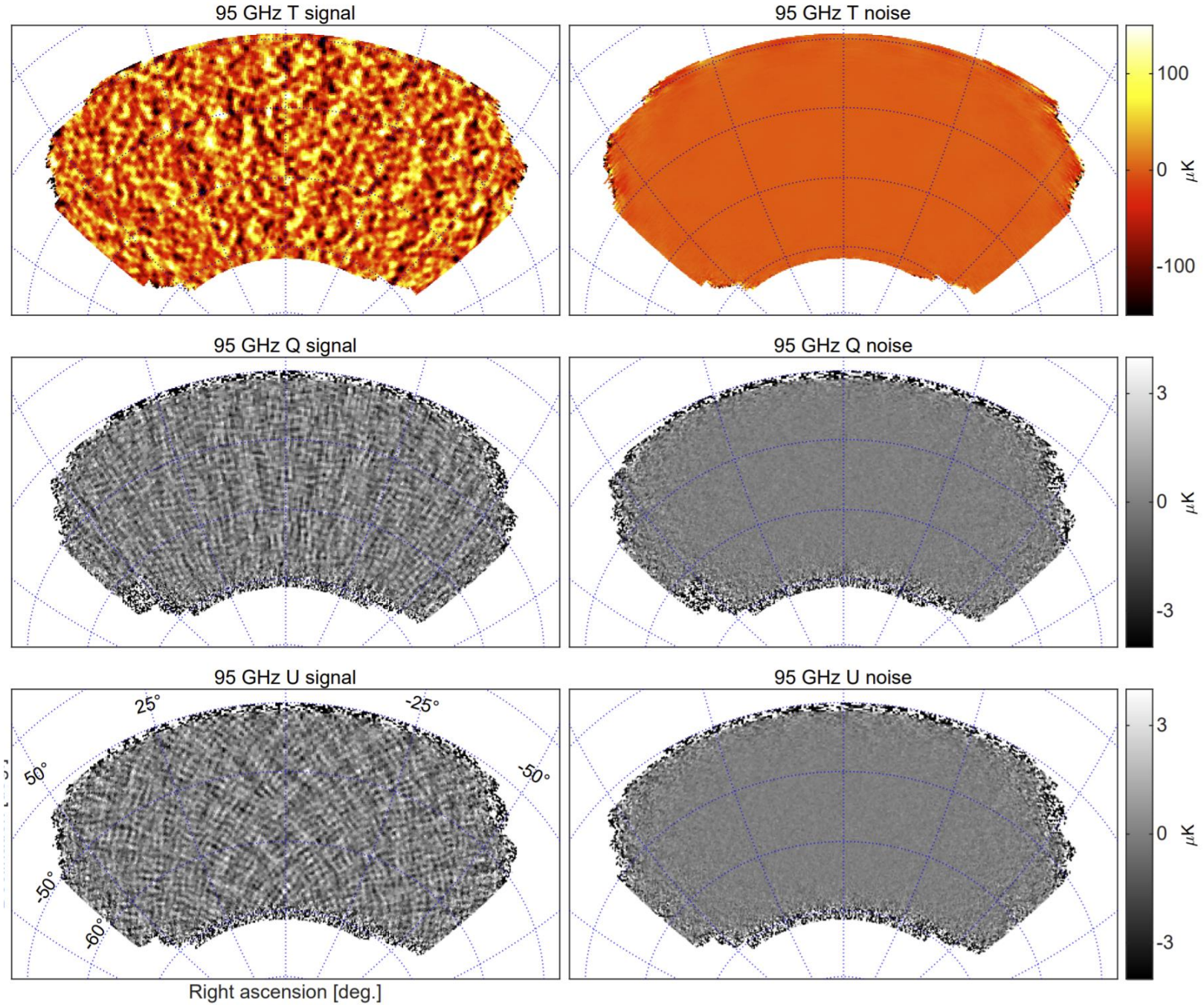

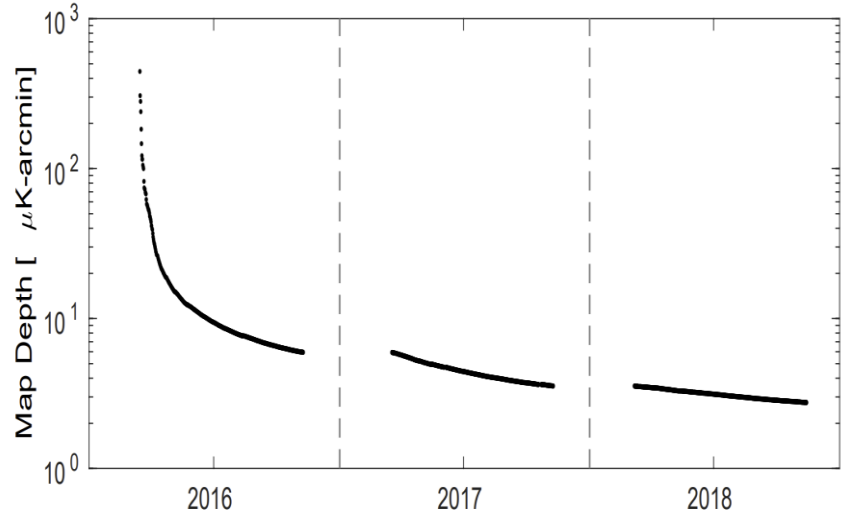

- The survey depth scales with the integration time as expected.
- Currently below 3 $\mu K \cdot arcmin$ approaching the cosmic variance / lensing limit

arXiv:2110.00483

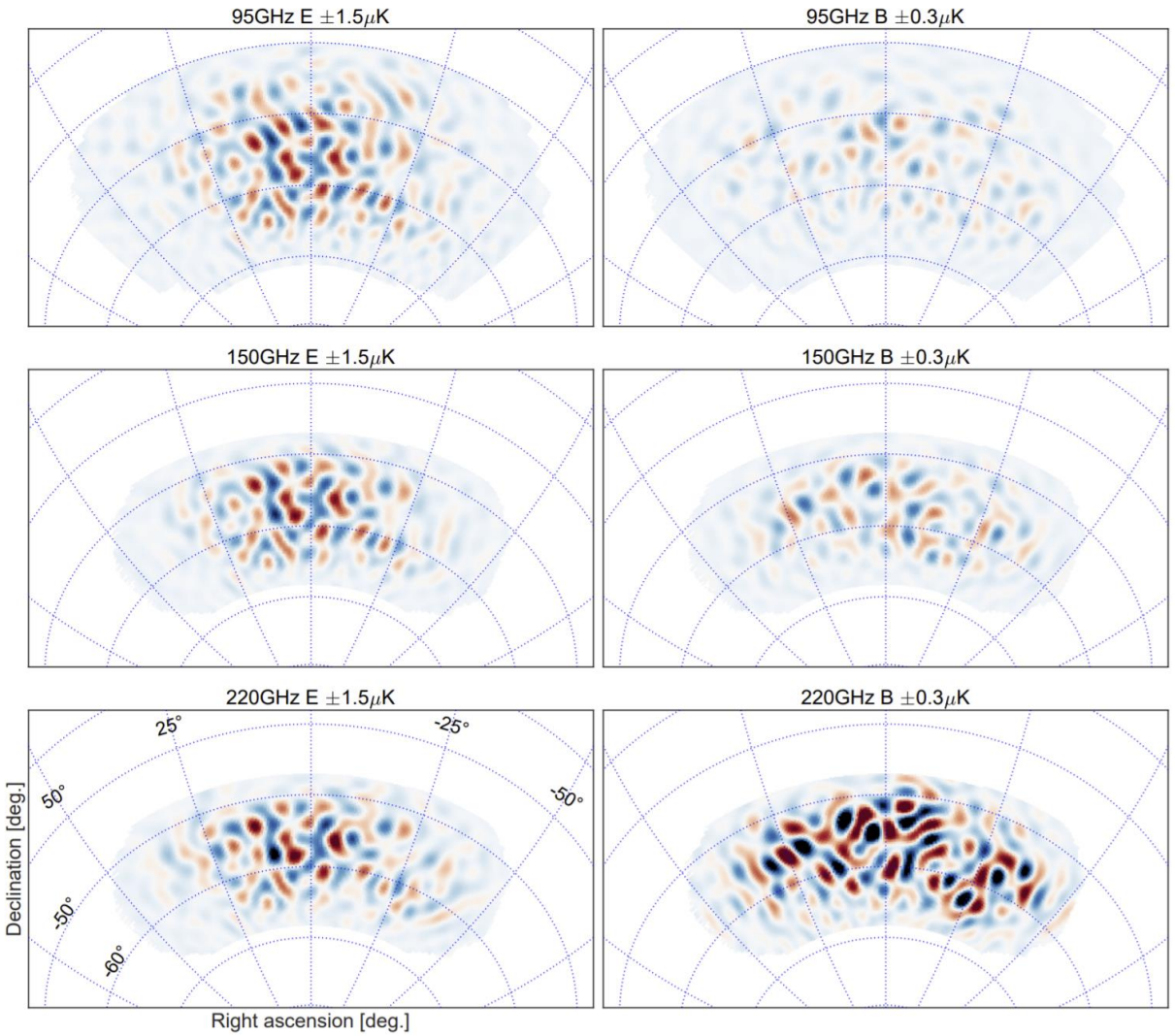

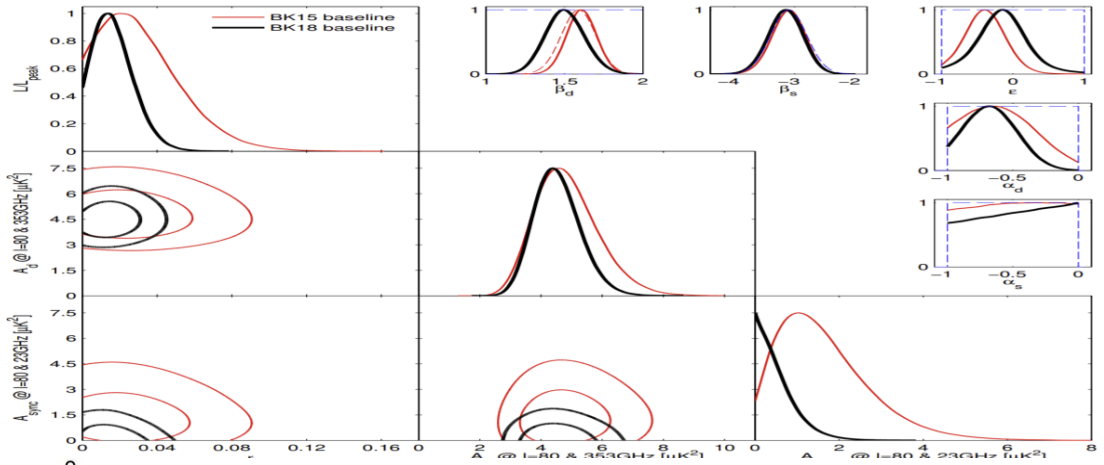

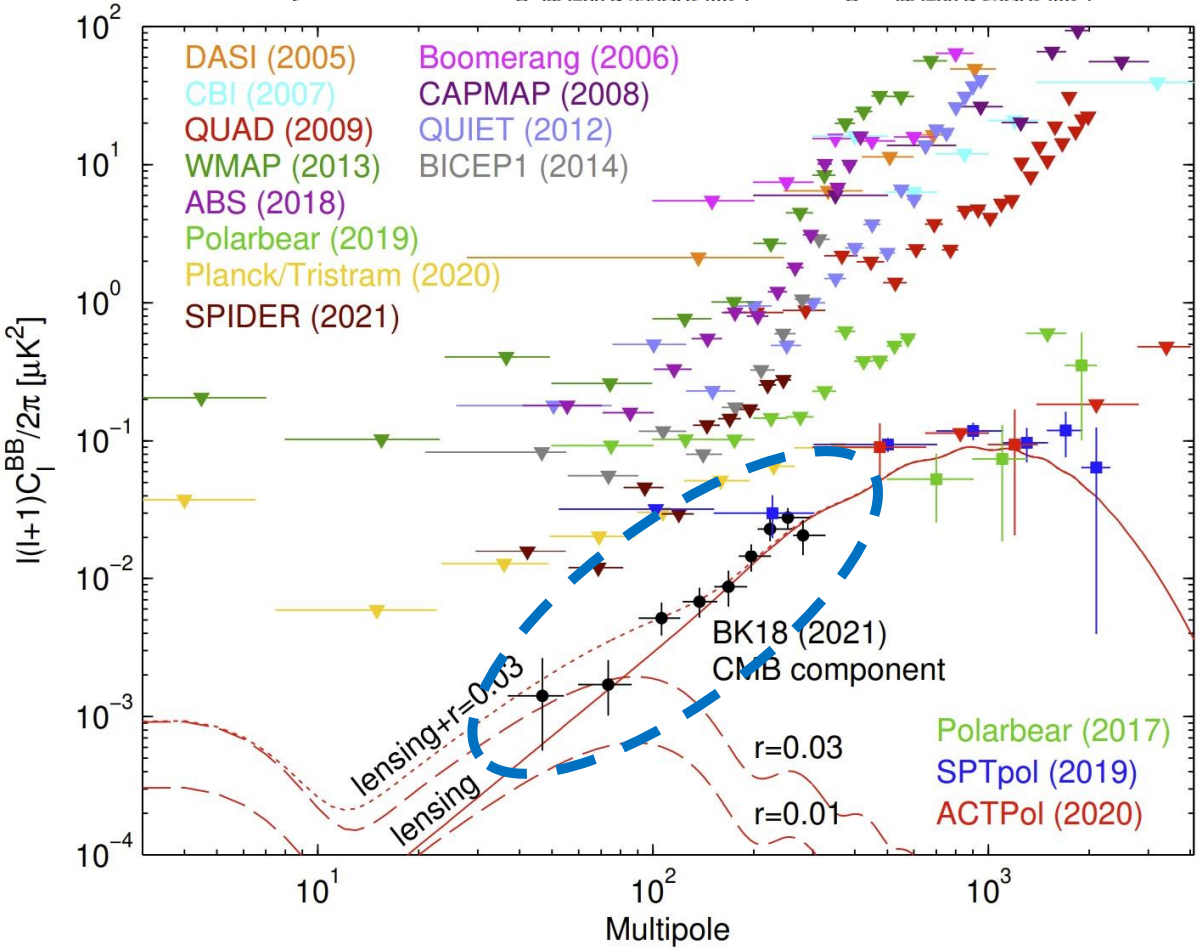

arXiv:2110.00483

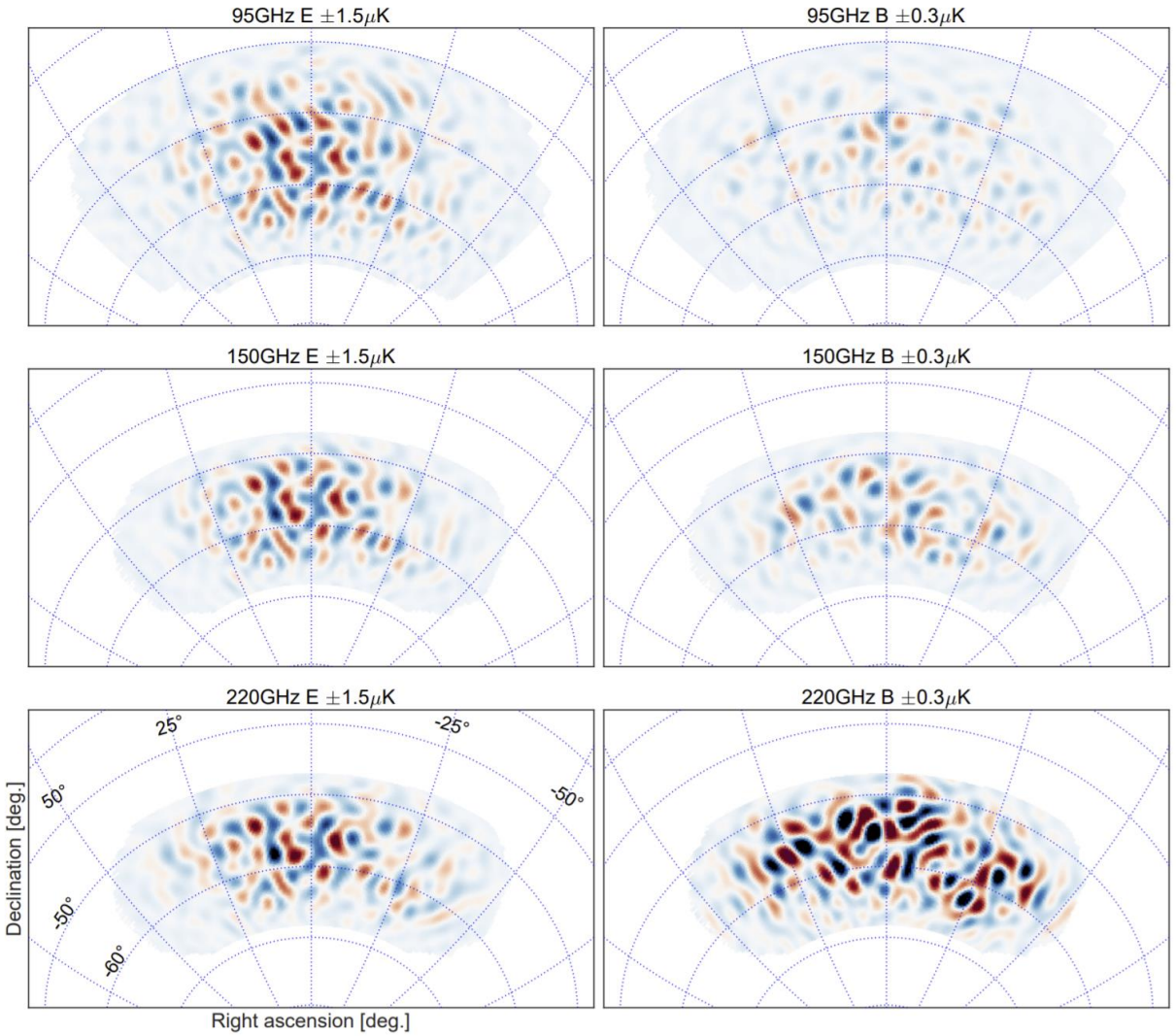

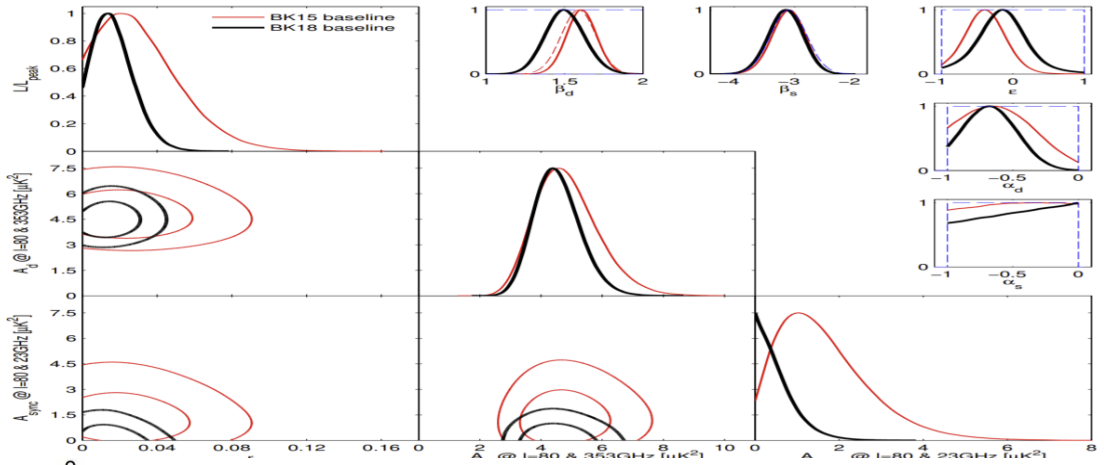

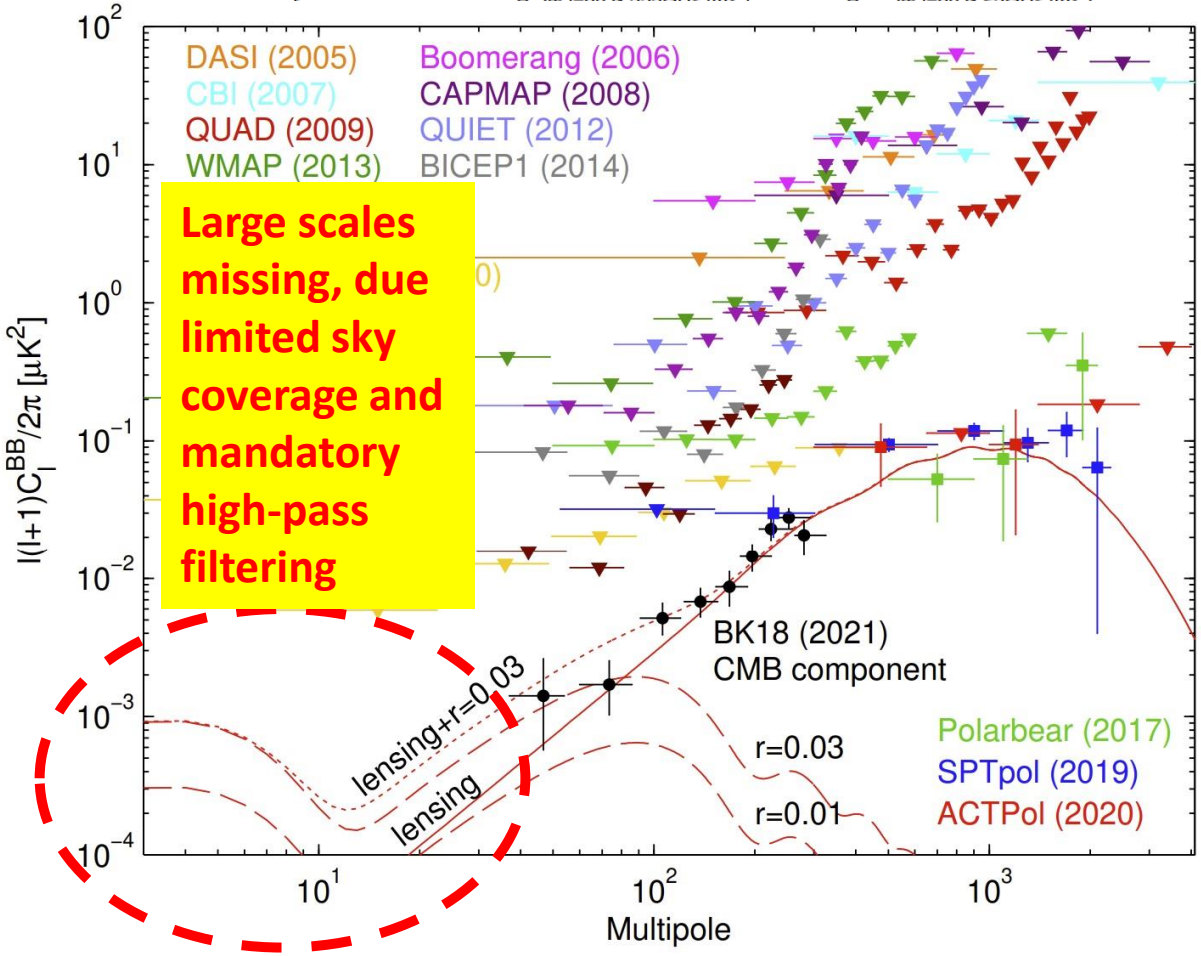

LSPE in a nutshell

- The **Large-Scale Polarization Explorer** is an experiment to measure the polarization of the CMB at large angular scales.
- **Science drivers / targets** :
  - The B-modes from inflation are mainly at large scales (*r*)
  - Polarization signatures from reionization (τ) are mainly at large scales
  - Rotation of the polarization angles (related to new physics)
  - Sensitive polarized dust survey at *f* close to the CMB ones
  - Sensitive polarized synchrotron survey at *f* close to the CMB ones
- **Instrumental approach** :
  - Frequency coverage: 40 – 250 GHz (5 bands)
  - 2 instruments covering the same northern sky
  - **STRIP** is a ground-based instrument working at 43 and 90 GHz
  - **SWIPE** works from near-space (balloon) at 145, 210, 240 GHz, with an internal polarization modulator to achieve the stability necessary for large scales.

LSPE : frequency coverage

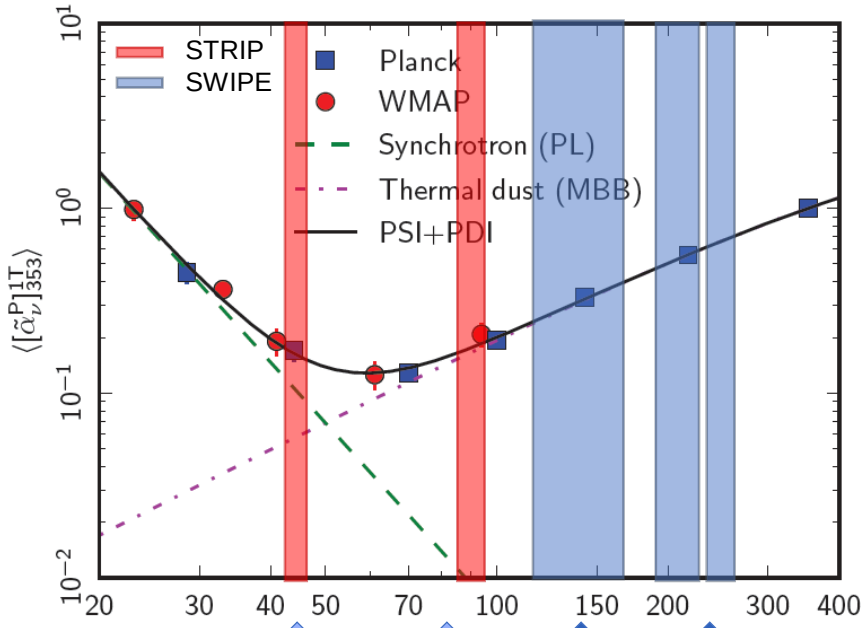

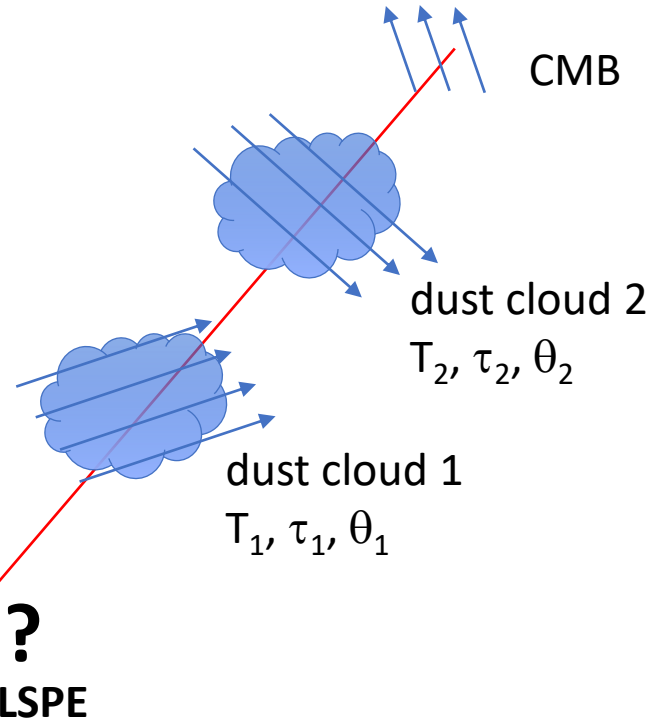

43 GHz (ground)
Monitor polarized synchrotron

90 GHz (ground)
Atmospheric monitor

145 GHz (balloon)
Main CMB channel

210 + 240 GHz (balloon)
Monitor **level, slope and possible rotation with frequency** of polarized dust emission.
To date: extrapolated from single frequency (Planck 353 GHz)

The LSPE collaboration

Addamo	G.
Farooqui	Z.
Lumia	M.
Paonessa	F.
Peverini	O.A.
Virone	G.
Battaglia	P.
Bersanelli	M.
Caccianiga	B.
Caprioli	S.
Cavaliere	F.
Colombo	L.
Franceschet	C.
Incardona	F.
Maino	D.
Mandelli	S.
Mandelli	L.
Mennella	A.
Paradiso	S.
Pezzotta	F.
Realini	S.
Tomasi	M.
Viganò	D.
Baschirotto	A.
Baù	A.
De Matteis	M.
Gervasi	M.
Ghigna	T.
Mainini	R.
Nati	F.
Passerini	A.
Pincella	C.
Tartari	A.
Zannoni	M.
Cuttaia	F.
De Rosa	A.
Morgante	G.
Ricciardi	S.
Sandri	M.
Terenzi	L.
Villa	F.

Gregorio	A.
Maris	M.
Sartor	S.
Zacchei	A.
Hill-Valler	J.
Jew	L.
Jones	M.
Taylor	A.
Watkins	B.
Gaier	T.
Soria	M.
Cleary	K.
Genova-Santos	R.
González Escalera	V.
Hoyland	R.
Perez	A.
Rebolo	R.
Rubiño-Martin	J. A.
Mena	P.
Pizarro	J.
Reyes	N.
Tapia	V.
Amico	G.
Battistelli	E. S.
Columbro	F.
Coppi	G.
Coppolecchia	A.
D'Alessandro	G.
de Bernardis	P.
De Petris	M.
Lamagna	L.
Marchetti	T.
Masi	S.
Paiella	A.
Panico	F.
Piacentini	F.
Presta	G.
Schillaci	A.
Boscaleri	A.

Biasotti	M.
Boragno	C.
Ceriale	V.
Corsini	D.
Fontanelli	F.
Fumagalli	E.
Gatti	F.
Giovannini	M.
Grosso	D.
Siri	B.
Baldini	A. M.
Cei	F.
Galli	L.
Grassi	M.
Incagli	M.
Moggi	A.
Nicolò	D.
Piendibene	M.
Signorelli	G.
Spinella	F.
Tartari	D.
Vaccaro	D.
Ade	P.A.R.
Pisano	G.
Tucker	C.
Coppi	G.
Martinis	L.
May	A.
McCulloch	M.
Melhuish	S.
Piccirillo	L.
Baccigalupi	C.
Farsian	F.
Krachmalnicoff	N.
Puglisi	G.
Matarrese	S.

Matarrese	S.
Forastieri	F.
Gruppuso	A.
Iacobellis	G.
Lattanzi	M.
Molinari	D.
Natoli	P.
Pagano	L.
Polastri	L.
Zavattini	G.
Bazzicchi	A.
Buzzelli	A.
Cabella	P.
Cesarini	E.
Cifaldi	M.
Coccia	E.
D'Antonio	S.
De Gasperis	G.
Fafone	V.
Haridasu	S.
Lorenzini	M.
Lukovich	V.
Migliaccio	M.
Rocchi	A.
Vittorio	N.
Polenta	G.
Tommasi	E.
Volpe	A.

Scientists from institutions in Italy, UK, USA, Spain, Chile:

CNR-TO
UniMI, INFN-MI
UniMIB, INFN-MIB
INAF-BO
INAF-OAT
UniTS
Oxford
JPL
Caltech
IAC
UniChile
UniGE, INFN Ge
INFN Pi
Sapienza Roma, INFN Roma
IFAC CNR
UniCardiff
UniManchester
SISSA
UniPD
UniFE, INFN Fe
Tor Vergata, INFN RM2
ASI

LSPE : Sky Coverage

STRIP

Ground telescope at 43 and 95 GHz located in Tenerife. Will measure for two years. Based on coherent polarimeters

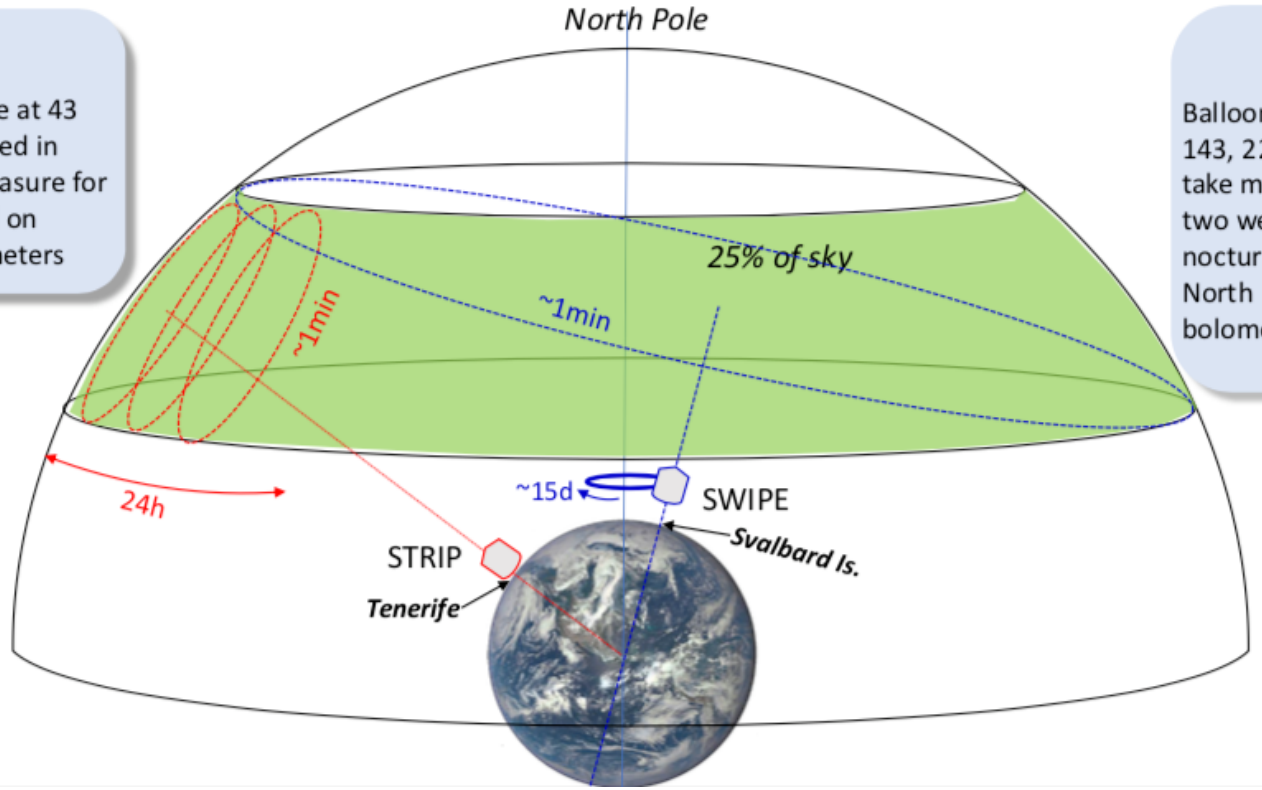

SWIPE

Balloon borne telescope at 143, 220 and 240 GHz. Will take measurements for two weeks during a LDB nocturnal flight around the North Pole. Based on TES bolometers

Credit A. Mennella

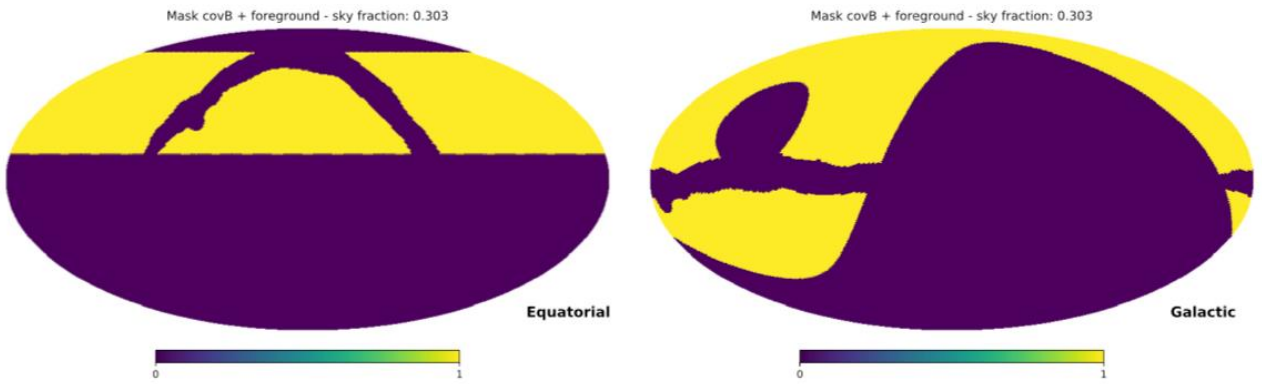

Credit L. Pagano, F. Piacentini

LSPE-STRIP in a nutshell

- Survey TeneRIfe Polarimeter
- Target: Polarized Synchrotron
- Two arrays of coherent polarimeters: 49 @44 GHz (QUIET) plus 7 @ 90 GHz.
- The measured response of the corrugated feedhorns confirms the expected performance down to -55 dB
- 1.5 m telescope (Clover)
- PI M. Bersanelli UNIMI

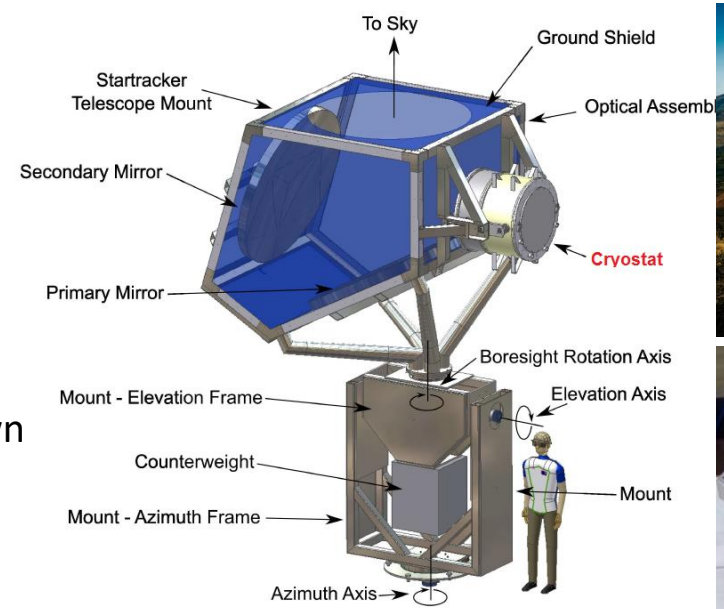

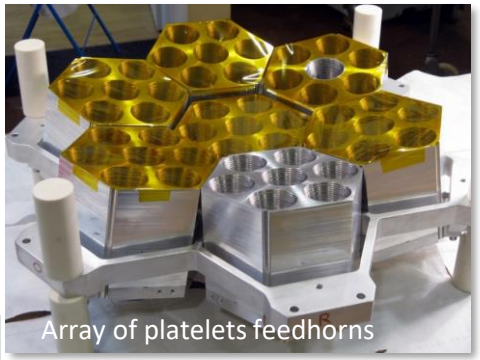

Instrument	STRIP	
Site	Tenerife	
Freq (GHz)	43	90
Bandwidth	17%	8%
Angular resolution FWHM (arcmin)	20	10
Detectors technology	HEMT	
Number of detectors N_{det}	49	6
Detector NET ($\mu K_{CMB}\sqrt{s}$)	515	1139
Mission duration	2 years	
Duty cycle	50%	
Sky coverage f_{sky}	37%	
Map sensitivity $\sigma_{Q,U}$ (μK_{CMB} · arcmin)	102	777
Noise power spectrum $(\mathcal{N}_\ell^{E,B})^{1/2}$ (μK_{CMB} · arcmin)	171	1330

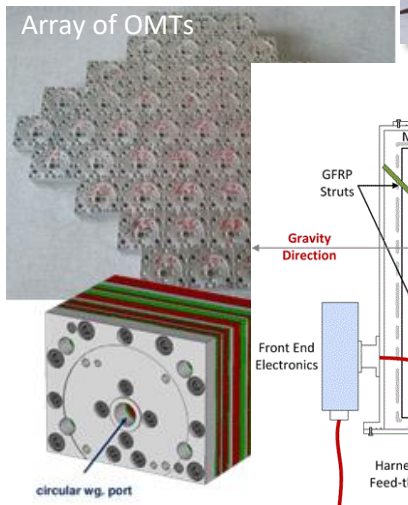

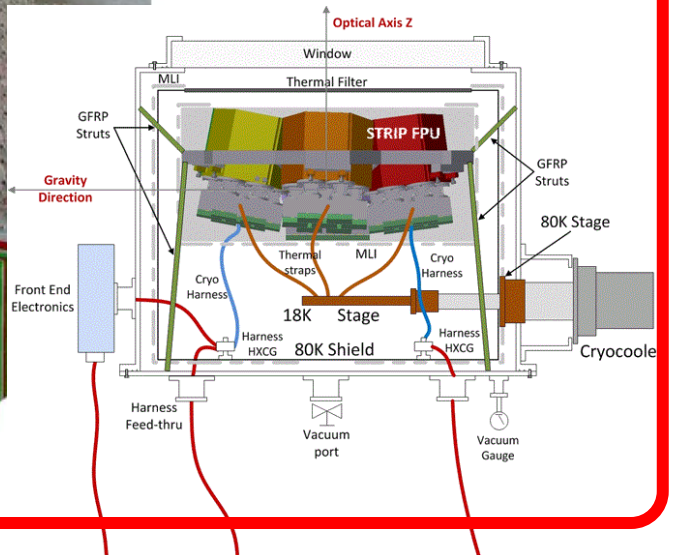

Provides essential information on polarized synchrotron

LSPE-SWIPE in a nutshell

- SWIPE is a multiband (145, 210, 220 GHz) array of Stokes polarimeters (163).
- Is flown on a stratospheric **balloon,** to avoid atmospheric noise at high *f,* including polarized radiation from ice crystals in tropospheric clouds (e.g. Takakura et al. 2018). **38%** of the sky covered in a 15d flight.
- SWIPE uses 326 **multimoded detectors** to improve the sensitivity wrt to Planck-HFI. The focal planes collect 8800 radiation modes. The resolution of each multimoded beam is 1.4° FWHM.
- Combined sensitivity: **10 μK arcmin per flight**
- SWIPE uses a **HWP-based polarization modulator as the first optically active element,** to solve several issues important at large scales (beam asymmetry leakage, bandpass mismatch, 1/f noise ... etc.)
- SWIPE uses a **single *large* polarizer, common** to the entire focal plane, to define the main axis of the polarimeter with high precision (< 0.1°): accurate absolute reconstruction of the pol. directions.
- PI P. de Bernardis (Sapienza)

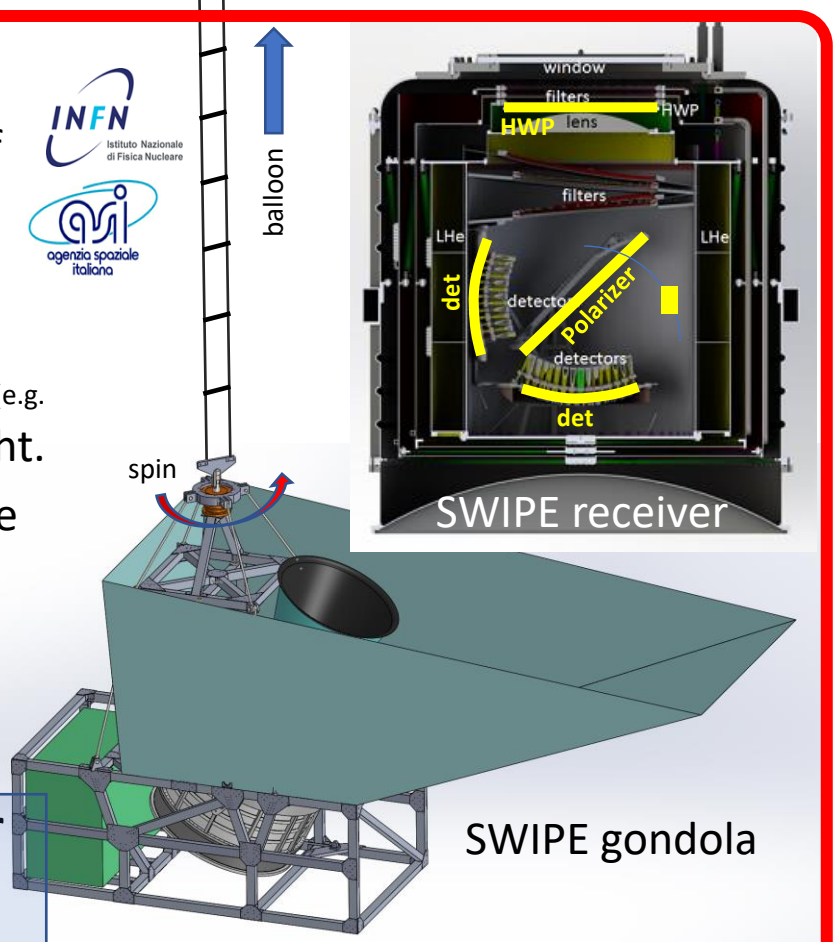

Instrument	SWIPE		
Site	balloon		
Freq (GHz)	145	210	240
Bandwidth	30%	20%	10%
Angular resolution FWHM (arcmin)	85		
Detectors technology	TES multimoded		
Number of detectors N_{det}	162	82	82
Detector NET ($\mu K_{CMB}\sqrt{s}$)	12.7	15.7	30.9
Mission duration	8 - 15 days		
Duty cycle	90%		
Sky coverage f_{sky}	38%		
Map sensitivity $\sigma_{Q,U}$ (μK_{CMB} · arcmin)	10	17	34
Noise power spectrum $(\mathcal{N}_\ell^{E,B})^{1/2}$ (μK_{CMB} · arcmin)	16	28	55

LSPE/SWIPE: photon background

To fully exploit the low radiative background: thin window

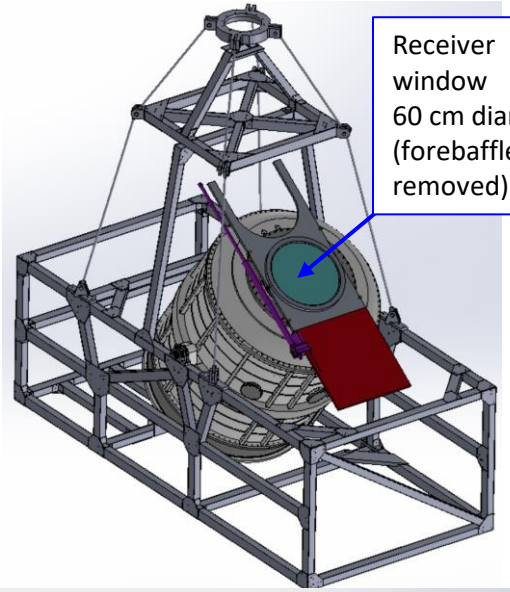

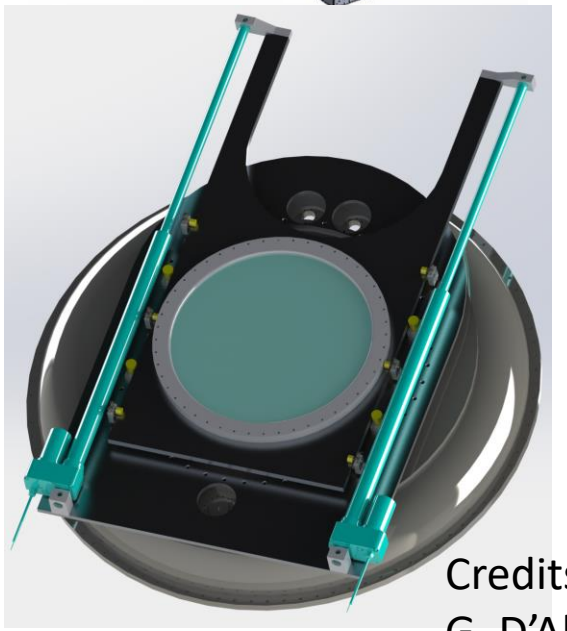

Credits:
G. D'Alessandro

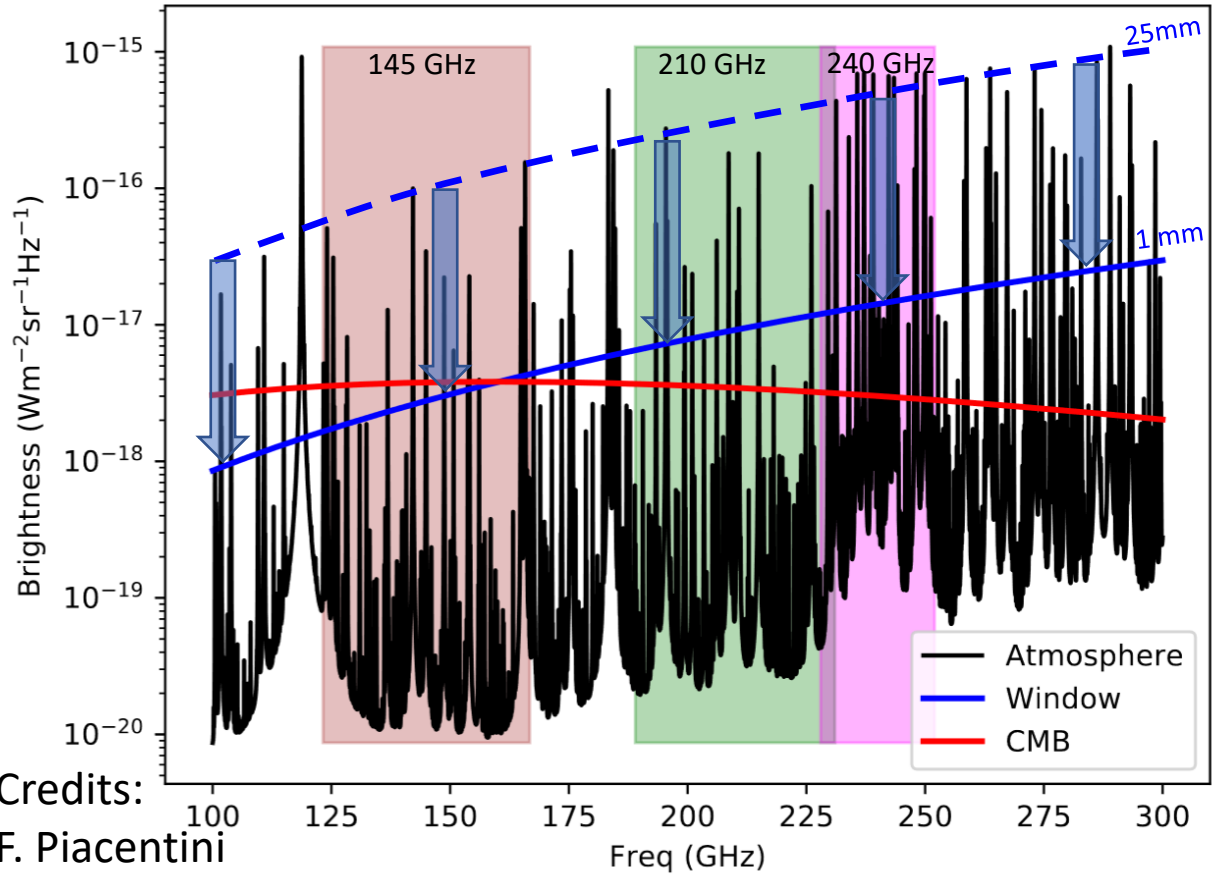

Credits:
F. Piacentini

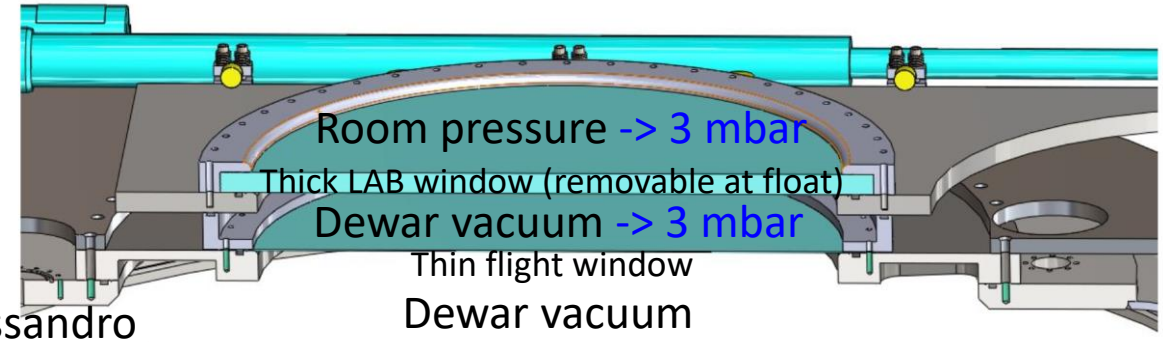

Reduction of the amplitudes of HWP-synchronous systematic effects

In a real Stokes polarimeter, the optical devices produce polarized emission, which can be in part modulated by the rotation of the HWP (e.g. Salatino & de Bernardis 2010, Columbro et al. 2019)

- Polarized emission/transmission of the lens, stop, field optics: mitigated using the HWP as the first optical element skywise.
- The HWP can have slightly different efficiencies for the fast and slow axes. This results in polarized emission & transmission of the HWP, modulated by the polarizer, i.e. a **$2f_{HWP}$** signal **(5 mK !)**. Mitigated by filtering the output signal (bandpass around $4f_{HWP}$)
- The polarizer emission can be reflected by the HWP and modulated: this results in a small **$4f_{HWP}$** signal. Mitigated by reducing the temperature of the polarizer (here 1.6K, so **few μK**). Can be removed by a dedicated pipeline (e.g. Ritacco & 2017).
- The polarized emission of the HWP can be reflected by the polarizer and by the HWP. This is a small $4f_{HWP}$ signal. In our case is very small, since the polarizer is tilted 45° wrt the HWP.

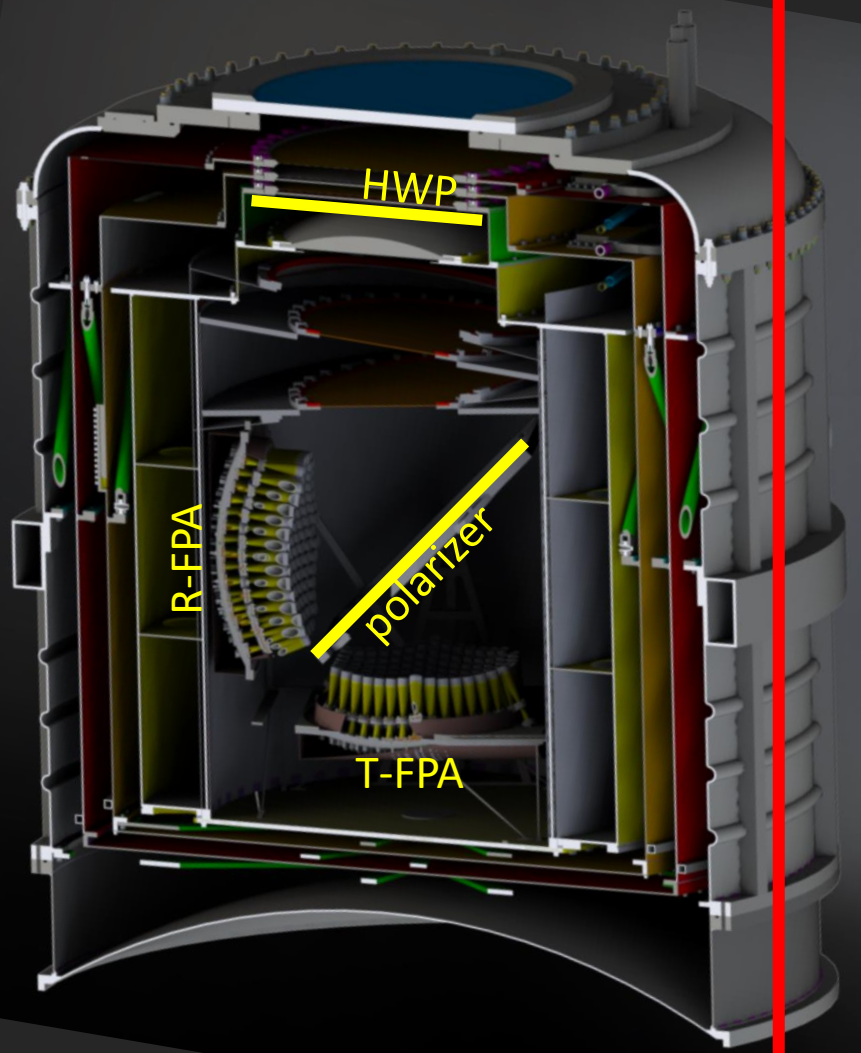

Reduction of the amplitudes of HWP-synchronous systematic effects

- There are other subtle systematic effects, an additional ones will be discovered.
- One of the main reasons of interest for this experiment is that we have the opportunity to study experimentally the performance of a Stokes polarimeter with cryogenic spinning HWP, a configuration which will be used in several ultresensitive experiments, including LiteBIRD.
- Real experimental tests are badly needed, in addition to simulations, to validate a very difficult meaurement !

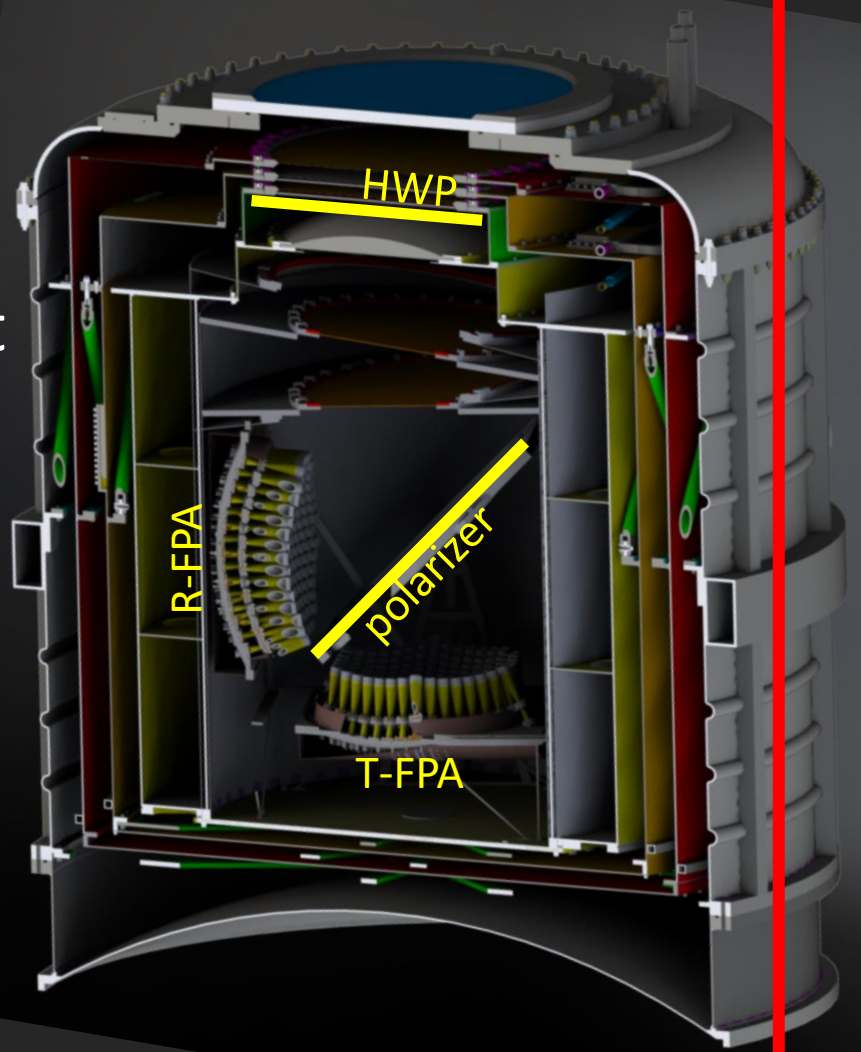

SWIPE – HWP

- Is a cold (2K), large (50 cm useful dia.), wide-band meta-materials HWP, placed immediately behind the window and thermal filters stack.
- HWP characteristics for the ordinary and extraordinary rays are well matched: $(T_o-T_e)/T_o < 0.001$, $X_{pol}<0.01$, over the 100-300 GHz band.
- Simulations show that continuous rotation has advantages in terms of 1/f noise mitigation and angles coverage.
- A custom superconductive rotator has been developed.

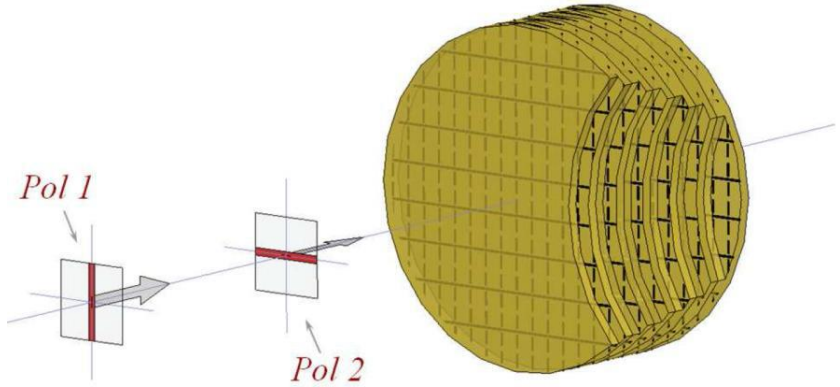

Pisano et al., Proc. SPIE, Vol. 9153, id. 915317 (2014)

SWIPE – HWP rotator - General layout

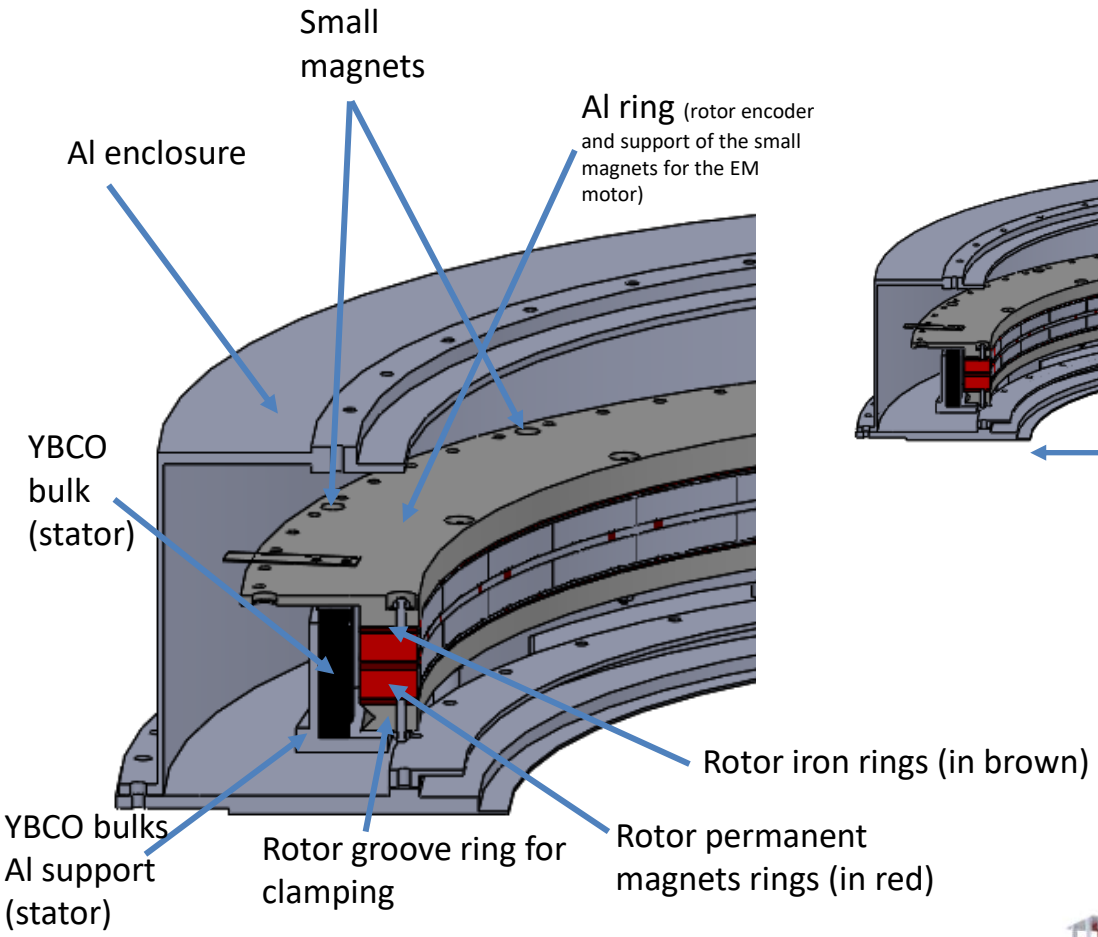

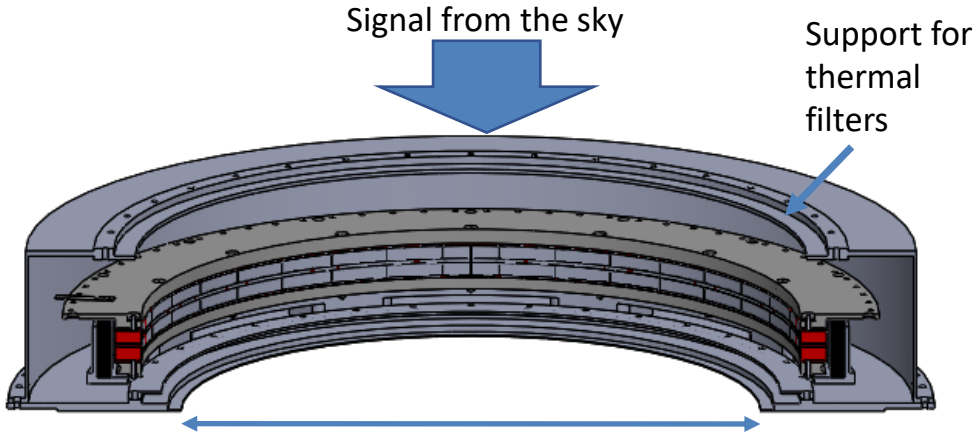

1T field strength in the gap. Total mass 9 kg.

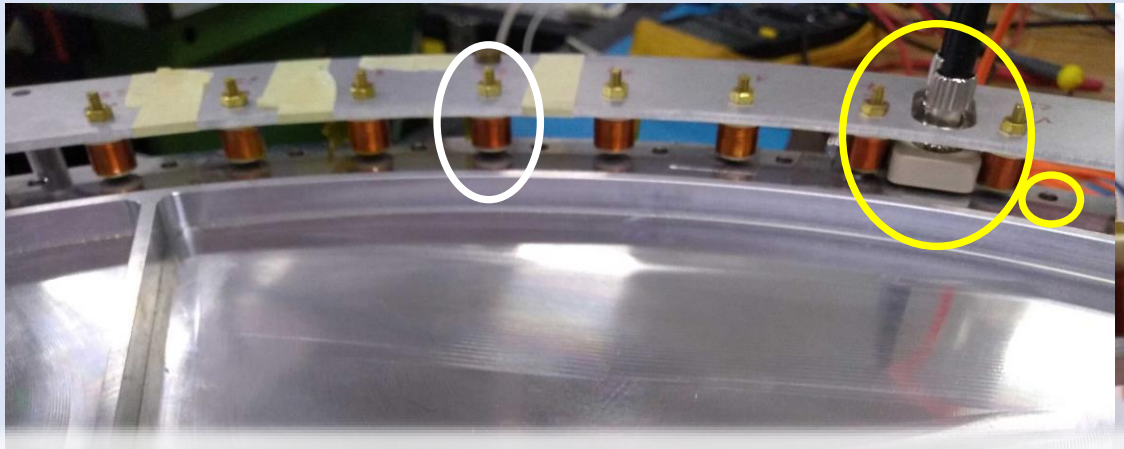

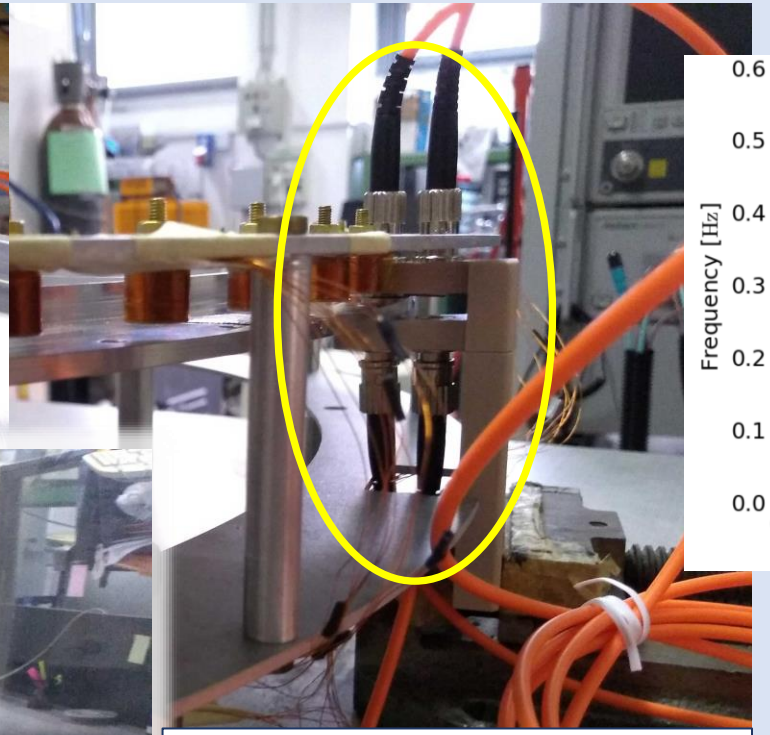

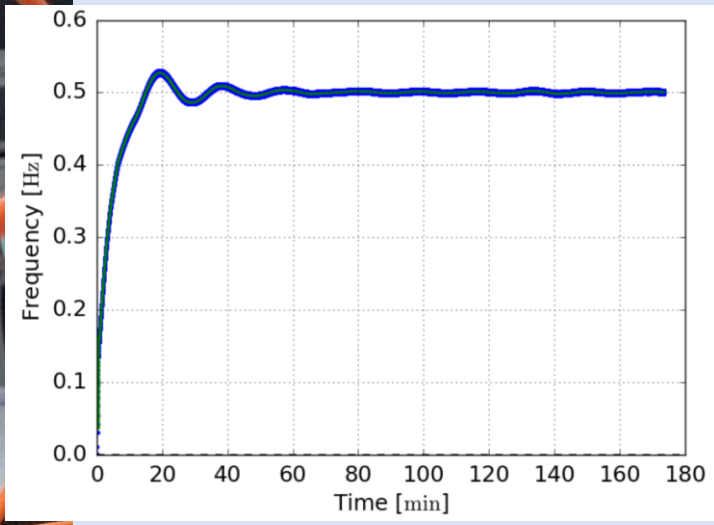

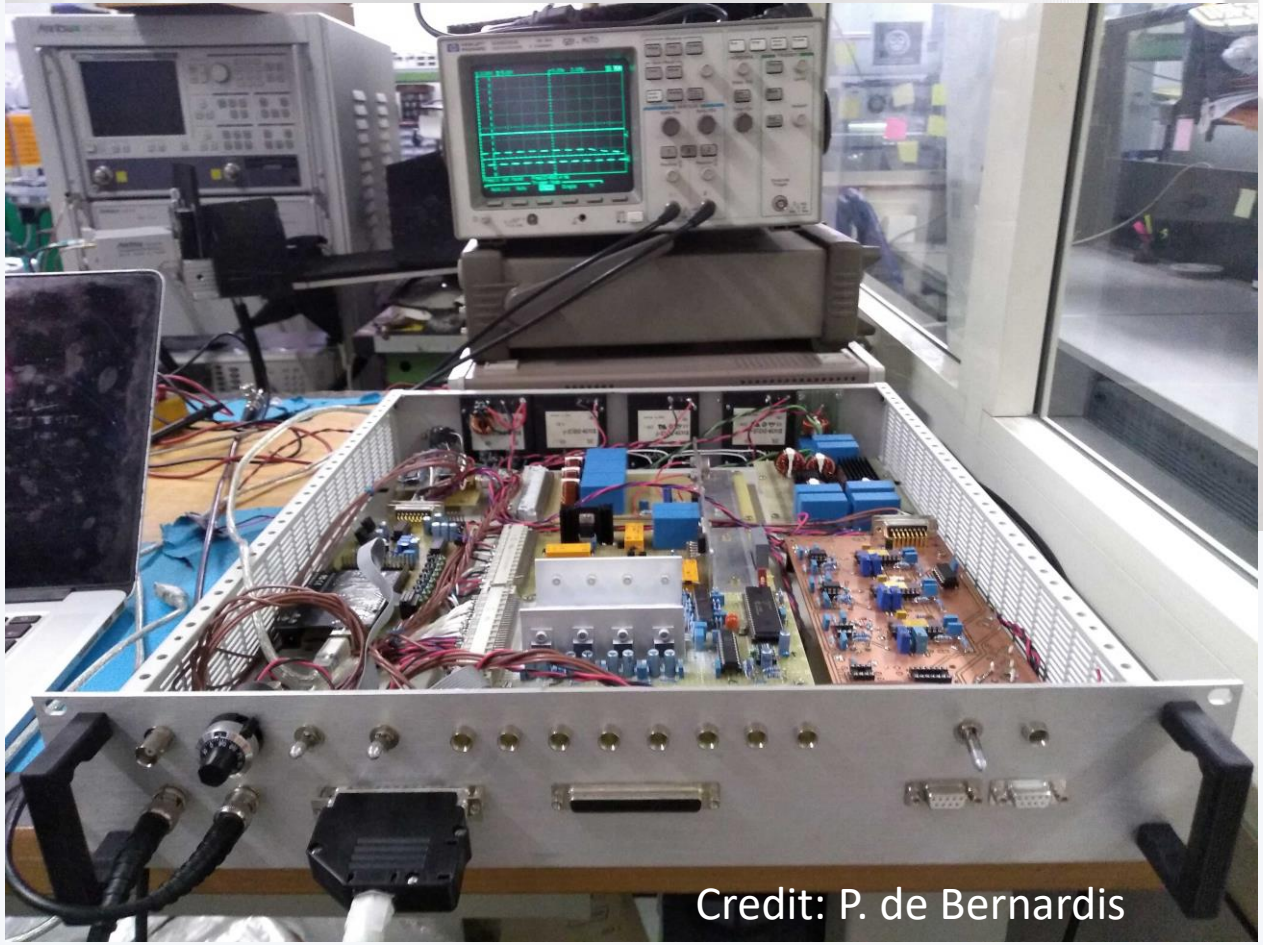

Custom brushless synchronous motor & control electronics:

- 8 phases
- 64 equalized coils (stator)
- 8 magnets (rotor)
- Smooth phased currents to minimize EMI & induced eddy currents
- 64-slits optical encoder
- High accuracy optical fibers readout (Δt=50μs)

Room-T testbed for motor & control: OK

Working for :

- Optimization of start
- Optimization of feedback algorithm (frequency, phase and amplitude)
- Minimization of driving currents
- FPGA board for precision time stamping
- Thermal/vac test

SWIPE: Focal Planes

- The distribution of colors in the pixels has been optimized with a simplified scheme for foregrounds (dust) removal.
- This distribution provides sufficient precision to extrapolate the dust signal from high frequency down to 150 GHz
- This configuration totalizes 4400 radiation modes for each focal plane (transmitted and reflected).

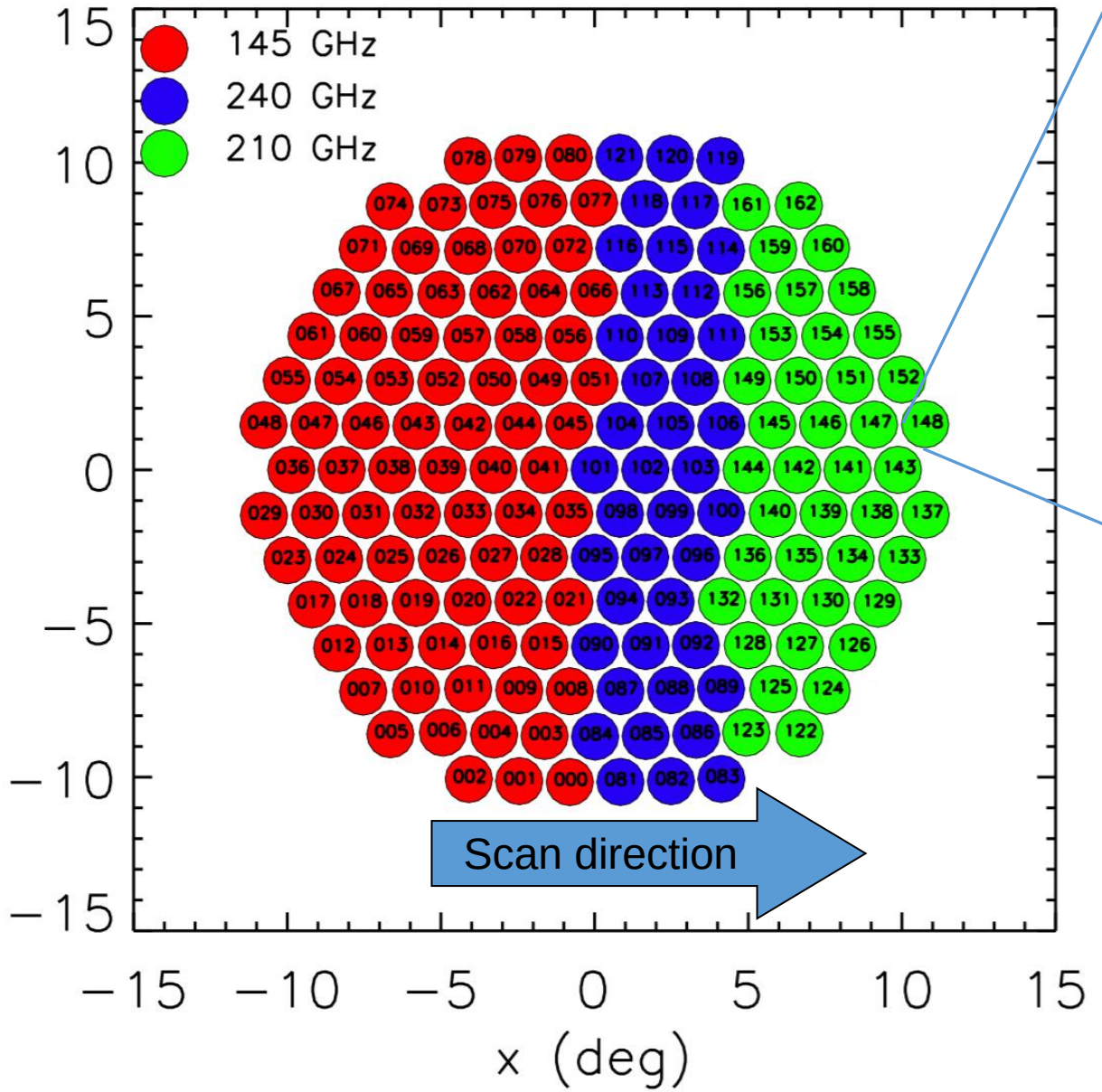

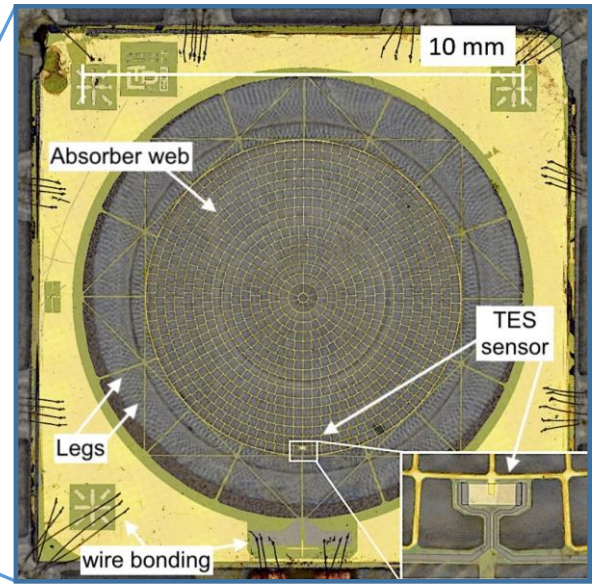

Large-throughput spider-web TES bolometer for LSPE-SWIPE: Au-Ti TES, 450 mK transition temperature, on a 1 μm thick Si_3N_4 web. τ=30 ms, NET=3x10^{-17}W/sqrt(Hz). (Genova, F. Gatti). With multimode feedhorn: AΩ=0.8cm^{2}sr

LSPE horns & bolo holders

Large Throughput multimode detectors: 8800 modes collected by 330 sensors

Focal plane detector flanges (gold plated Al6061, 40 cm side).

LSPE/SWIPE: noise estimates

Background power on each detector :

$$W = \int f_\nu \alpha A \Omega I_\nu d\nu$$

Optical throughput :

$$A\Omega = n_{\rm modes} \lambda^2$$

Photon noise :

$$\mathrm{NEP}^2_{\rm ph} = 2 \int f_\nu \alpha A \Omega I_\nu h\nu \left(1 + \frac{f_\nu \alpha c^2 I_\nu}{h\nu^3}\right) d\nu.$$

Detector noise :

$$\mathrm{NEP}_{\rm detector} = \sqrt{4 k_B T_c^2 G F}$$

The power of multimoded bolometers …

Ideal noise performance estimate

band (GHz)	145	210	240
bandwidth	30%	20%	10%
$n_{\rm modes}$	[10,17]	[23,32]	[32,39]
$A\Omega$ (m^2 sr)		$n_{\rm modes}\lambda^2$	
efficiency α	0.3	0.3	0.3
Power on cryostat entrance			
$W_{\rm CMB}$ (pW)	9.1	7.9	3.9
$W_{\rm atm}$ (pW)	0.9	1.9	9.8
$W_{\rm window}$ (pW)	6.9	21.4	18.4
$W_{\rm total}$ (pW)	16.9	31.2	32.1
Power on detector			
$W_{\rm total\text{-}detector}$ (pW)	5.1	9.4	9.6
Noise on detector			
$\mathrm{NEP}_{\rm ph\text{-}CMB}$ (aW/$\sqrt{\rm Hz}$)	23.5	25.9	19.3
$\mathrm{NEP}_{\rm ph\text{-}atm}$ (aW/$\sqrt{\rm Hz}$)	8.4	13.7	38.5
$\mathrm{NEP}_{\rm ph\text{-}window}$ (aW/$\sqrt{\rm Hz}$)	20.6	43.3	42.8
$\mathrm{NEP}_{\rm ph\text{-}total}$ (aW/$\sqrt{\rm Hz}$)	32.3	52.3	60.8
Thermal cond. G (pW/K)	86.2	158.9	163.5
$\mathrm{NEP}_{\rm detector}$ (aW/$\sqrt{\rm Hz}$)	37.9	51.5	52.3
$\mathrm{NEP}_{\rm total}$ (aW/$\sqrt{\rm Hz}$)	49.8	73.4	80.1
Optical noise			
$\mathrm{NEP}_{\rm optical\text{-}total}$(aW/$\sqrt{\rm Hz}$)	166	245	267
NET ($\mu\mathrm{K}_{\rm CMB}\sqrt{\rm s}$)	12.7	15.7	30.9

LSPE: ideal performance forecast

- TOD simulations > Components separation > Power spectra > Parameters (r, τ)
- see JCAP 2021(08):008

Table 7. Component separation wieghts for each component in each channel for the minimal case: Planck + LSPE (STRIP, SWIPE).

f (GHz)	Probes	w_{CMB}	w_{Dust}	w_{Synch}
30	P	-1.5×10^{-2}	2.7×10^{-3}	8.7×10^{-1}
43	ST	-2.6×10^{-3}	-4.5×10^{-4}	3.9×10^{-1}
145	SW	1.4	-4.1×10^{-1}	-1.6
210	SW	-1.9×10^{-1}	2.4×10^{-1}	2.8×10^{-2}
240	SW	-2.02×10^{-1}	1.6×10^{-1}	3.4×10^{-1}

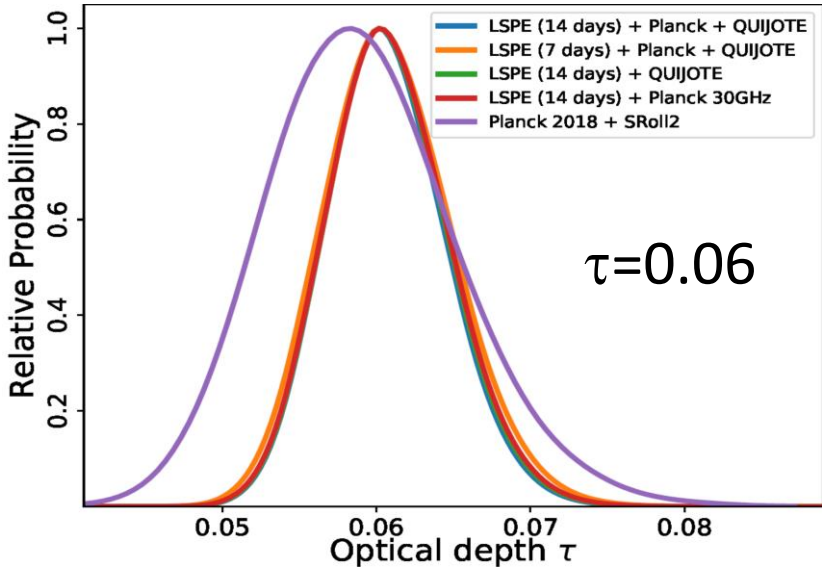

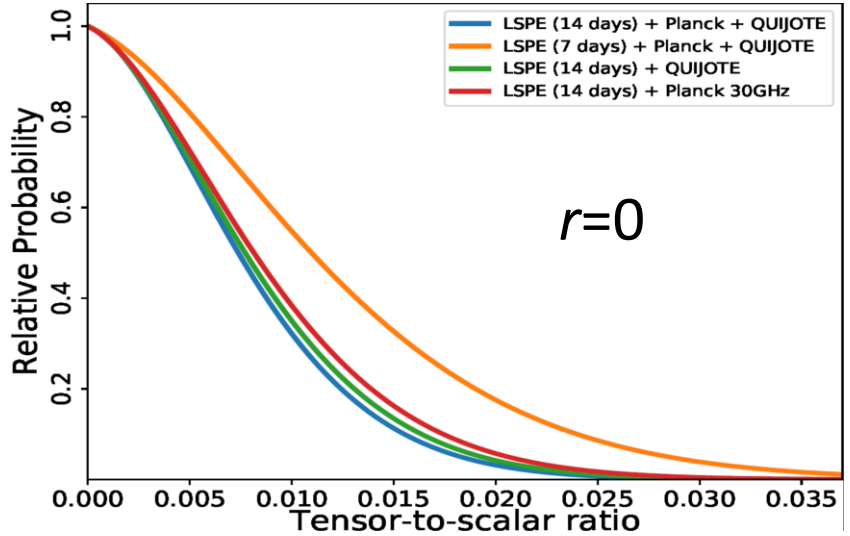

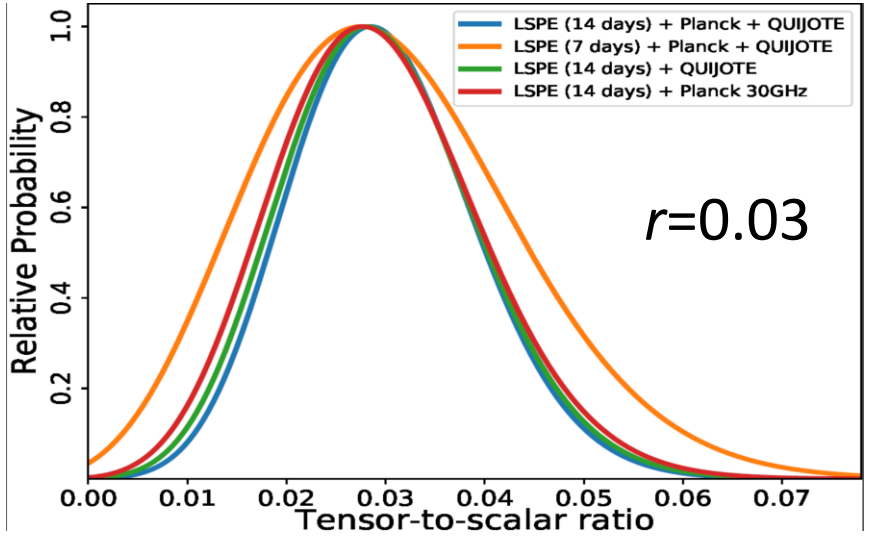

LSPE/SWIPE : polar night flight

- Uses the winter stratospheric polar vortex
- Less stable than the summer vortex used in Antarctica
- Reliable forecast tools needed

16/Dec/2019: polar vortex

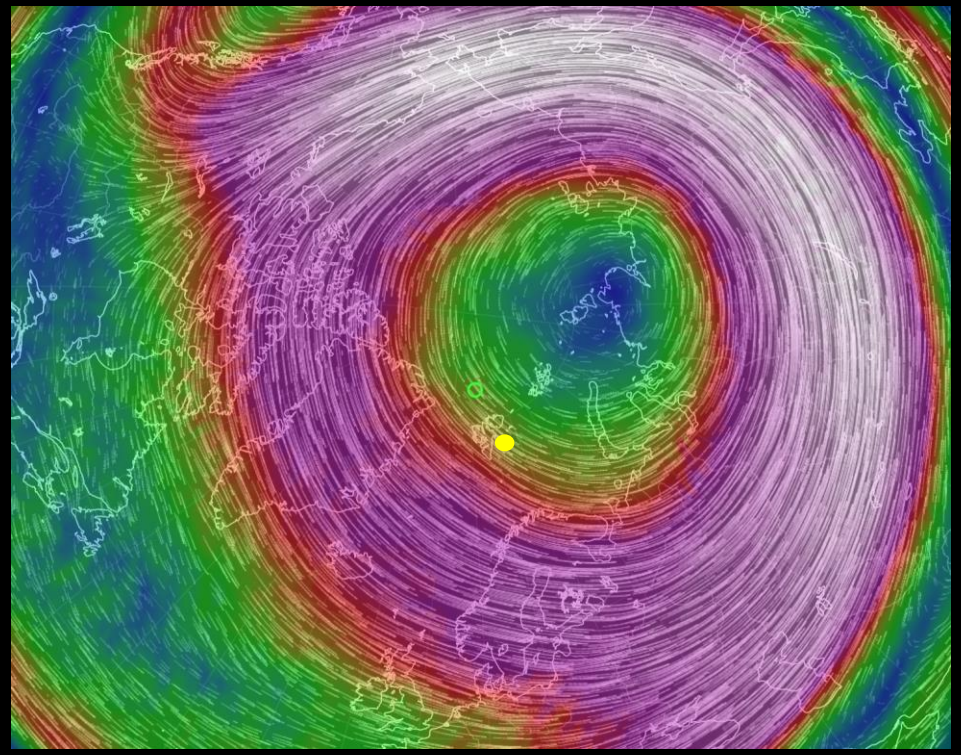

Credit: earth.nullschool.net

16/Dec/2019: flight forecast: 14 days

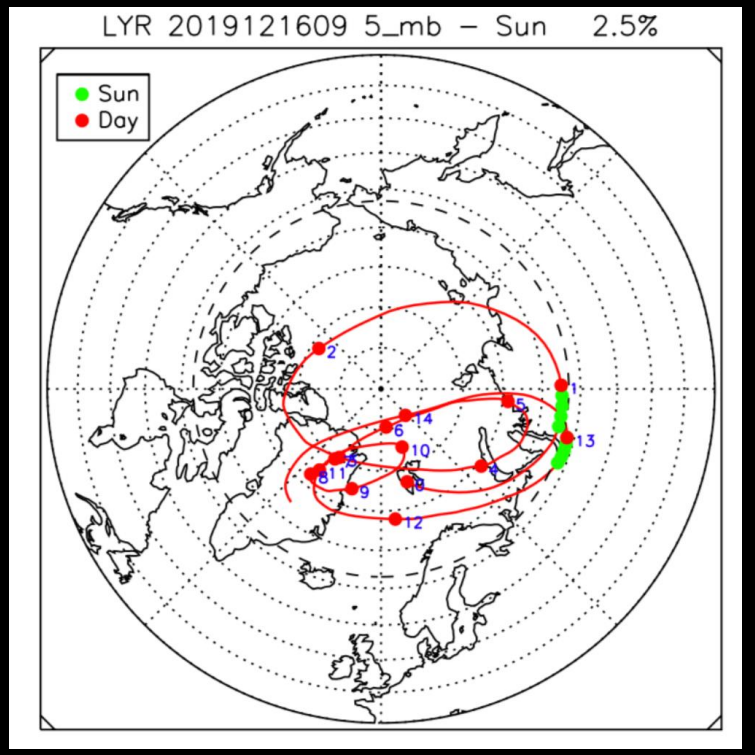

Credit: Piacentini

LSPE/SWIPE : night polar flight

- Flight managed by ASI, orgirnally scheduled for end of 2023 - Longyearbyen – Svalbard or Kiruna Sweden
- Several test flights already carried out
- On hold due to Russia-Ukraina war.

QUBIC, the Q&U Bolometric Interferometer for Cosmology

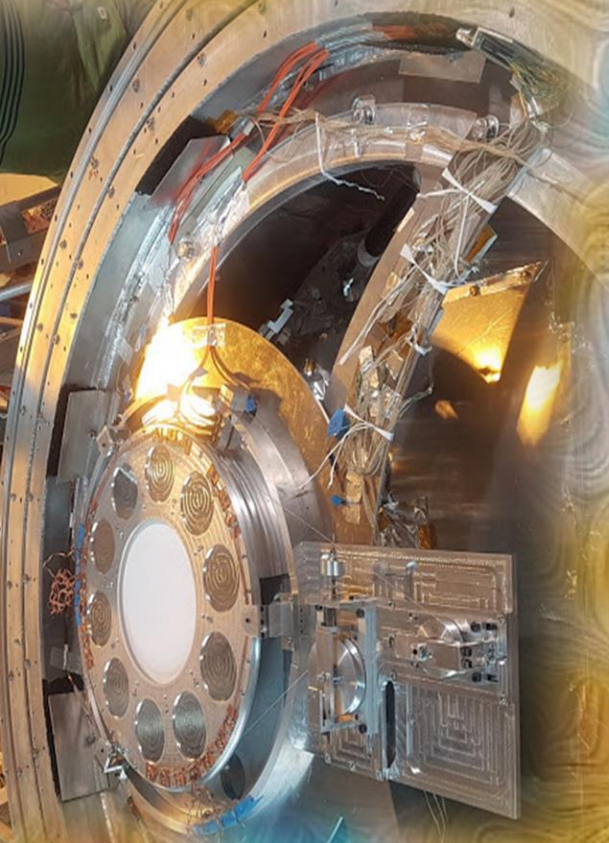

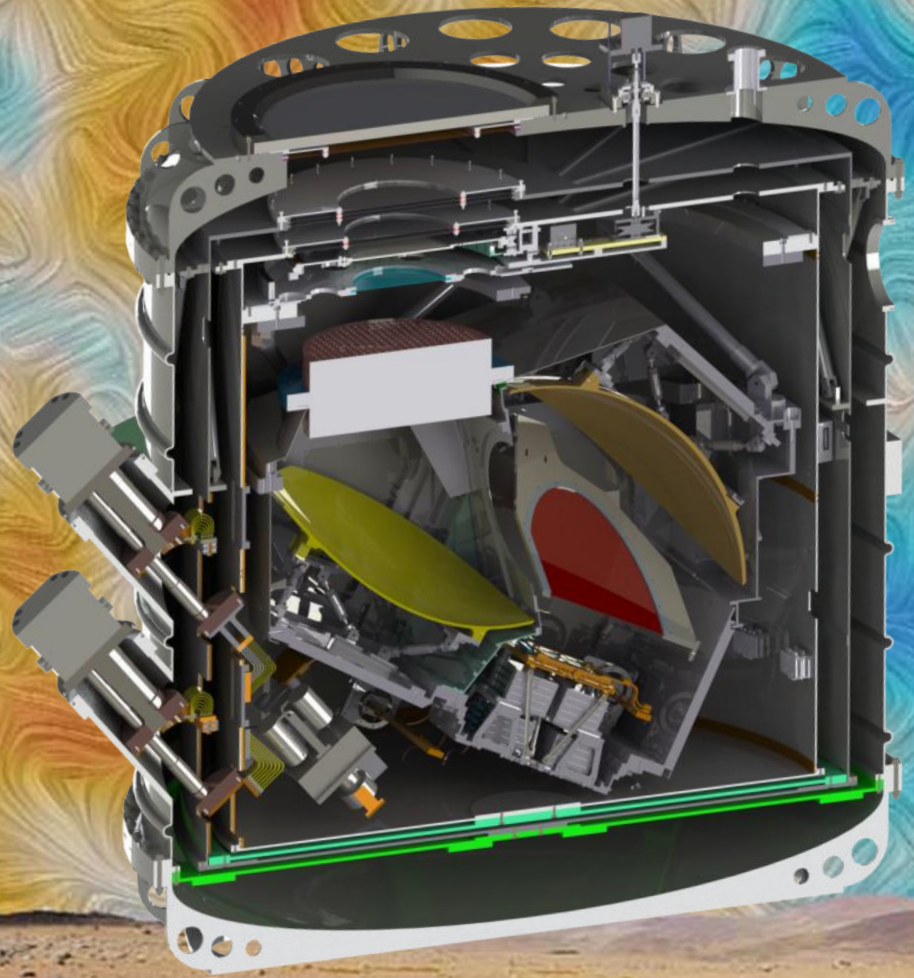

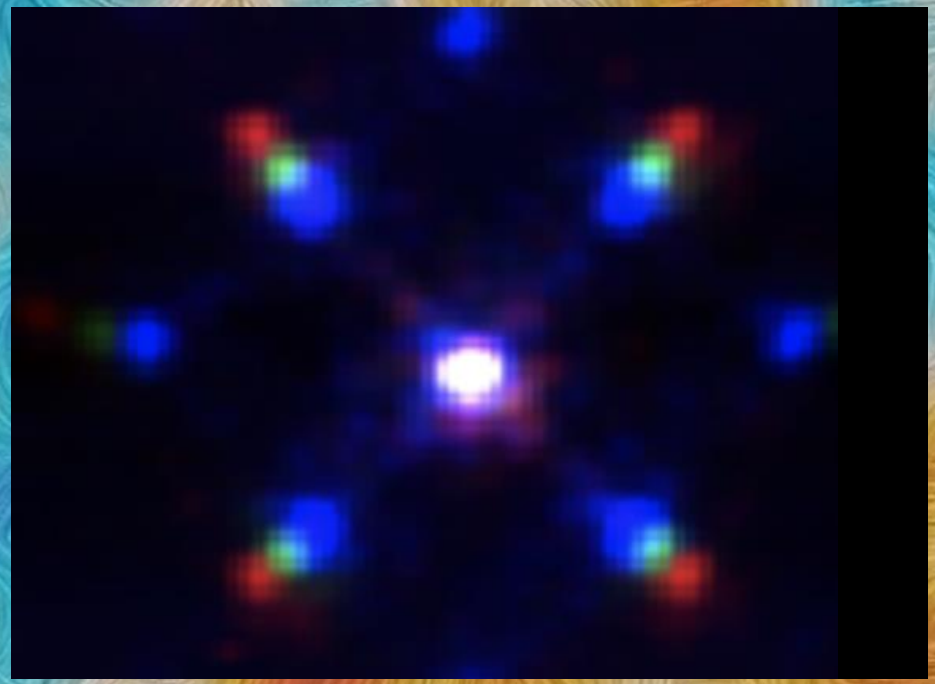

QUBIC

http://qubic.in2p3.fr/

a Q&U Bolometric Interferometer for Cosmology

APC Paris, France
C2N Orsay, France
CSNSM Orsay, France
IAS Orsay, France
IRAP Toulouse, France
LAL Orsay, France
Universita di Milano-Bicocca, Italy
Universita degli studi di Milano, Italy
Universita La Sapienza, Roma, Italy
Maynooth University, Ireland
Cardiff University, UK
University of Manchester, UK
Brown University, USA
Richmond University, USA
University of Wisconsin, USA
Centro Atómico Constituyentes, Argentina
GEMA, Argentina
Comisión Nacional de Energía Atómica, Argentina
Facultad de Cs Astronómicas y Geofísicas, Argentina
Centro Atómico Bariloche and Instituto Balseiro, Argentina
Instituto de Tecnologías en Detección y Astropartículas, Argentina
Instituto Argentino de Radioastronomía, Argentina

a large collaboration:

J.Ch. Hamilton, L. Mousset, E.S. Battistelli, M.-A. Bigot-Sazy, P. Chanial, R. Charlassier, G. D'Alessandro, P. de Bernardis, M. De Petris, M.M. Gamboa Lerena, L. Grandsire, S. Lau, S. Marnieros, S. Masi, A. Mennella, C. O'Sullivan, M. Piat, G. Riccardi, C. Scóccola, M. Stolpovskiy, A. Tartari, S.A. Torchinsky, F. Voisin, M. Zannoni, P. Ade, J.G. Alberro, A. Almela G. Amico, L.H. Arnaldi, D. Auguste, J. Aumont, S. Azzoni, S. Banfi, B. Bélier, A. Baù, D. Bennett, L. Bergé, J.-Ph. Bernard, M. Bersanelli, J. Bonaparte, J. Bonis, E. Bunn, D. Burke, D. Buzi, F. Cavaliere, C. Chapron, A.C. Cobos Cerutti, F. Columbro, A. Coppolecchia, G. De Gasperis, M. De Leo, S. Dheilly, C. Duca, L. Dumoulin, A. Etchegoyen, A. Fasciszewski, L.P. Ferreyro, D. Fracchia, C. Franceschet, K.M. Ganga, B. García, M.E. García Redondo, M. Gaspard, D. Gayer, M. Gervasi, M. Giard, V. Gilles, Y. Giraud-Heraud, M. Gómez Berisso, M. González, M. Gradziel, M.R. Hampel, D. Harari, S. Henrot-Versillé, F. Incardona, E. Jules, J. Kaplan, C. Kristukat, L. Lamagna, S. Loucatos, T. Louis, B. Maffei, W. Marty, A. Mattei, May, M. McCulloch, L. Mele, D. Melo, L. Montier, L.M. Mundo, J.A. Murphy, J.D. Murphy, F. Nati, E. Olivieri, C. Oriol, A. Paiella, F. Pajot, A. Passerini, H. Pastoriza, A. Pelosi , C. Perbost, M. Perciballi, F. Pezzotta, F. Piacentini, L. Piccirillo, G. Pisano, M. Platino, G. Polenta, D. Prêle, R. Puddu, D. Rambaud, P. Ringegni, G.E. Romero, E. Rasztocky, J.M. Salum, A. Schillaci, S. Scully, S. Spinelli, G. Stankowiak, A.D. Supanitsky, J.-P. Thermeau, P. Timbie, M. Tomasi, C. Tucker, G. Tucker, D. Viganò, N. Vittorio, F. Wicek, M. Wright, A. Zullo

QUBIC is looking for Primordial B-mode Polarization in the Cosmic Microwave Background

Very weak signal

- **Focal Plane:**
  - 2x1024 TES with NEP ~ $5x10^{-17}$ $W.Hz^{-½}$
  - 128:1 SQUIDs+ASIC Mux Readout
  - **End-To-End Sims. show σ(r)=0.015 (3 years ops.)**

Instrumental Systematics

- **Cryogenic Optics after HWP and Polarizer + Full power detectors**
  - Instrumental X-Polarization has small effect
- **400 elements Interferometer**
  - Synthesized Imaging (well controlled beam) – angular resolution 23.5 arcmin
  - Self-Calibration using switches + active source

Polarized Foregrounds

- **Two wide bands: 150 and 220 GHz**
- **Spectro-Imaging allows forming ≳ 4 sub-bands for each band**
  - Increased Frequency Resolution
  - Complex dust models can be constrained «locally»

QUBIC: a Stokes polarimeter plus an adding interferometer

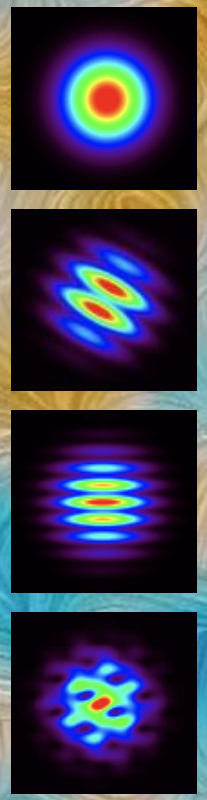

1 Horn open

2 Horns open

2 Horns open

All Horns open

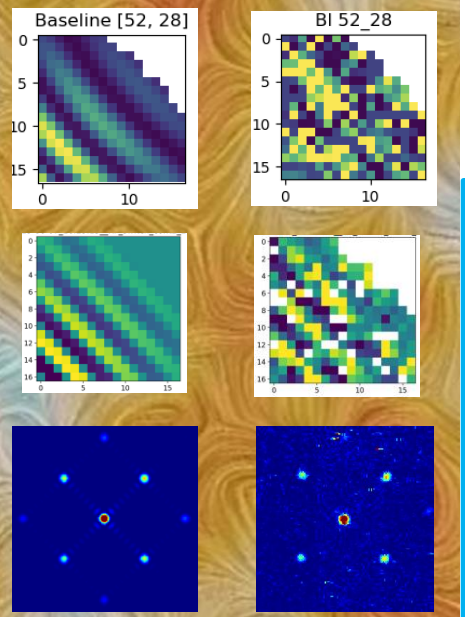

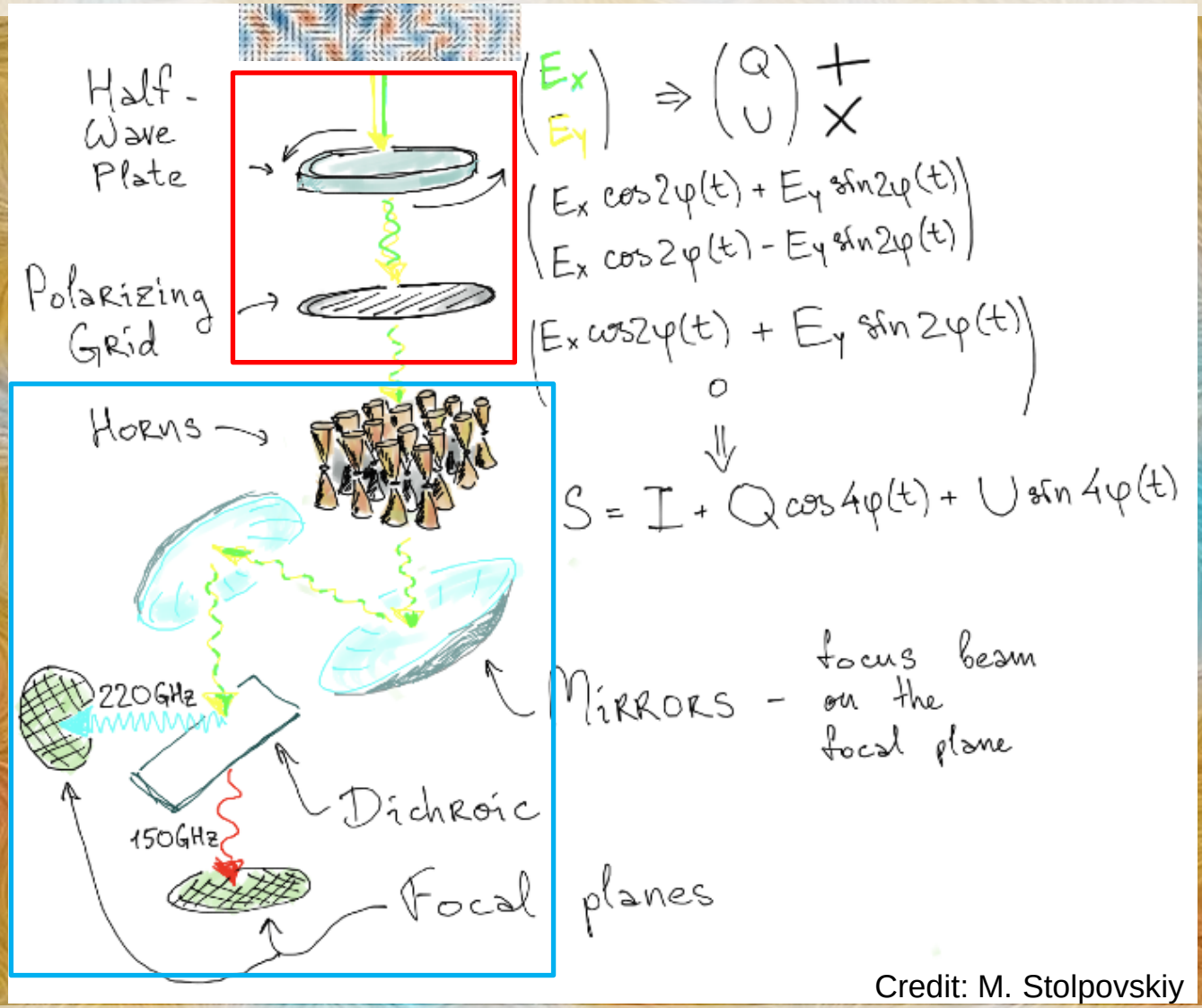

NB: Optical combiner + bolometer array is equivalent to a multi-elements coherent correlator

- 400 elements interf. (same bw) with usual correlators: 400x399/2x5x1000$ ~ 400 M$

Credit: M. Stolpovskiy

Fringe and Synthesized Beam data: [Torchinsky et al., QUBIC III, arXiv:2008.10056v3] (JCAP submitted)

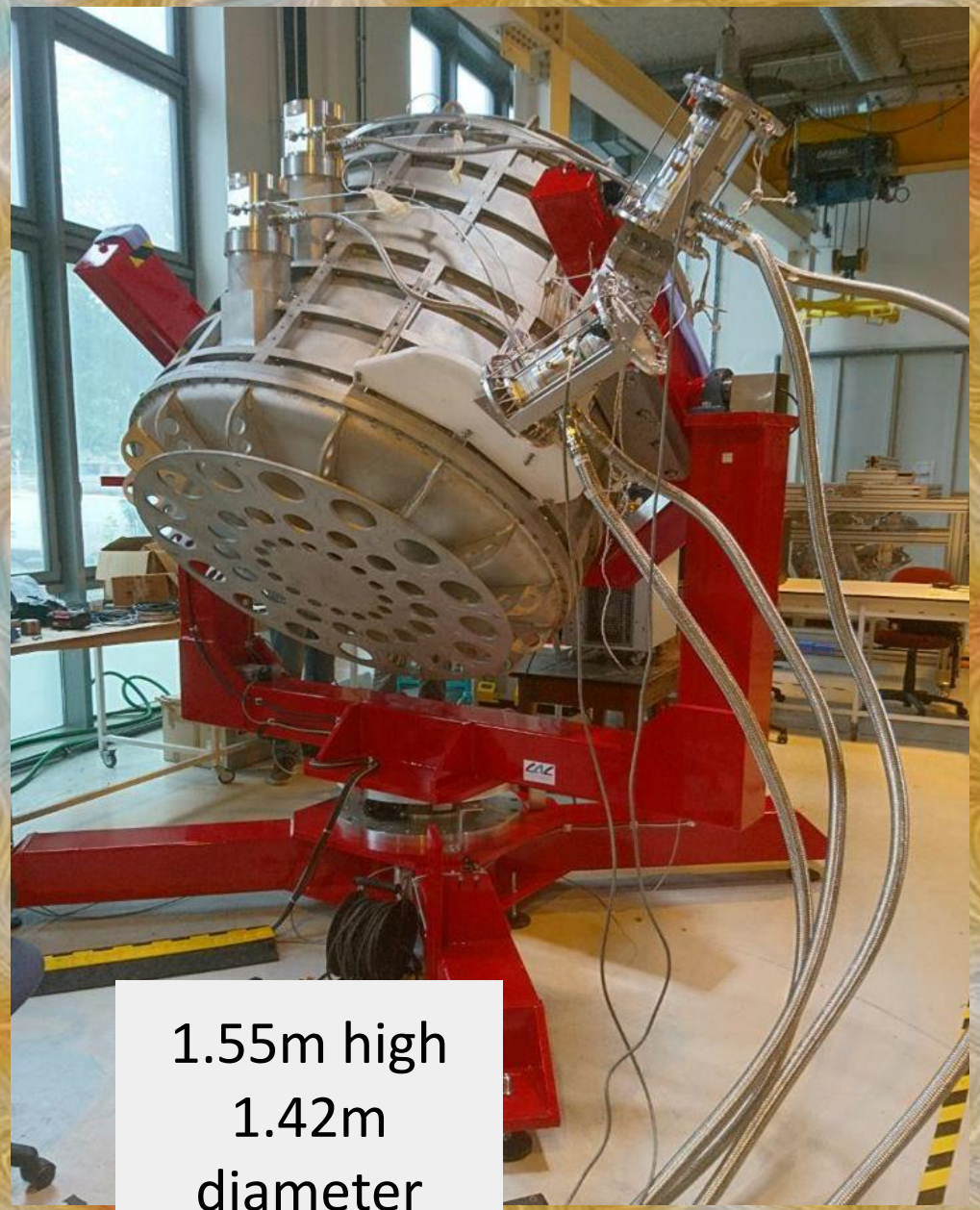

1.55m high
1.42m diameter
About 800kg

- **Main cryostat: Roma1**
- 1K Box / detectors: APC, CSNSM / IRAP
- Sub-K refrigerators: Manchester
- **Optics: Roma1** / **Milano** / Maynooth / Cardiff
- **Feedhorns arrays & Switches: Milano**
- **Cryogenic rotator of polarization modulator: Roma1**
- Mount: La Plata
- Site: CNEA
- Calibration Mount: IJCLab
- Integration, Calibration and testing: APC

Tests showed:

- Expected behavior and performance of the instrument
- Bolometric Interferometry in the laboratory

Inauguration:
November 22, 2022
In **Alto Chorrillo**
4980 m osl

Now commissioning

Space-borne: LiteBIRD (JAXA, 2029)

	ID	ν [GHz]	$\delta\nu$ [GHz] ($\delta\nu/\nu$)	Beam size [arcmin]	No. of detectors	NET$_{\rm arr}$ [μK$\sqrt{\rm s}$]	Sensitivity [μK-arcmin]
LFT	1	40	12 (0.30)	70.5	48	18.50	37.42
LFT	2	50	15 (0.30)	58.5	24	16.54	33.46
LFT	3	60	14 (0.23)	51.1	48	10.54	21.31
LFT	4	68	16 (0.23)	(41.6, 47.1)	(144, 24)	(9.84, 15.70)	(19.91, 31.77)
comb.						8.34	16.87
LFT	5	78	18 (0.23)	(36.9, 43.8)	(144, 48)	(7.69, 9.46)	(15.55, 19.13)
comb.						5.97	12.07
LFT	6	89	20 (0.23)	(33.0, 41.5)	(144, 24)	(6.07, 14.22)	(12.28, 28.77)
comb.						5.58	11.30
LFT/	7	100	23 (0.23)	30.2/	144/	5.11/	10.34
MFT				37.8	366	4.19	8.48
comb.						3.24	6.56
LFT/	8	119	36 (0.30)	26.3/	144/	3.8/	7.69
MFT				33.6	488	2.82	5.70
comb.						2.26	4.58
LFT/	9	140	42 (0.30)	23.7/	144/	3.58/	7.25
MFT				30.8	366	3.16	6.38
comb.						2.37	4.79
MFT	10	166	50 (0.30)	28.9	488	2.75	5.57
MFT/	11	195	59 (0.30)	28.0/	366/	3.48/	7.05
HFT				28.6	254	5.19	10.50
comb.						2.89	5.85
HFT	12	235	71 (0.30)	24.7	254	5.34	10.79
HFT	13	280	84 (0.30)	22.5	254	6.82	13.80
HFT	14	337	101 (0.30)	20.9	254	10.85	21.95
HFT	15	402	92 (0.23)	17.9	338	23.45	47.45
Total					4508		2.16

Target: r=0.001 !

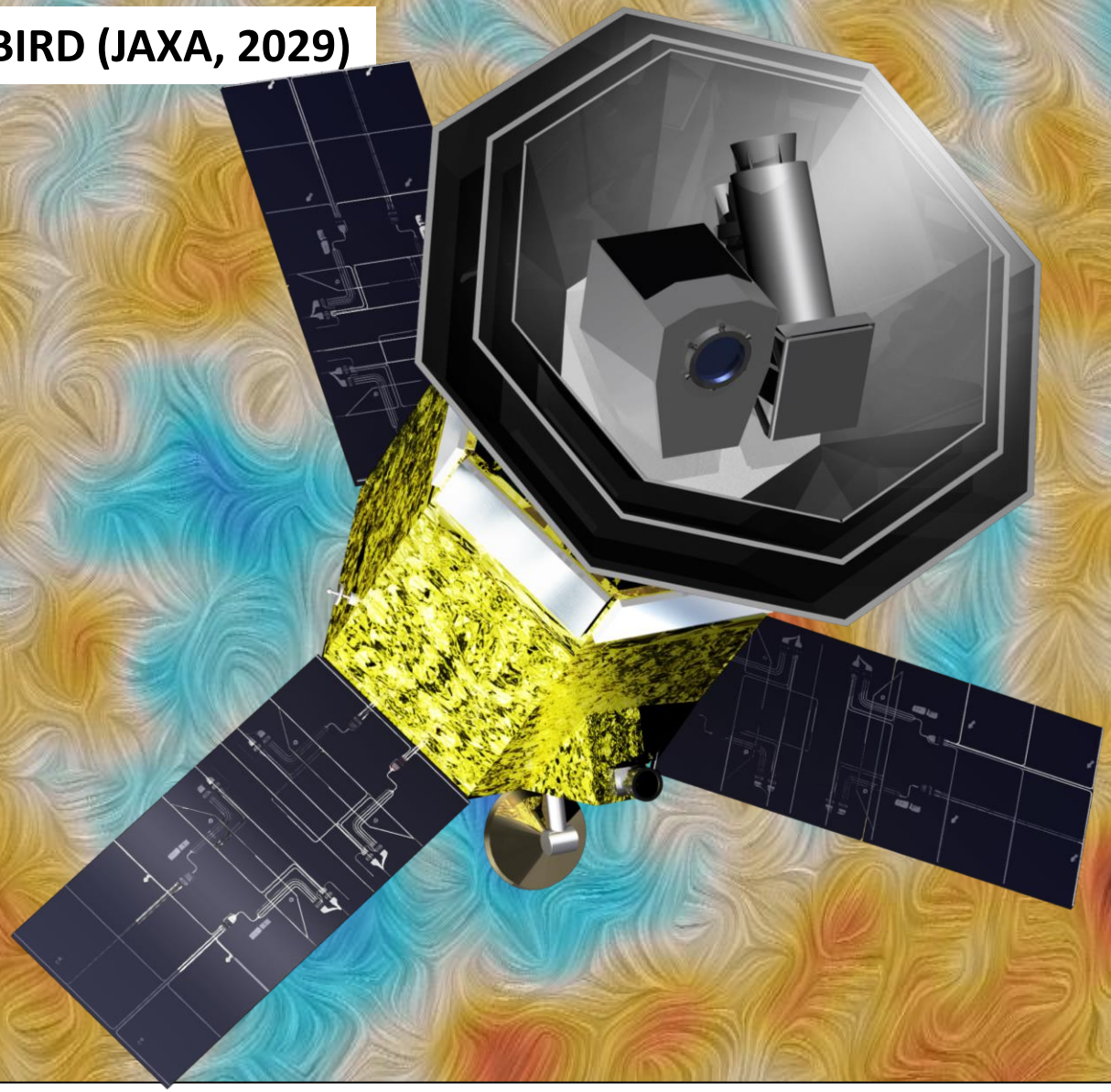

Probing Cosmic Inflation with the LiteBIRD Cosmic Microwave Background Polarization Survey, *Progress of Theoretical and Experimental Physics*, ptac150 (2022) arXiv-2202.02773

Probing Cosmic Inflation with the LiteBIRD Cosmic Microwave Background Polarization Survey, *Progress of Theoretical and Experimental Physics*, ptac150 (2022) arXiv-2202.02773

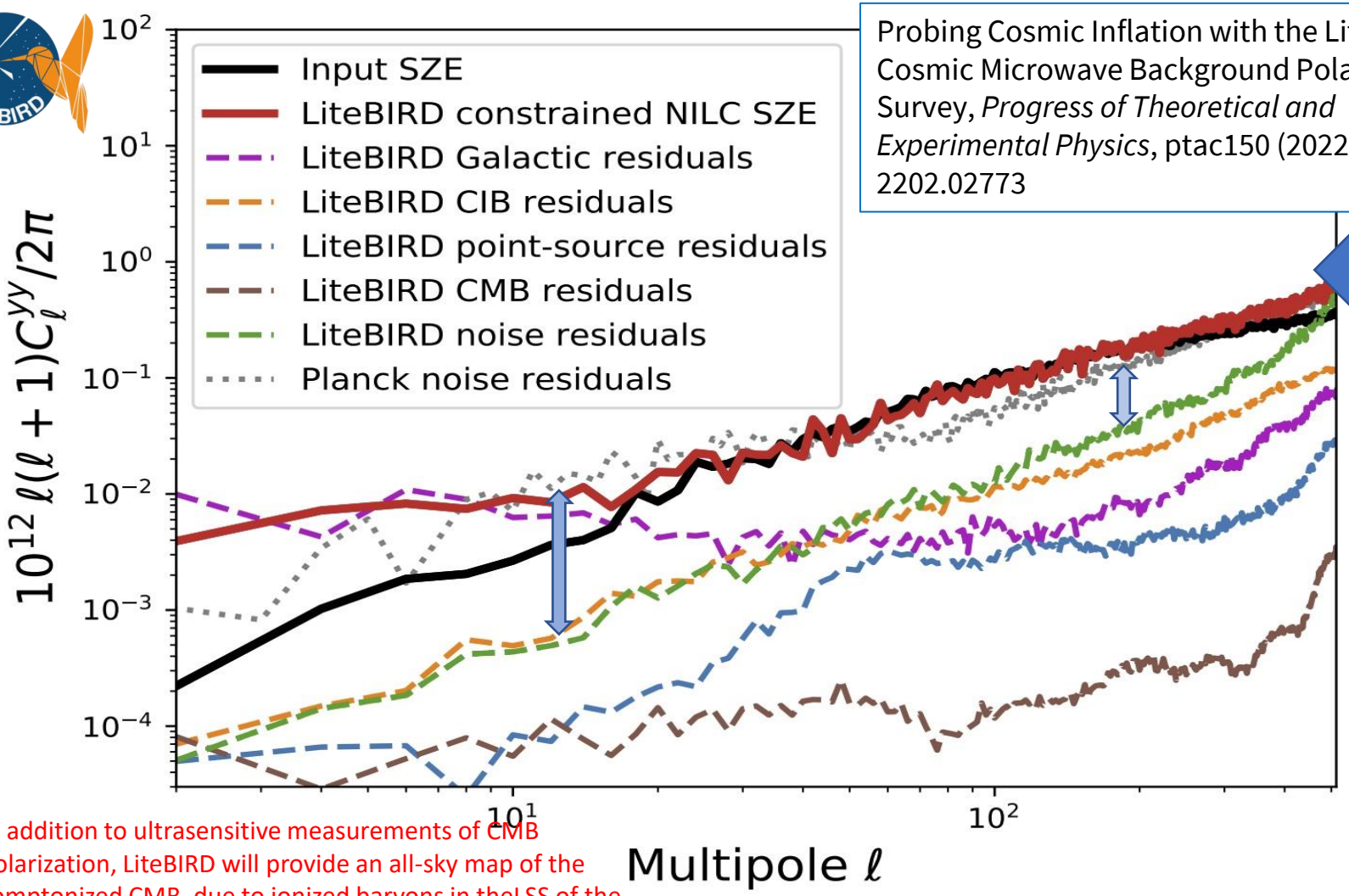

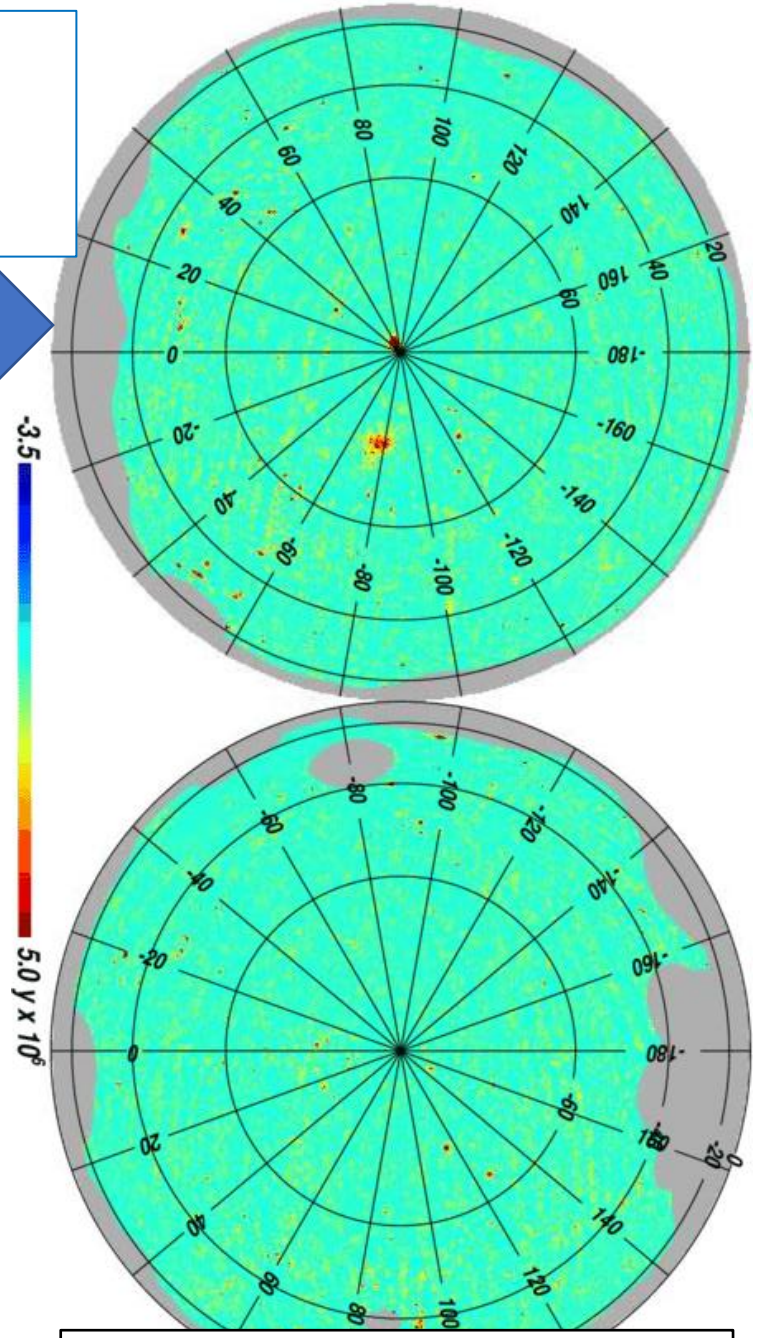

In addition to ultrasensitive measurements of CMB polarization, LiteBIRD will provide an all-sky map of the comptonized CMB, due to ionized baryons in theLSS of the universe, improving over Planck by a significant factor.

Fig. 52: Reconstructed power spectrum of the thermal SZ effect from a simulation of *LiteBIRD* (red line), compared with the input one (black line). Both agree well except at $\ell < 20$, which still shows residuals from the Galactic emission; however, such low multipoles suffer from large non-Gaussian cosmic-variance error bars in any case. The noise power spectrum of *LiteBIRD* (green dashed line) is much lower than that of *Planck* (gray dotted line), showing the substantially improved sensitivity and fidelity of the thermal SZ map from *LiteBIRD*.

https://irsa.ipac.caltech.edu/data/Planck/release_2/all-sky-maps/foregrounds.html

ACT / ACTpol

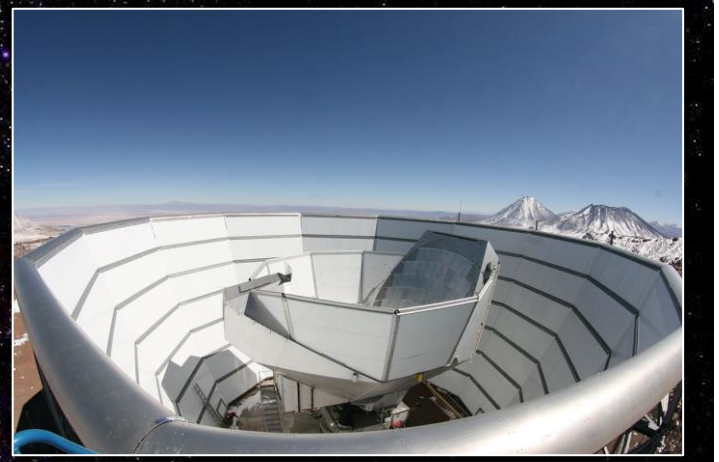

The six-meter Atacama Cosmology Telescope (ACT) in Chile was built to measure the cosmic microwave background (CMB) at *arcminute* angular scales.
Operates from Cerro Toco @ 5200 m osl.
A large steady ground shield and a comoving shield surround an 6m off-axis telescope with a large format bolometric receiver.
Main results in Aiola+ arXiv:2007.07288. Data are availability Mallaby-Kay arXiv: 2103.03154. Way more than polarization power spectra ! e.g. lensing maps and SZ cluster catalogue with 4000+ clusters.

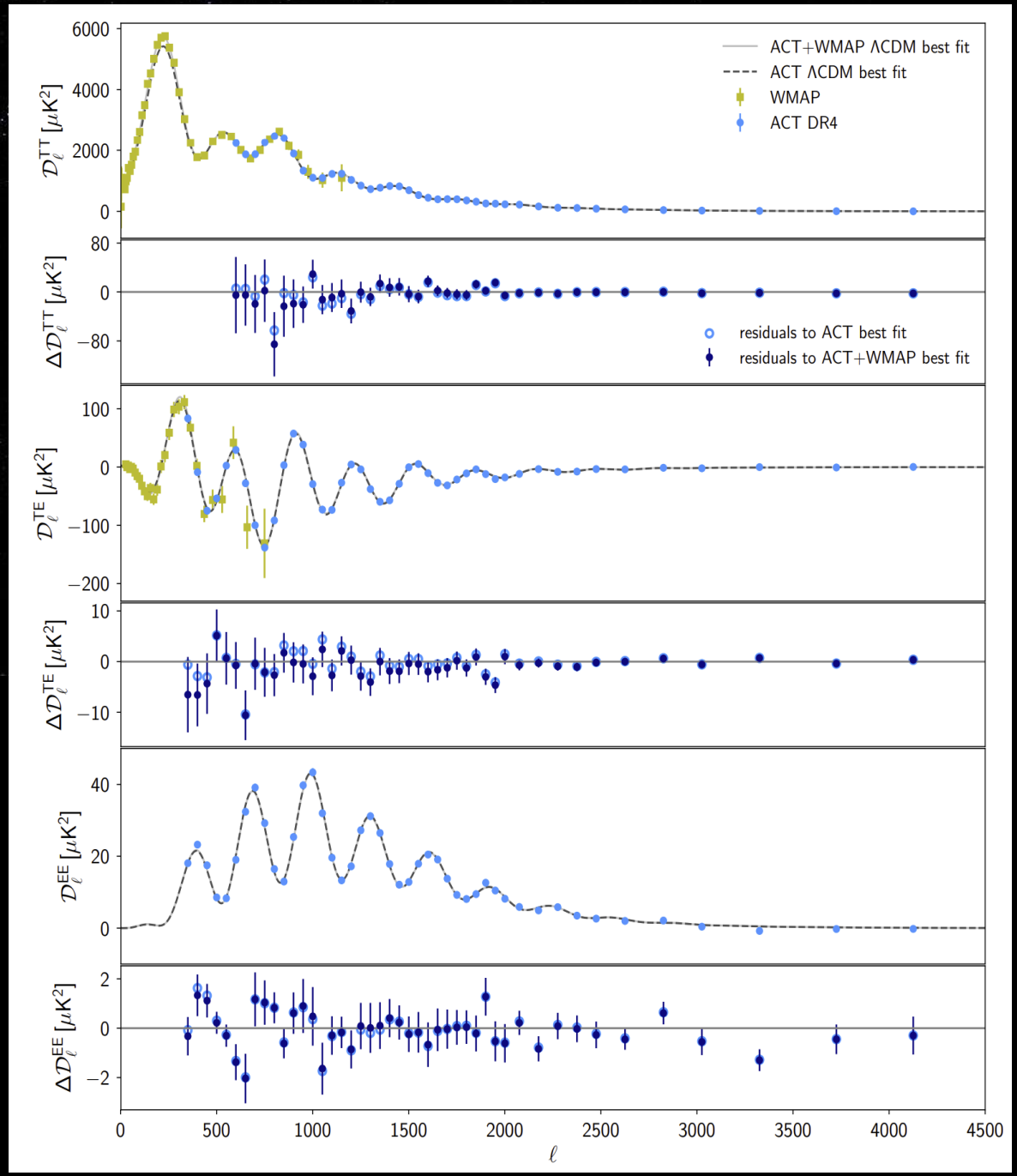

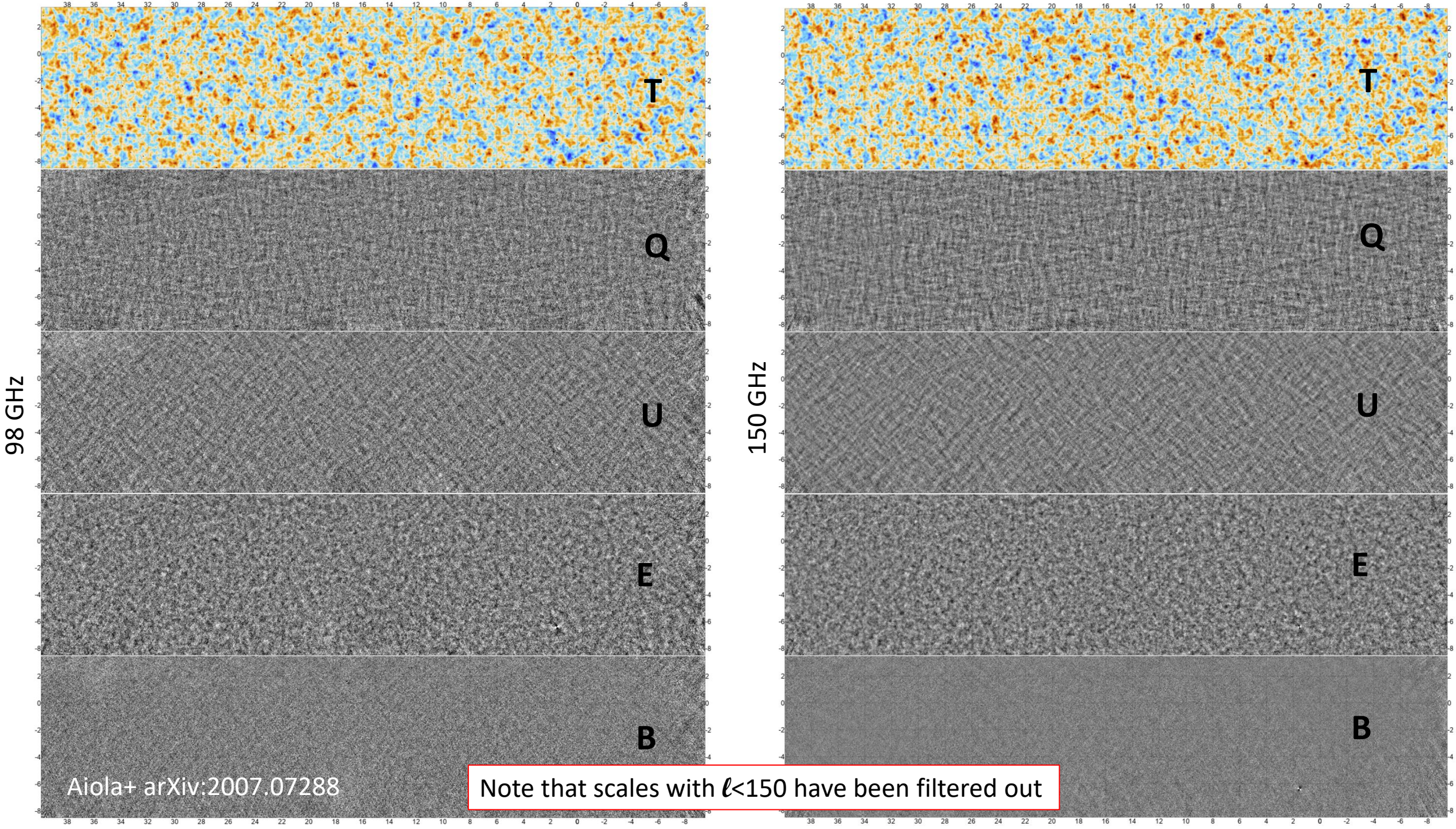
98 GHz
150 GHz
T
Q
U
E
B
Aiola+ arXiv:2007.07288
Note that scales with ℓ<150 have been filtered out

- Two ways to constrain post recombination large-scale structures using CMB anisotropy and polarization experiments:
- Using the lensing deflection (due to *all* the mass) Lewis, A., & Challinor, A., Phys. Rep., **429**, 1 (2006). Correlating with CIB / galaxy z surveys it is possible in principle to obtain matter density tomography up to high redshifts.
- Using the Sunyaev-Zeldovich effect (due to *ionized baryons*) J.E. Carlstrom & ARAA, **40**, 643 (2002). This can be observed in clusters but also in filaments. The thermal component maps the density, while the kinetic part maps the velocity (and possibly turbulence) of the ionized medium. Linear with *n*, so more sensitive than X-rays in low density regions (filaments).
- Simulations from CMB-S4 Science Case, Reference Design, and Project Plan - arXiv-1907.04473
- Angular resolution is very important !

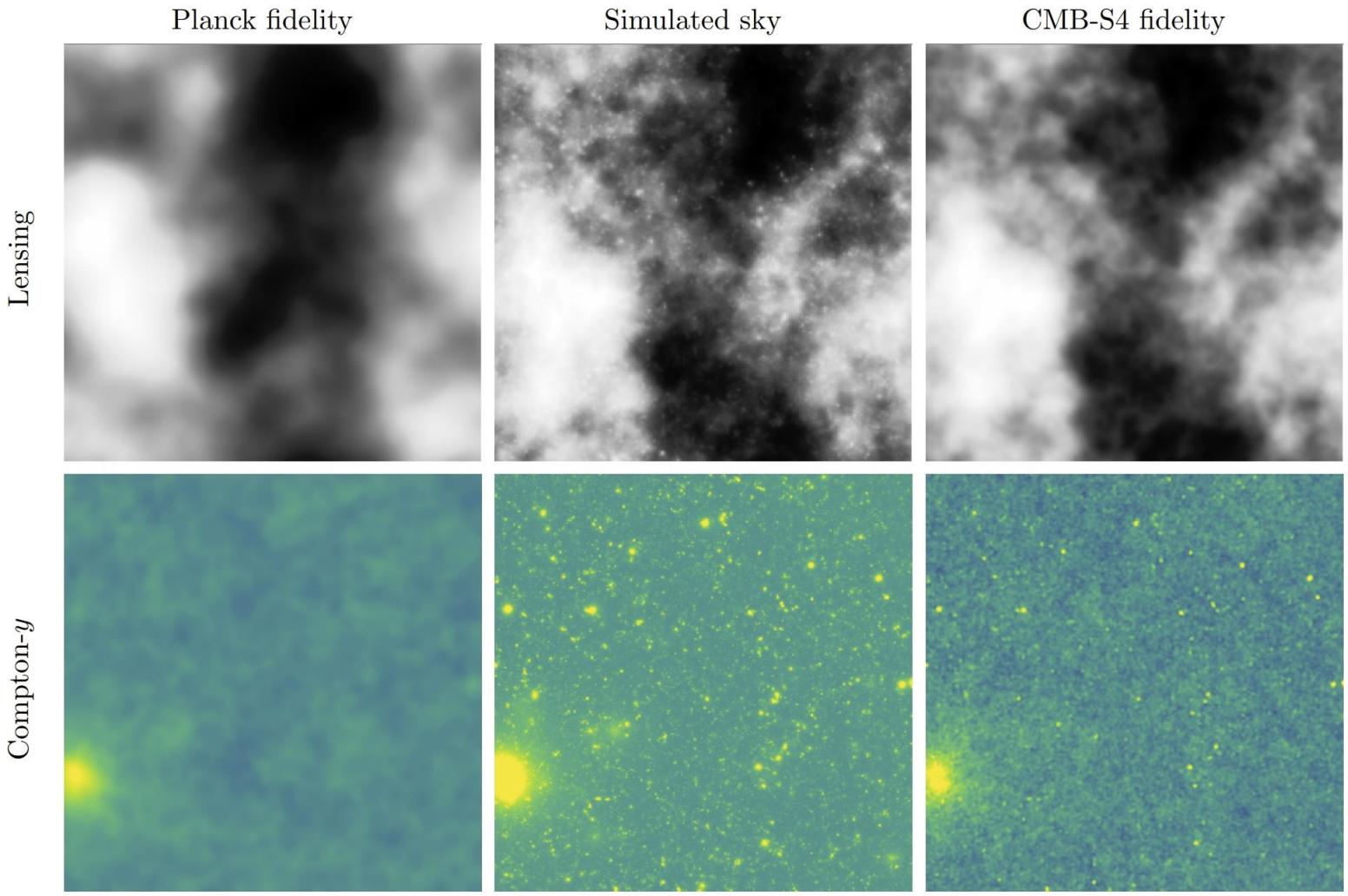

Figure 3. *Example lensing-deflection maps (top) and thermal SZ (Compton y-maps, bottom) reconstructed with Planck (left) and CMB-S4 data (right). The center panels show a 25 deg^2 patch of the all-sky lensing-deflection field in the WebSky simulations (top) and Compton y (bottom). The left panels show Wiener-filtered maps of the signal after adding (Gaussian) noise and residual foregrounds with levels corresponding to the Planck 2018 lensing-deflection map (top) and the Planck 2015 "Needlet Internal Linear Combination" tSZ map (bottom). The right panel shows analogous Wiener-filtered maps with noise expected for CMB-S4 (top) and residual foregrounds determined by the CMB-S4 + Planck tSZ noise power spectrum in Fig. 20. The significantly higher fidelity of the CMB-S4 reconstruction is evident.*

Clusters and the Sunyaev-Zeldovich effect

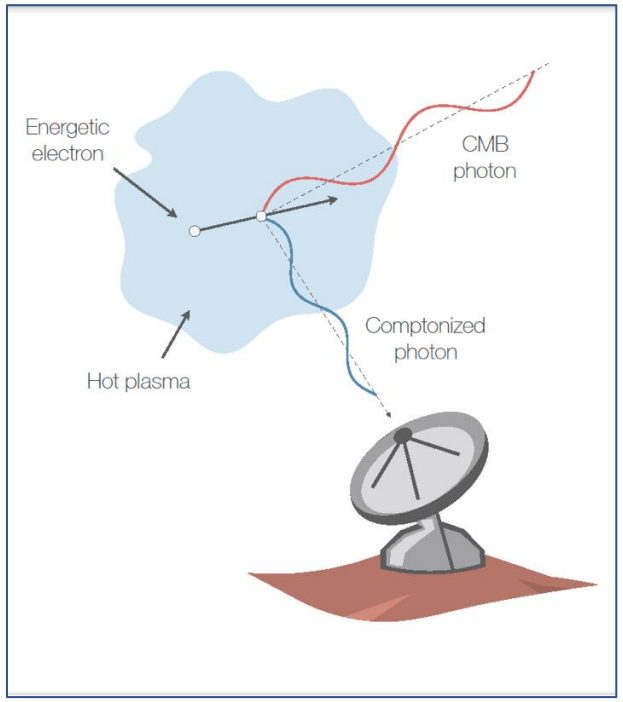

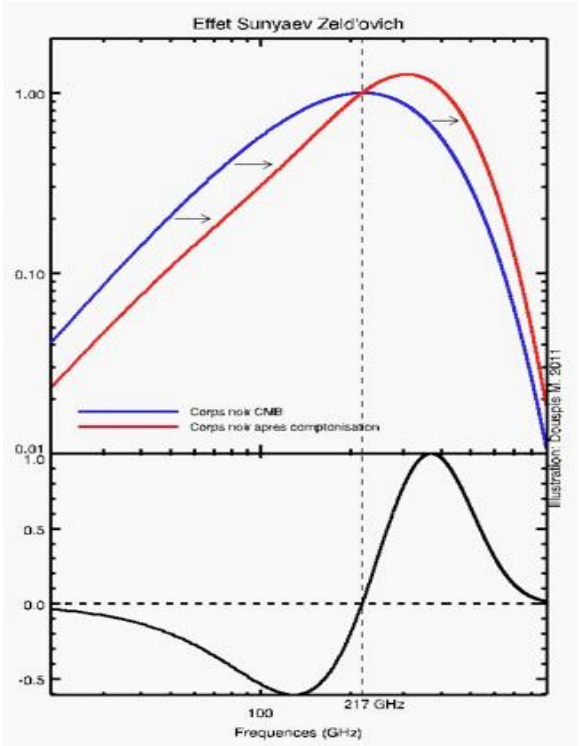

$$\Delta I(x) = \mathrm{y I_0\, g(x)}$$ Thermal SZ

$$\mathrm{y} = \int n_e \sigma_T \frac{k_B T_e}{m_e c^2} dl = \tau \theta_e$$

$$\mathrm{g(x)} = \mathrm{x}^4 \frac{e^x}{(e^x - 1)^2} \left[x \cdot coth\left(\frac{x}{2}\right) - 4 \right]$$

while X.Ray Bremmstrahlung $X_{br} \propto n_e^2 \cdot \sqrt{T_e} \cdot l$

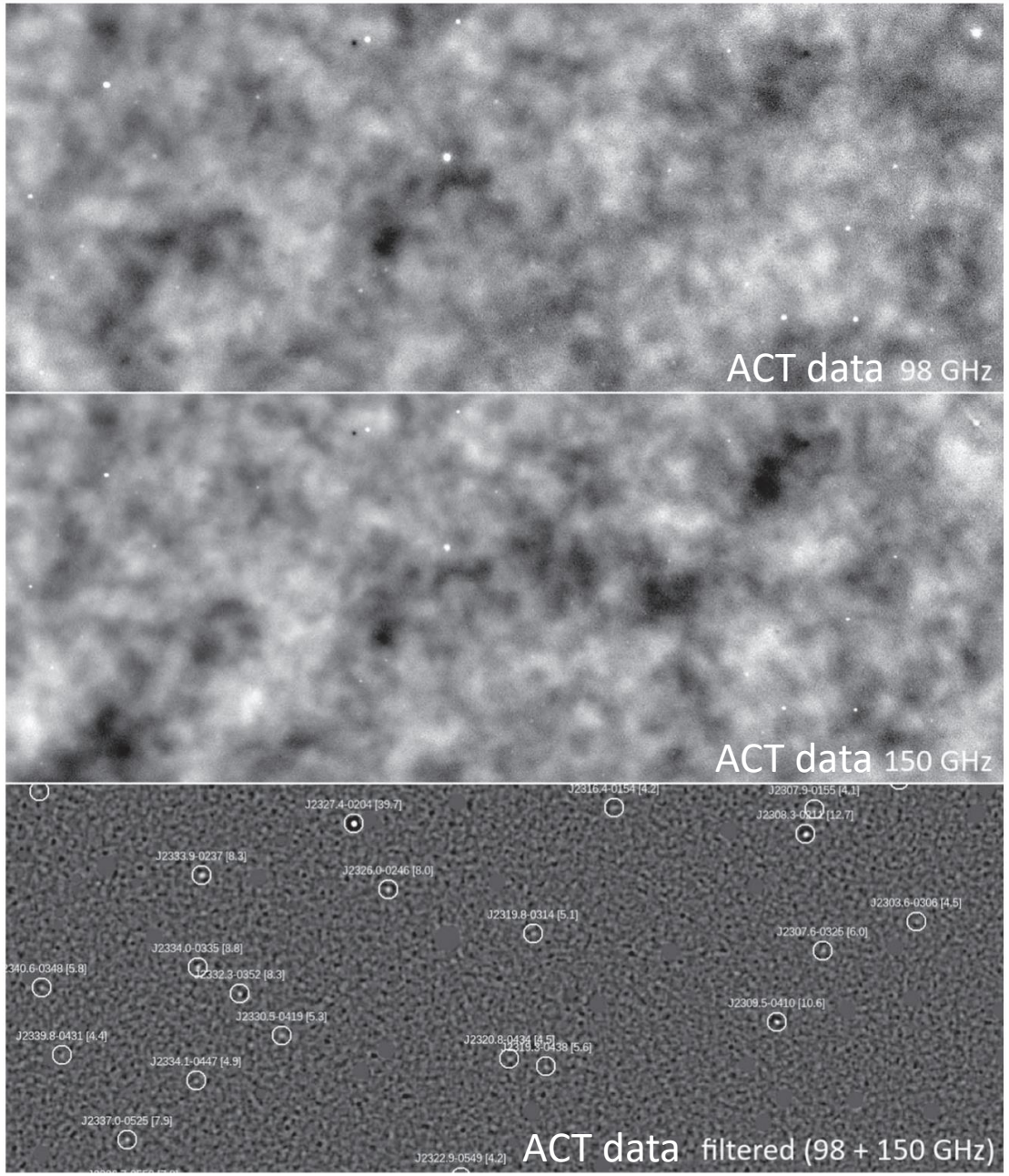

Figure 3. Comparison between the unfiltered 98 and 150 GHz maps and the filtered S/N map, for an approximately 10 deg × 4 deg patch of sky. In the unfiltered maps, clusters appear as decrements (dark spots) in the map. Point sources appear as white spots, and CMB fluctuations dominate at large angular scales. In the filtered S/N map, clusters appear as white spots (marked with white circles to guide the eye; the number given in brackets is $S/N_{2.4}$), and point sources have been masked. The brightest object visible is the $z = 0.70$ cluster ACT-CL J2327.4-0204 (center left, near the top left of the image), which is an $S/N_{2.4} = 39.7$ detection.

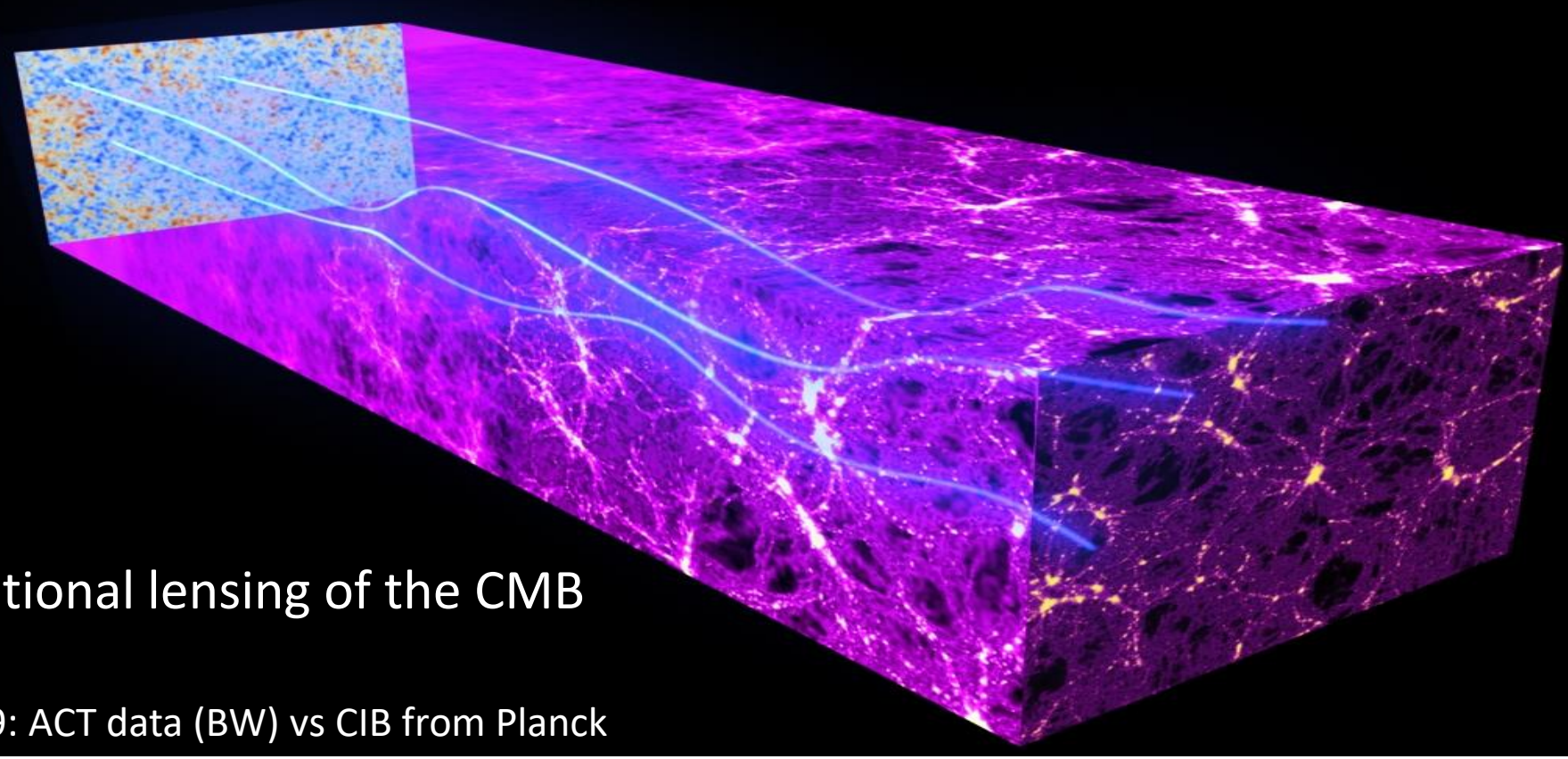

Weak gravitational lensing of the CMB

arXiv:2004.01139: ACT data (BW) vs CIB from Planck

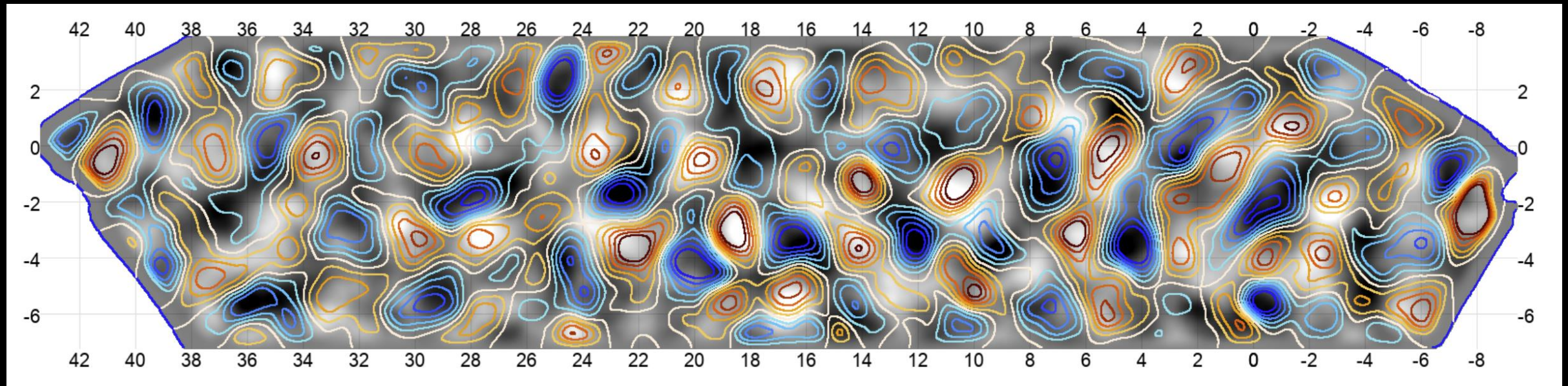

Ground-based: CMB S-4 (DOE, >2030)

LATs

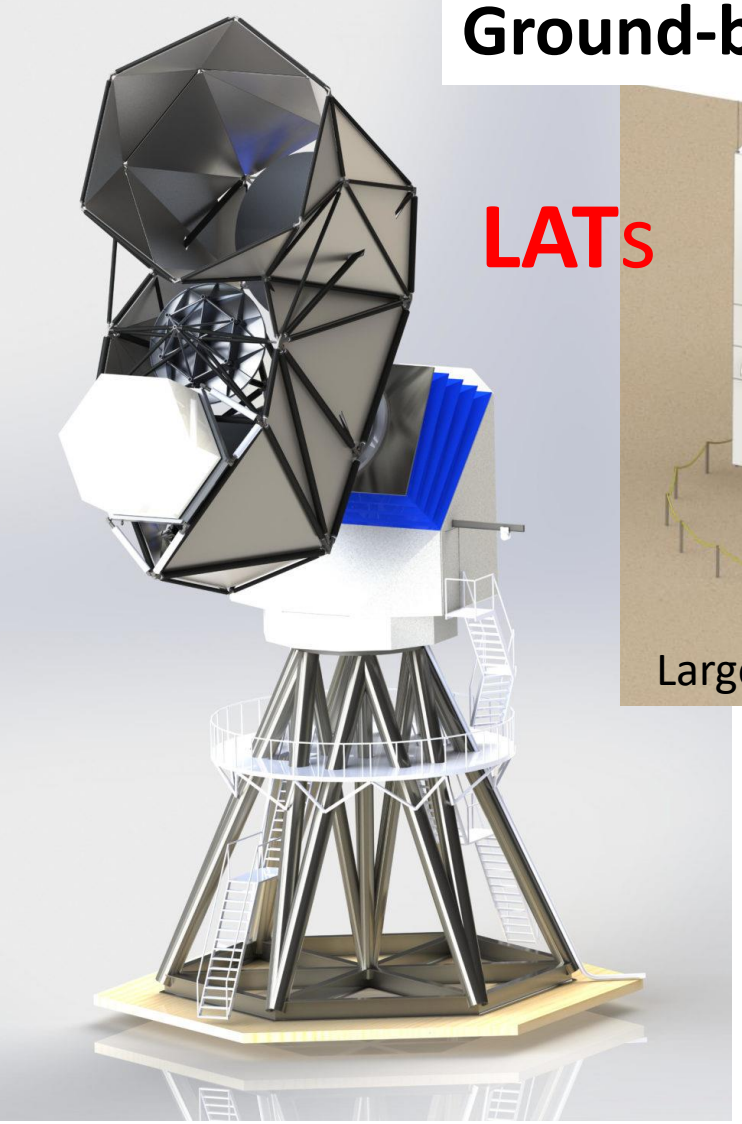

Large-Aperture (5m) Telescope (South Pole)
150000 superconducting detectors

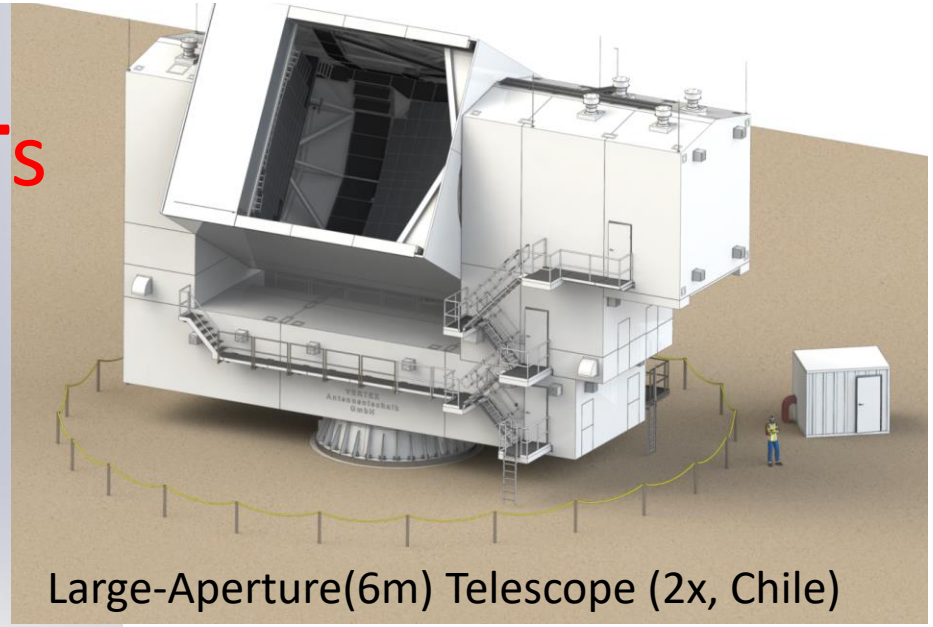

Large-Aperture(6m) Telescope (2x, Chile)

1.5’ FWHM @150 GHz
each with 130000
superconducting detectors

SATs

18 Small-Aperture
(0.5m) Telescopes
(Chile)
30-300 GHz
150000
superconducting
detectors

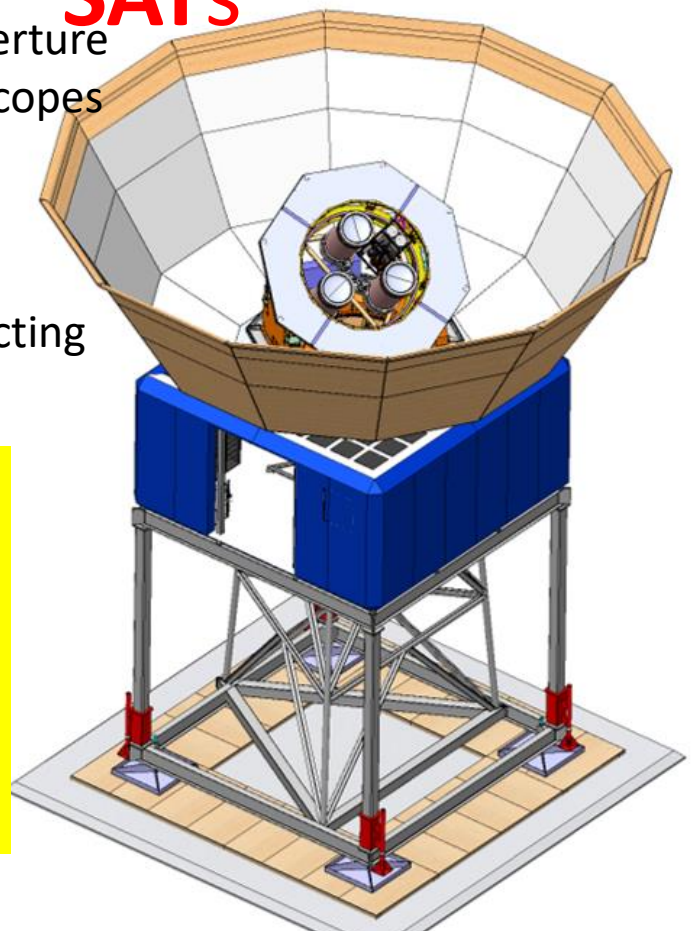

For the study of LSS, clusters and filaments, LATs will be incredibly effective, boosting the number of measured SZ clusters by a factor >10 wrt current knowledge.

Study of clusters and filaments with the SZ

- Mainstream:
  - Simon Observatory, CCAT, CMB-S4: large area ~ arcmin resolution surveys for clusters catalogues in the entire Hubble volume
- Two main instrumental improvement avenues:
  - Higher Angular Resolution (substructures, internal dynamics, …)
  - Higher frequencies (more accurate measurements, high resolution, dust & CIB monitoring …)
  - Implementation:
    - Low-frequency: very large ground-based telescopes: NIKA2@ IRAM30m, MISTRAL @ SRT, Mustang2 @GBT , ….
    - Balloon-borne telescopes (OLIMPO, Exclaim, ….) and, in the long term, a space mission (PICO, ESA-Voyage-2050 …).

First example of **synergy** in clusters/filaments studies: ACT + Planck provide “low” resolution map, Mustang2@GBT provides high resolution for complementary fluctuations analysis.

 MNRAS 510, 3335–3355 (2022)

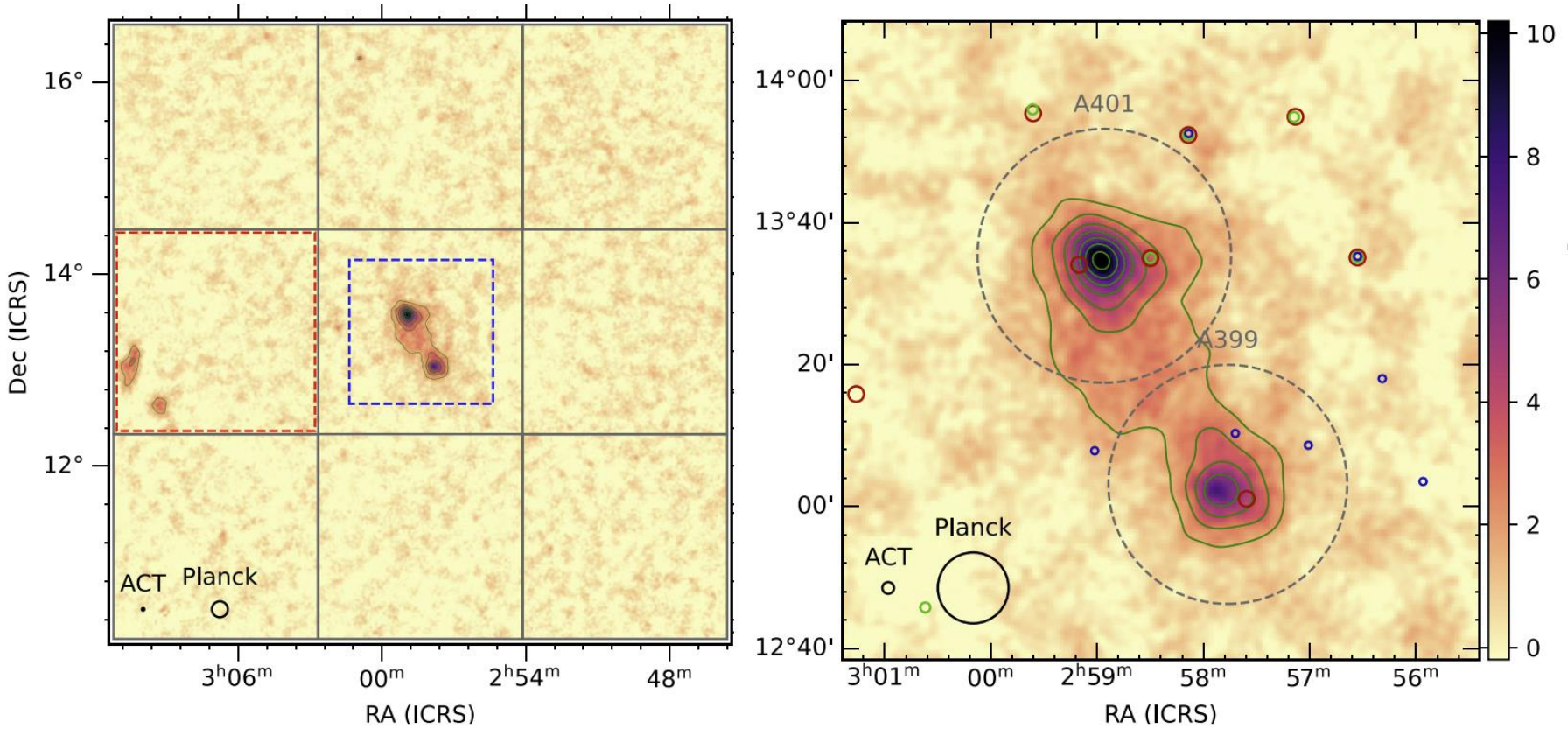

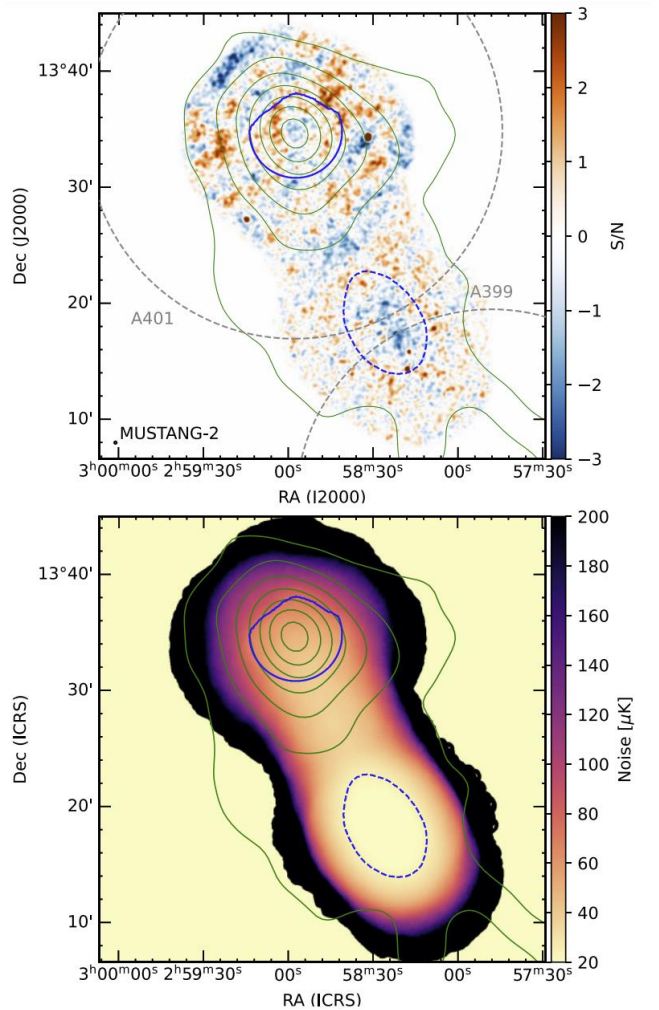

Figure 1. Left-hand panel: Compton-y map of A401 (north-east) and A399 (south-west) made with ACT and *Planck* data (see the text for details). Contour levels are at 3, 5, 7, 9, 11, 13, and 15σ. Of the eight perimeter regions (grey boxes), the region to the east (marked with a dashed red box) is excluded from the covariance analysis due to dust contamination. The dashed blue region denotes the zoom-in shown to the right. Right-hand panel: The panel shows a zoom-in on the dashed blue region in the left-hand panel, with the clusters denoted by dashed circles corresponding to their measured R_{500c} (the radius inside of which the average density of the cluster is 500 times the critical density of the Universe; see Table 4). The solid black circles in the lower left of each panel show the 1.65 arcmin effective beam size of our map, driven by ACT's high resolution, as well as the 10 arcmin resolution of the *Planck*-only MILCA y-map (see Section 4.1). Compact sources detected in the ACT maps are represented by coloured circles, where the sizes reflect the FWHM of the beam at that frequency and the colours – red, blue, and green – indicate the 98, 150, and 224 GHz data. The colour scale is the same in both panels.

igure 2. The images show (top) the MUSTANG-2 signal-to-noise (S/N) nd (bottom) the MUSTANG-2 RMS (noise per beam) map, respectively. he effective resolution (12.7 arcsec) of the smoothed map is depicted as a mall circle in the lower left-hand corner of the top panel. The regions used or pressure fluctuation analysis (Section 5) are shown with solid and dashed lue regions, corresponding to A401 and the bridge region, respectively. The ontours and R_{500c} regions from the left-hand panel of Fig. 1 are overlaid (in reen) for reference. We note that the region mapped by MUSTANG-2, and isplayed here, was only a portion of that displayed in Fig. 1, and A399 was ot included in these MUSTANG-2 observations.

OLIMPO

- Extend SZ measurements to high frequencies:
- Telescope on a stratospheric balloon. At 300 - 400 GHz, a 2.6m aperture telescope matches the resolution of ground based 10m telescopes operating at 150 GHz.
- Focus on selected targets to get *accurate* multiband photometry
- Use nearby clusters to study internal structure of thermal ICM + relativistic component
- Use thermal and kinetic SZ to study the dynamics -> energetics
- Payload flown with ASI + SSC in 2018 – very successful technology demonstration. (see Masi+ *JCAP* 07 (2019) 003)
- Now proposed to NASA for Antarctic LDB science flight (Hanany & Masi 2022).

OLIMPO LDB

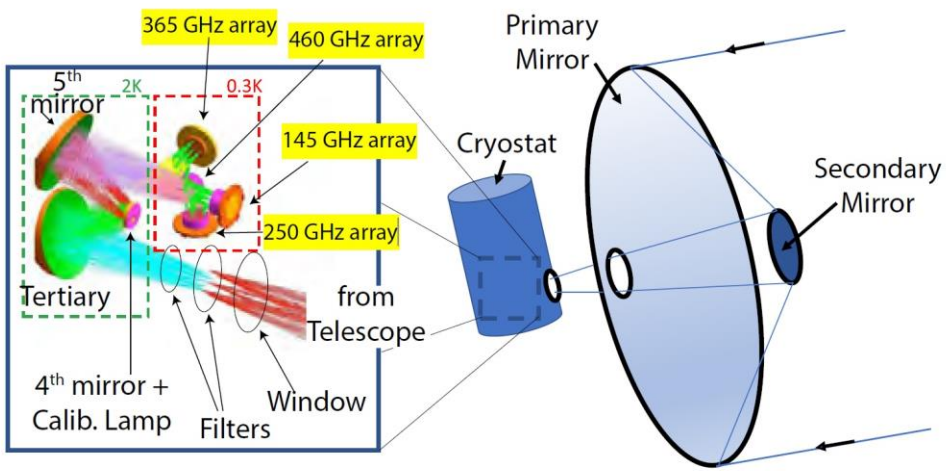

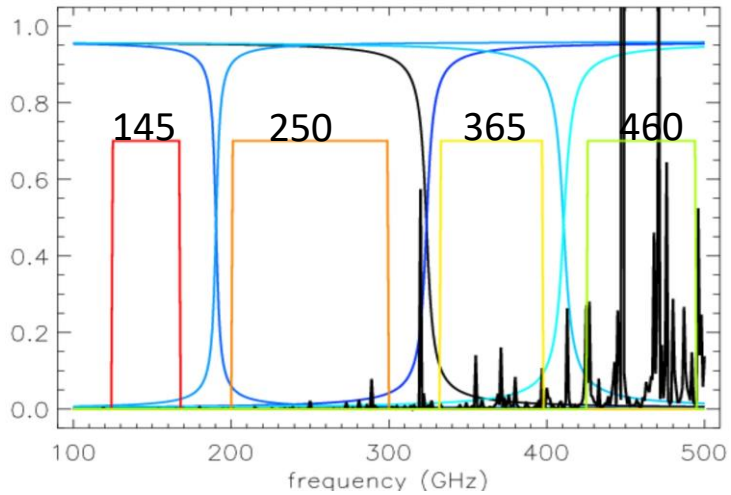

Figure 8: **Two left panels:** Schematic diagram of the OLIMPO instrument. From right to left: a two-mirror Ritchey-Chretien telescope feeding a cryogenic receiver with reimaging optics and four arrays at frequencies between 145 and 460 GHz. **Right:** The OLIMPO payload on the launch pad in Svalbard, Norway, in 2018.

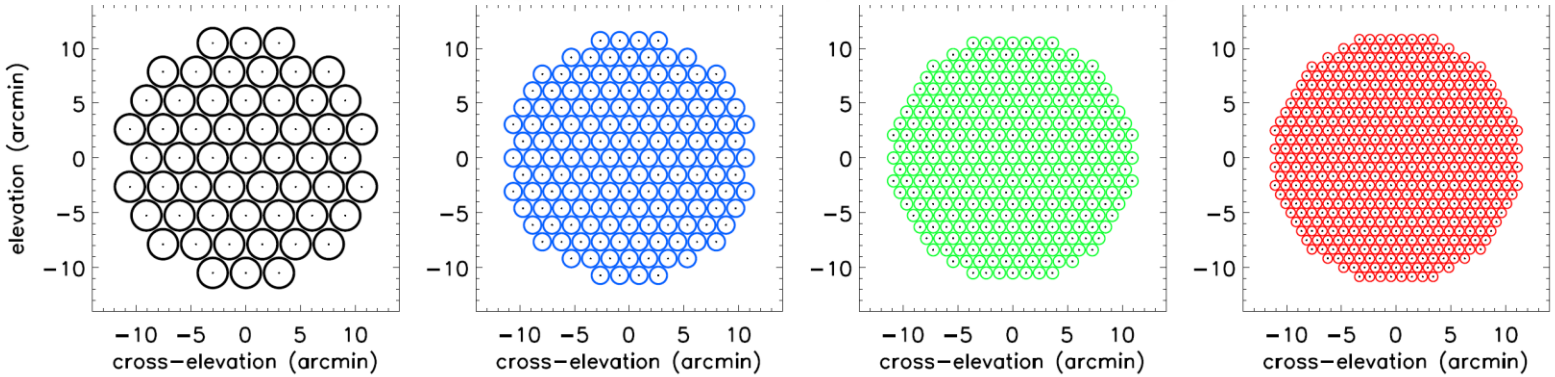

Figure 9: Focal plane arrays projected on the sky. Circles represent the $1F\lambda$ diameter of the pixels. The centers of the arrays coincide on the sky enabling efficient, simultaneous, multi-band observations of our targets.

Band (GHz)	145	250	365	460	Total
Number of detectors	55	151	313	511	1030
FWHM (arcmin)	3.3	1.9	1.3	1.0	-
Detector NEP ($\times 10^{18}$ W/$\sqrt{\text{Hz}}$)	9.4	11	7.0	7.2	-
Detector NET[a] ($\times 10^{6}$ K$\sqrt{\text{s}}$)	58	70	255	834	-
Array NET[a] ($\times 10^{6}$ K$\sqrt{\text{s}}$)	8	6	15	39	4.6

Table 4: Specifications of the OLIMPO focal plane. Noise equivalent temperature (NET) refers to T_{CMB}. The array NET includes a detector yield factor of 0.9, matching the yield for the 2018 flight [*101*] and the yield of other foundries [*105*–*107*].

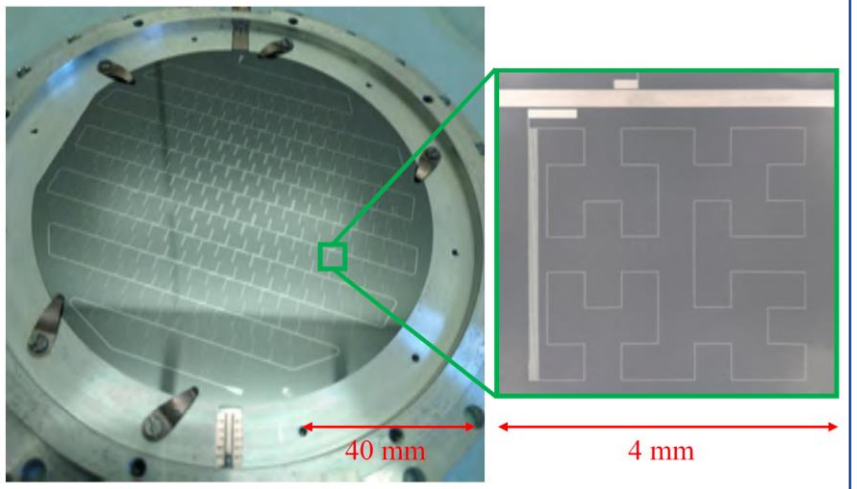

Array of >400 KIDs for the CMB
(Sapienza + CNR-IFN Roma)

OLIMPO LDB: science goals

- Probe the dynamics and characterize the WHIM in several showcase clusters / filaments systems.
- OLIMPO mm-wave data will be analyzed in correlation with e-ROSITA and radio data to get the most complete description of both the ICM plasma and the relativistic plasma, up to the periphery of the cluster, where the X-ray signal is very faint.
- Extensive simulations show that observations of the selected clusters will provide maps of the **SZ brightness** and of the **velocity of the ICM** with 0.2 Mpc resolution, with typically **10σ SNR** and **50 km/s** uncertainty. The velocity dispersion resolution in 0.2 Mpc annuli can be as low as 15 km/s, depending on the target.
- We have identified four emission bridges covered by the e-ROSITA and Planck surveys, in the observable region of OLIMPO. The surface brightness excess due to a filament is expected to be measurable at >25σ. We expect to measure density and temperature of the WHIM in the filaments at a significance of 5σ.

The (far) future of high frequency CMB surveys:

MICROWAVE SPECTRO-POLARIMETRY OF MATTER AND RADIATION ACROSS SPACE AND TIME

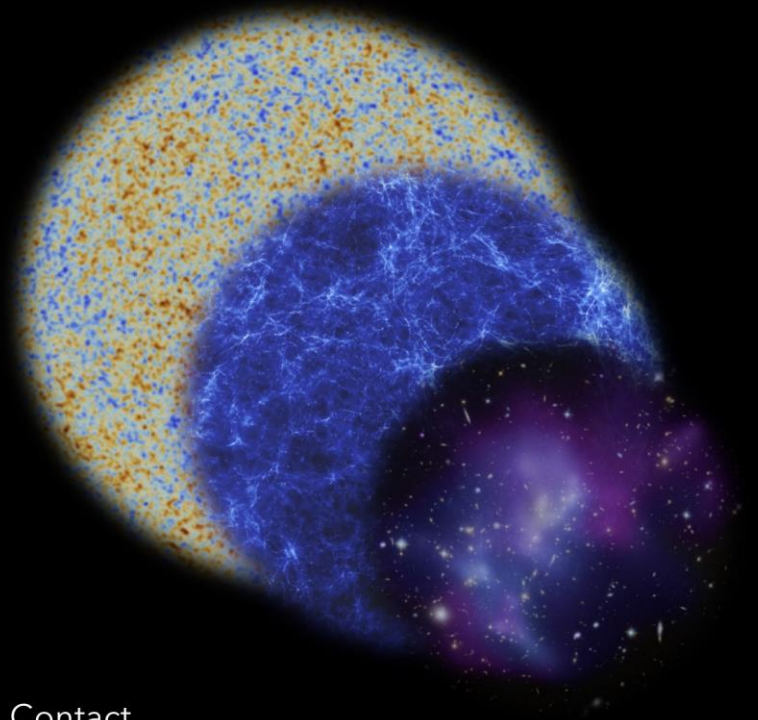

Contact
Jacques DELABROUILLE

Laboratoire APC, 10 rue A. Domon et L. Duquet, 75013 PARIS - FRANCE
email: delabrouille@apc.in2p3.fr phone: +33 6 72 91 19 54

ESA Voyage 2050 Science White Paper

A Space Mission to Map the Entire Observable Universe using the CMB as a Backlight

Corresponding Author:

Name: Kaustuv Basu
Institution: Argelander-Institut für Astronomie, Universität Bonn, D-53121 Germany
Email: kbasu@astro.uni-bonn.de, Phone: +49 228 735 658

Co-lead Authors:

Mathieu Remazeilles (Manchester; *proposal writing coordinator*),
Jean-Baptiste Melin (IRFU Saclay)

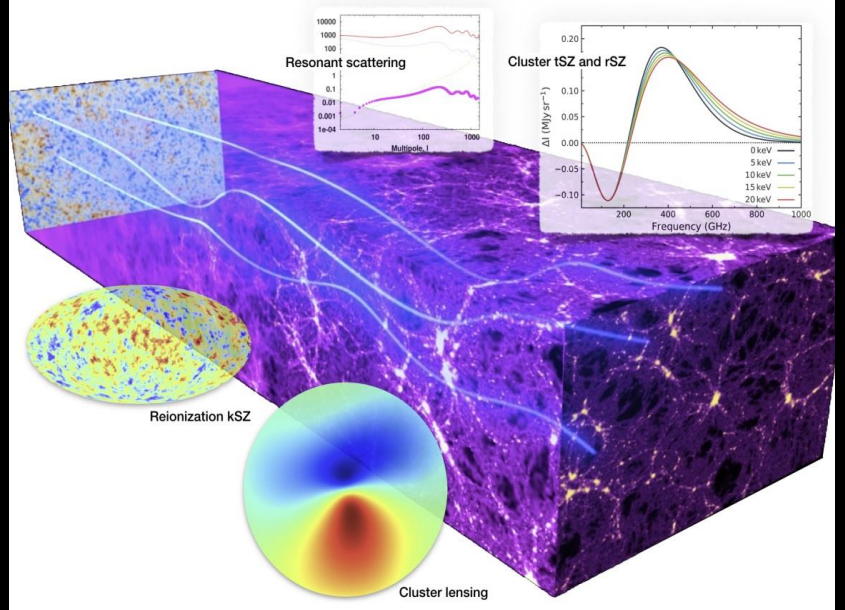

PICO

PROBE OF INFLATION AND COSMIC ORIGINS

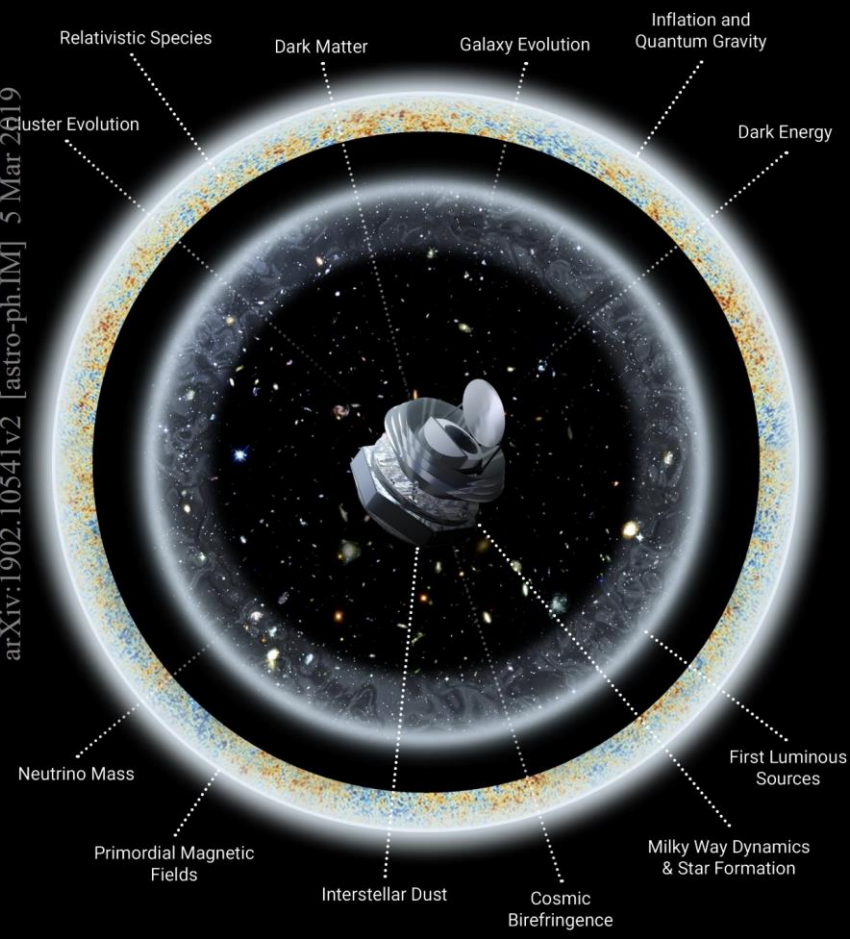

MISTRAL @ SARDINIA RADIO TELESCOPE

The near future of High Resolution SZ surveys

Picture acknowledgment: Sergio Poppi

- The Sardinia Radio Telescope (SRT) Lat. 39.4930 N -Long. 9.2451 E, is a multipurpose 64m aperture radiotelescope operated either as a single dish or VLBI.
- The **MISTRAL** W-band camera will be accommodated at the Gregorian focus cabin.
- 408 KID pixels (80-100 GHz).
- FOV = 4'
- FWHM= 12.2"
- Pixel separation = 10.6"
- Expected sensitivity: 0.9 10^{-16} W/√Hz = 0.30mJy/beam
- Commissioning: Early 2023.
- **See Paiella & JLTP 209, 889 (2022)**

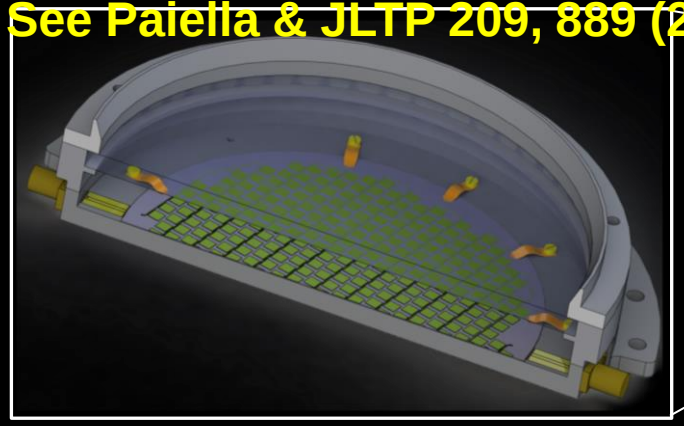

MISTRAL @ SARDINIA RADIO TELESCOPE

The near future of High Resolution SZ surveys

Picture acknowledgment: Sergio Poppi

- The Sardinia Radio Telescope (SRT) Lat. 39.4930 N -Long. 9.2451 E, is a multipurpose 64m aperture radiotelescope operated either as a single dish or VLBI.
- The **MISTRAL** W-band camera will be accommodated at the Gregorian focus cabin.
- 408 KID pixels (80-100 GHz).
- FOV = 4'
- FWHM= 12.2"
- Pixel separation = 10.6"
- Expected sensitivity: 0.9 10^{-16} W/√Hz = 0.30mJy/beam
- Commissioning: Early 2023.
- **See Paiella & JLTP 209, 889 (2022)**
- Converting to **y parameter maps**: 1h of observation of a 4' diameter region under optimal atmospheric conditions provides a **y uncertainty of $2x10^{-6}$ per beam**

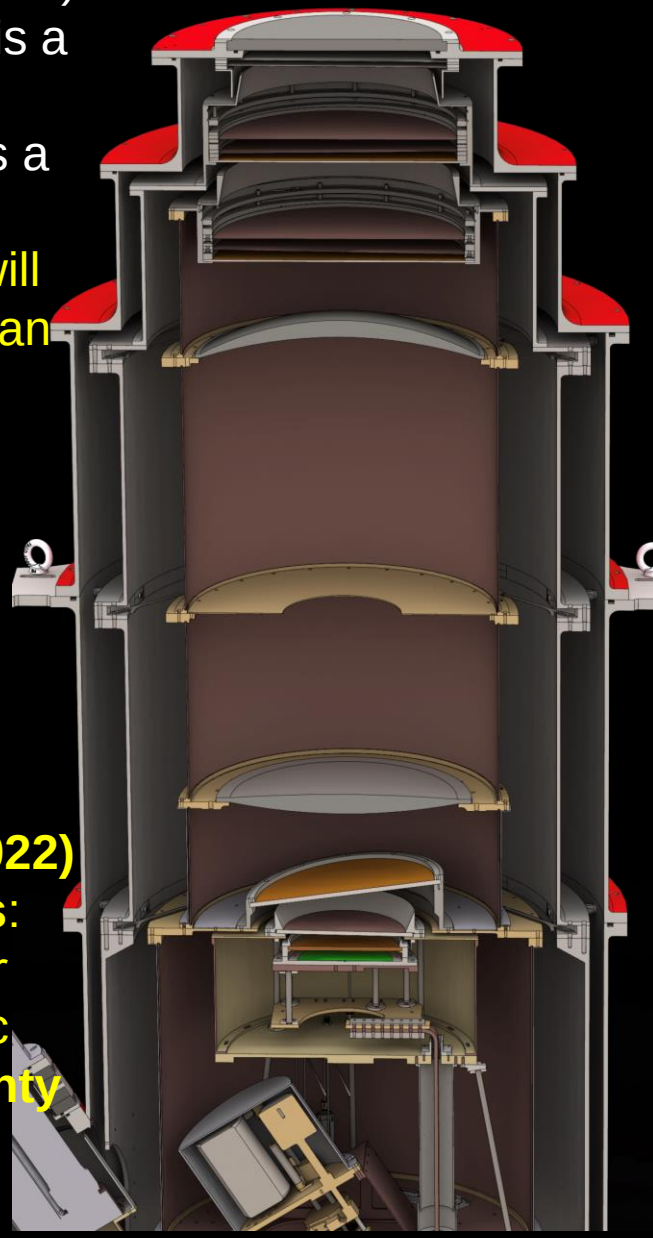

MISTRAL @ SARDINIA RADIO TELESCOPE

The near future of High Resolution SZ surveys

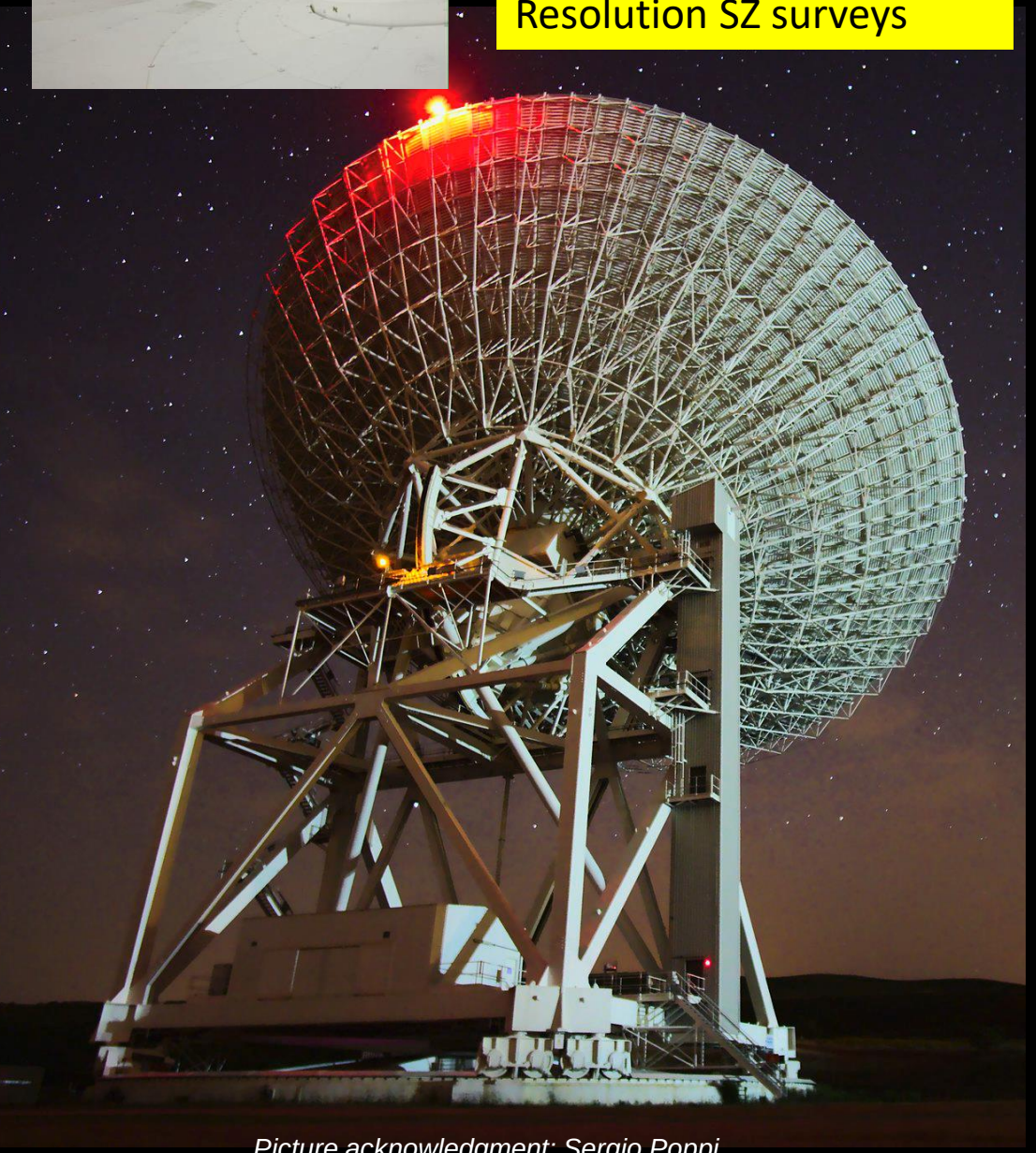

Picture acknowledgment: Sergio Poppi

This will allow a number of science cases:

- Understanding the self-similarity of Galaxy Clusters: non relaxed/merging clusters
- Study of the pressure profile and fluctuations of the ICM
- Point sources contamination
- Pressure/temperature/mass profiles
- AGN feedback
- Unveil the hierarchical growth of clusters
- Detect the cosmic web
- ….

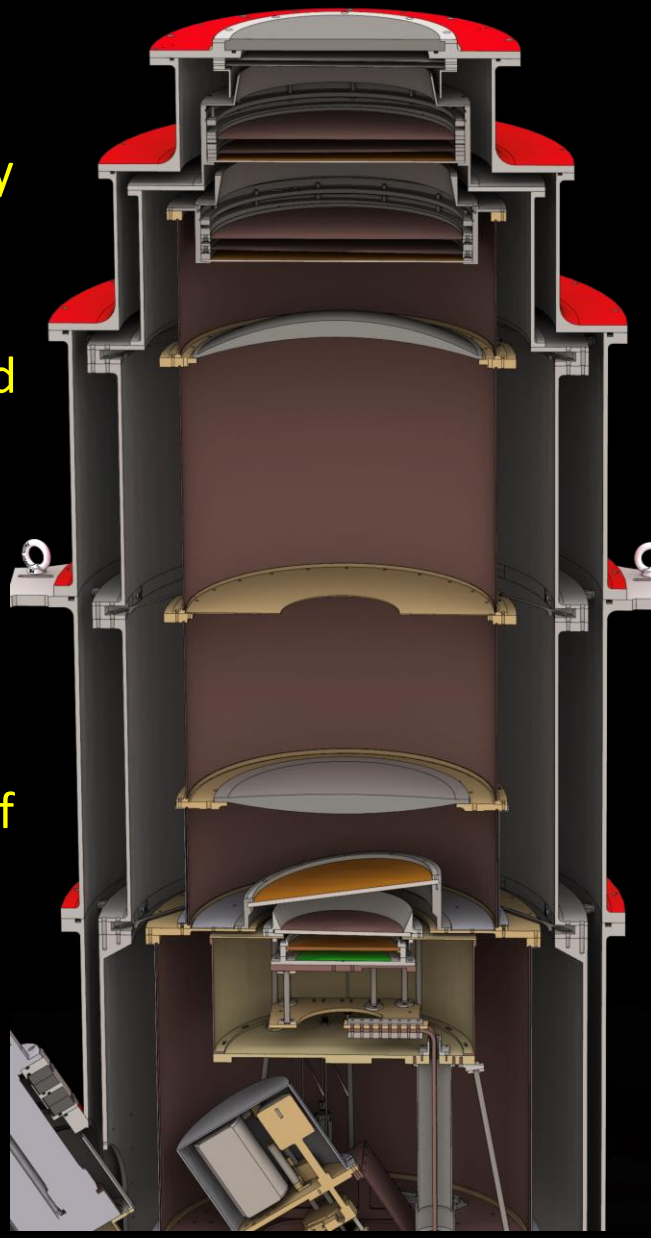

Short conclusions:

- CMB anisotropy and polarization measurements promise to provide breaktroughs in the physics of early universe (B-mode polarization), but also in the study of the large scale structure, providing, in the long run, maps of the ionized and dark matter integrated along the line of sight to recombination.
- Correlation of these data with galaxy redshift surveys, CIB, intensity mapping data etc. will provide tomographic information, complementary to all other probes.
- Deep observations of specific targets (clusters/filaments) in SZ will provide very interesting probes of cluster dynamics, ICM temperature, relativistic gas etc., complementary and synergic to radio and X-ray probes.